Micro- & Optoelectronics

FY 2003 Programs and Accomplishments

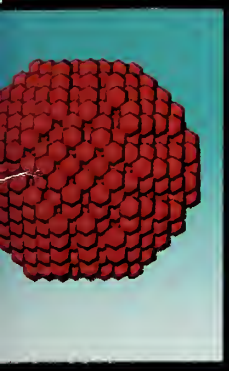
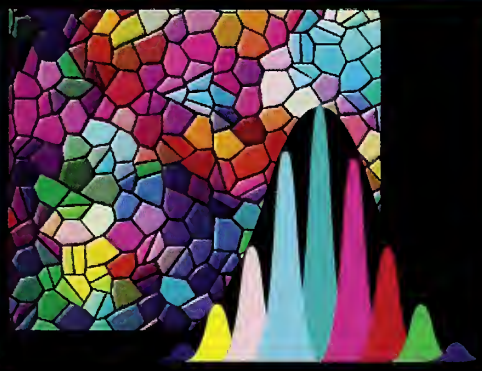

MSEL

NIST
National Institute of Standards and Technology
Technology Administration
Department of Commerce
NISTIR 7019
November 2003

On the Cover:

From the front cover and continuing on to the back, right to left, the images refer to:

2D SAXS image, p.9.

Pyrochlore structure, p.12.

Two-magnon model, p.18.

MD simulation of agglomerated spheres of copper atoms, p.32.

NIST Website: **http://www.msel.nist.gov/**
Voice Phone: 301-975-2000

National Institute of Standards and Technology
Arden L. Bement, Jr.
Director

Technology Administration
Phillip J. Bond
Undersecretary of Commerce for Technology

U.S. Department of Commerce
Donald L. Evans
Secretary

Materials Science and Engineering Laboratory

FY 2003 Programs and Accomplishments

MSEL Materials for Micro- and Optoelectronics

Frank W. Gayle
Deputy Chief, Metallurgy Division

NISTIR 7019

November 2003

Certain commercial entities, equipment, or materials may be identified in this document in order to describe an experimental procedure or concept adequately. Such identification is not intended to imply recommendation or endorsement by the National Institute of Standards and Technology, nor is it intended to imply that the entities, materials, or equipment are necessarily the best available for the purpose.

Table of Contents

Executive Summary

Introduction

U.S. microelectronics and related industries are in fierce international competition to design and produce smaller, lighter, faster, more functional, and more reliable electronics products more quickly and economically than ever before. At the same time, there has been a revolution in recent years in new materials used in all aspects of microelectronics fabrication.

Since 1994, the NIST Materials Science and Engineering Laboratory (MSEL) has worked closely with the U.S. semiconductor, component, packaging, and assembly industries. These efforts led to the development of an interdivisional MSEL program committed to addressing industry's most pressing materials measurement and standards issues central to the development and utilization of advanced materials and material processes. The vision that accompanies this program — to be the key resource within the Federal Government for materials metrology development for commercial microelectronics manufacturing — is targeted through the following objectives:

- Develop and deliver standard measurements and data;
- Develop and apply *in situ* measurements on materials and material assemblies having micrometer- to nanometer-scale dimensions;
- Quantify and document the divergence of material properties from their bulk values as dimensions are reduced and interfacial effects become increasingly important;
- Develop models of small, complex structures to substitute or provide guidance for experimental measurement techniques; and
- Develop fundamental understanding of materials needed in future micro- and opto-electronics.

With these objectives in mind, the program presently consists of projects led by the Metallurgy, Polymers, Materials Reliability, and Ceramics Divisions that examine and inform industry on key materials-related issues. These projects are conducted in concert with partners from industrial consortia, individual companies, academia, and other government agencies. The program is strongly coupled with other microelectronics programs within government and industry, including the National Semiconductor Metrology Program (NSMP) at NIST.

The present report describes the major technical activities and accomplishments in the area of Materials for Micro- and Optoelectronics within MSEL in FY2003 (October 2002 through September 2003).

In this report, we have tried to provide insight into how MSEL research programs meet the needs of our customers, how MSEL capabilities are being used to solve problems important to the national economy and the materials metrology infrastructure, and how MSEL interacts with its customers to establish new priorities and programs. Feedback and suggestions on how we can better serve the needs of our customers and encourage increasing collaboration to this end are welcomed.

Mission

Our mission is to provide critical leadership in the development of measurement methods and standards, as well as fundamental understanding of materials behavior needed by the U.S. microelectronics and optoelectronics industries to remain competitive in the changing global marketplace. As an essential part of this mission, we are responsible not only for developing new measurement methods with broad applicability across micro- and optoelectronics classes and industries, but also for working with individual industry groups to develop and integrate measurements, standards, software tools, and evaluated data for specific, technologically important applications.

Establishing Priorities

In the development of this technical program, a wide range of research opportunities is first examined. Choices for the research portfolio are based on several criteria: the match to the NIST mission, the magnitude and immediacy of industrial need, the degree to which NIST's contribution is critical for success, the anticipated impact relative to the investment, ability to respond in a timely fashion with high-quality output, and the opportunity to advance mission science. This requires that MSEL establish its research priorities through extensive consultation and collaboration with customers in U.S. industry and with counterparts in the international metrology community, using a variety of methods including workshops, technical meetings, standards committee participation, and individual consultation with our customers. Materials metrology needs are also identified through industry groups and roadmaps, including the International Technology Roadmap for Semiconductors (ITRS), the IPC Lead-free Solder Roadmap, the National Electronics Manufacturing Initiative (NEMI) Roadmap, the Optoelectronics Industry Development Association (OIDA) roadmaps, and the Information Storage Industry Consortium (INSIC).

This program deals almost exclusively with rapidly evolving technologies, where advances in measurement science are needed to understand the limitations on system behavior. MSEL focuses its efforts to address these needs in order to have the best chance to have an impact on the course of technology.

Research Portfolio

Although there is increasing integration within various branches of microelectronics and optoelectronics, the field can be considered to consist of three main areas. The first, microelectronics, includes needs ranging from integrated circuit fabrication to component packaging to final assembly. MSEL programs address materials metrology needs in each of these areas including, for example, polymer photoresists for next-generation lithography and electrodeposition of interconnects; electrical, mechanical, and physical property measurement of dielectrics (interlevel, packaging, and wireless applications); and packaging and assembly processes (lead-free solders, solder interconnect design, and thermal stress analysis). New areas this year include critical dimension measurement with small angle scattering (p. 8), computational methods for multiscale modeling (pp. 31–32) and new methods for characterizing defects and interfaces in electronic ceramics (p. 34). In addition, a long-term project supporting industrial adoption of Pb-free solders was completed (p. 37).

The second major area is optoelectronics, which includes work that often crosses over into electronic and wireless applications. Projects currently address residual stress measurement in optoelectronic films, performance of III–V optical materials, and wide bandgap semiconductors. In particular, the wide bandgap program has grown as a collaboration with the NIST Electronic and Electrical Engineering Laboratory (EEEL). Building on the existing projects on metal interconnects for GaN (Metallurgy Division) and on interface and bulk defects in GaN (Ceramics Division), the EEEL/MSEL program is developing a comprehensive suite of measurement methods for characterizing interface and bulk defects limiting the application of GaN and related materials.

A third, complementary area is magnetic data storage, where the market potential is vast and growing, and the technical challenges extreme. INSIC plans to demonstrate a recording density of 1 terabit per square inch — 40 times today's level — by 2006. To reach these goals, new materials are needed that have smaller grain structures, can be produced as thin films, and can be deposited uniformly and economically. New lubricants are needed to prevent wear as spacing between the disk and head becomes smaller than the mean free path of air molecules. Some measurements require calibration of magnetometers using certified magnetic standards in several different shapes and magnetic strengths, and with a wide range in magnetic character. These standards are now being produced under this program. MSEL is working with the magnetic recording industry to develop measurement tools, modeling software, and standards to help achieve these goals. Staff expertise at MSEL spans all fields relevant to magnetic data storage, including materials science, electrical engineering, physics, mathematics and modeling, manufacturing engineering, chemistry, metrology, and computer science, with the Materials Science and Engineering Laboratory, the Electronics and Electrical Engineering Laboratory, the Physics Laboratory, the Information Technology Laboratory, and the Manufacturing Engineering Laboratory working as partners in this effort.

Project Output

An integral part of our research programs is the dissemination of our technical accomplishments. Project output exists in a variety of forms, ranging from a fundamental understanding of micro- and optoelectronics behavior to new measurement techniques required for anticipated developments in materials use or design. These outputs are conveyed through the scientific literature and oral presentations, standard reference materials, evaluated data and online databases, software tools, and sensors for on-line process control.

Technical Highlights

The following Technical Highlights section includes expanded descriptions of research projects that have broad applicability and impact. These projects generally continue for several years. The results are the product of the efforts of several individuals. The Technical Highlights include:

- Advanced Metallizations for Sub-100 nm Electronics
- Pore Size Distributions in Low-k Dielectric Thin Films from SANS Porosimetry
- Critical Dimension Metrology of Nanoscale Structures with Small Angle X-ray Scattering
- NEMI–NIST–TMS Workshop on Tin Whiskers: Cause and Effect
- Crystal Chemistry of Novel Wireless Dielectrics: Bi-Zn-Nb-O Pyrochlores
- Biaxial Stress Dependence of Raman and Photoluminescence Lines in $Al_xGa_{1-x}As$
- Artifacts in Ballistic Magnetoresistance Measurements
- Modeling Dynamics, Damping and Defects for Perpendicular Magnetic Recording Media
- Nanoscale Measurement of the Amount of Complex Hydrocarbon Molecules on Magnetic Hard Disks

Advanced Metallizations for Sub-100 nm Electronics

Electrodeposited copper is rapidly replacing aluminum for on-chip "wiring" because of its lower electrical resistivity, superior electromigration behavior, and the ability to fill fine features without the formation of seams or voids. As feature dimensions go below 100 nm, difficulties in maintaining performance are anticipated. We are addressing these issues through a combination of modeling and experimental efforts. In FY2003, we have pushed the quantitative limits of the Curvature Enhanced Accelerator Coverage (CEAC) mechanism developed in the Metallurgy Division of NIST. Exploration of the mechanism has yielded new electrochemical processing routes for improved metallization and is guiding the development of advanced metallizations beyond copper as well as new processing routes such as ruthenium barriers for seedless electrodeposition of copper.

Thomas P. Moffat and Daniel Josell

This project is meeting the microelectronics industry's need for improved device metallizations by exploring advanced materials and process models for superconformal film growth. In FY2003 we have:

- Developed a two-step process for obtaining superfill during silver electrodeposition;
- Demonstrated superconformal feature filling using ruthenium barriers without copper seeds;
- Described an exact solution for feature filling under conditions of fixed total catalyst coverage;
- Extended the CEAC mechanism to explain surface stabilization of planar deposits during deposition of metals in electrolytes containing surfactant additives;
- Quantified consumption of adsorbed catalyst (neglected in previous CEAC models) which can substantially affect feature filling under certain deposition conditions.

Technical Details

Filling of trenches and vias with silver and copper is quantitatively explained by the Curvature Enhanced Accelerator Coverage Mechanism (CEAC) developed at NIST. Our current measurement and modeling effort is focused on copper and silver metallizations, the latter metal having the lowest resistivity of any element and, thus, having potential on-chip applications.

A two-step process for superfill of high aspect ratio features during silver deposition was demonstrated for the first time. In this process, the catalyst is adsorbed on the patterned wafer prior to metal deposition; in traditional copper processing, a single electrolyte contains both the catalyst and the metal ions. As explained by the CEAC mechanism, this process offers the possibility of improved filling of finer features with higher aspect ratios through minimization of the conformal "incubation" period of growth. In addition, the plating bath requires fewer components and is thus easier to maintain under industrial conditions.

In a review of NIST research by International Sematech in November 2000, Aaron Frank, Program Manager for Copper Deposition, requested that we also examine a growing problem for on-chip interconnects: poor deposition of seed layers as features shrink. In response to this request, we demonstrated in FY 2003 that superconformal electrodeposition directly on ruthenium barrier layers on *patterned* substrates eliminates the difficulties associated with sputter-depositing copper seeds on tantalum and titanium nitride barriers, again allowing filling of finer features with higher aspect ratios (See Figure 1).

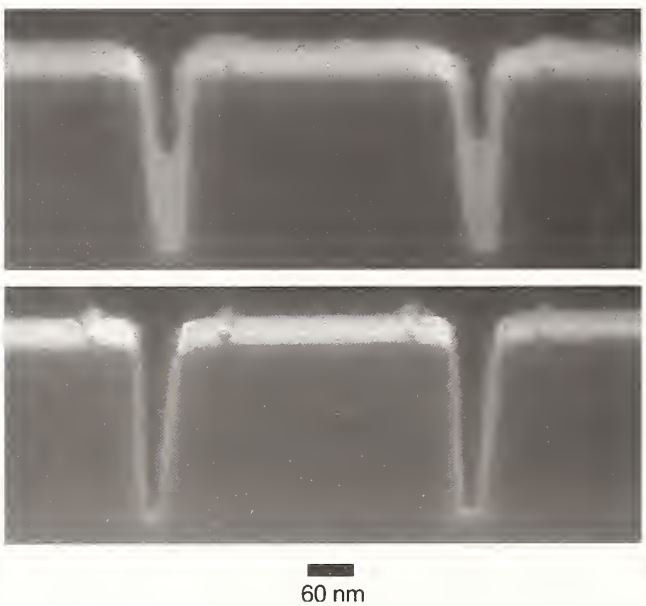

Figure 1: *Bottom-up copper fill during electrodeposition in 50 nm wide trenches with no copper seed is visible in the top image. The patterned dielectric with the ruthenium barrier alone is visible in the bottom image.*

Computer codes, that quantitatively predict superconformal deposition in fine features through the CEAC mechanism, evaluate concentration fields in the electrolyte as well as surface coverage of adsorbed catalyst on a moving boundary. Our closed-form solution for fixed initial coverage of catalyst can be used to assess the accuracy of these codes, increasing the reliability of

their predictions when applied to more complex conditions including catalyst accumulation and consumption.

In a development with application far beyond the microelectronics industry, our recent publication on the CEAC mechanism of brightening is the first to quantitatively explain the impact of adsorbed catalyst on surface stabilization during growth. This work is possibly the most significant advance in understanding surface stabilization since the growth of surface perturbations due to concentration gradients was first described. It is as significant to creating shiny electrodeposits of metal on a car bumper as it is to reducing defect-inducing surface roughness in feature filling for microelectronics.

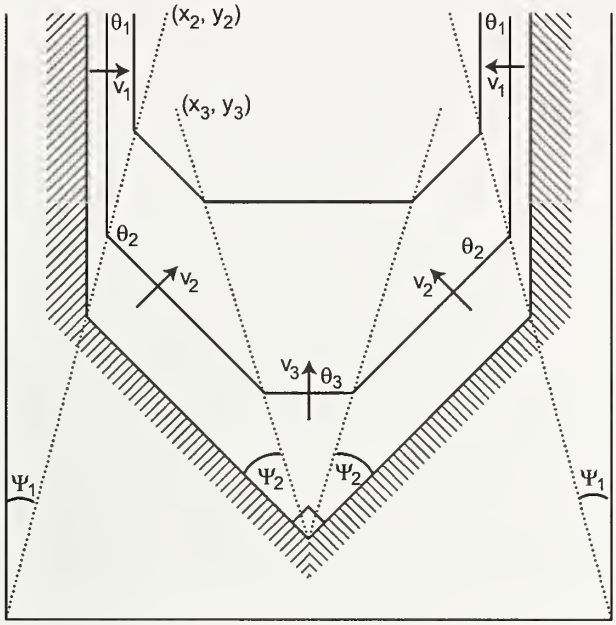

Figure 2: *The geometry used to define the exact solution for the superconformal filling of a trench. The metal deposits at the bottom corners of the trench have met in the middle where a new, even more rapidly moving, growth front emanates.*

Electrochemical and surface analytical measurements on planar substrates were used in FY2003 to establish rates of catalyst consumption that affect both feature filling and, quite likely, the microstructure of the metal deposits. Previous CEAC-based models have discounted such consumption, and this work demonstrates the reasonableness of such assumptions for the previously studied conditions. It also extends the understanding of CEAC mechanism operation to the less than ideal deposition conditions for which catalyst consumption is significant.

Selected Project Publications for FY2003

D. Josell, T.P. Moffat, and D. Wheeler. "An Exact, Algebraic Solution for the Incubation Period of Superfill," *J. Electrochem. Soc., (in press).*

D. Josell, D. Wheeler, C. Witt, and T.P. Moffat. "Seedless Superfill: Copper Electrodeposition in Trenches with Ruthenium Barriers." *Electrical and Solid-State Letters, (in press).*

G.B. McFadden, S.R. Coriell, T.P. Moffat, D. Josell, D. Wheeler, W. Schwarzacher, and J. Mallett. "A Mechanism for Brightening: Linear Stability Analysis of the Curvature Enhanced Accelerator Coverage Model." *J. Electrochem. Soc., (in press).*

D. Josell, S. Kim, D. Wheeler, T.P. Moffat, and S.G. Pyo. "Interconnect Fabrication by Superconformal Iodine-Catalyzed Chemical Vapor Deposition of Copper." *J. Electrochem. Soc.*, **150**(5), C368–C373 (2003).

D. Wheeler, D. Josell, and T.P. Moffat. "Modeling Superconformal Electrodeposition Using the Level Set Method." *J. Electrochem. Soc.*, **150**(5), C302–C310 (2003).

B.C. Baker, C. Witt, D. Wheeler, D. Josell, and T.P. Moffat. "Superconformal Silver Deposition Using KSeCN Derivitized Substrates." *Electrochemical and Solid-State Letters*, **6**(5), C67–C69 (2003).

T.P. Moffat, B. Baker, D. Wheeler, and D. Josell. "Accelerator Aging Effects During Copper Electrodeposition." *Electrochemical and Solid-State Letters*, **6**(4), C59–C62 (2003).

S.G. Pyo, S. Kim, D. Wheeler, T.P. Moffat, and D. Josell. "Seam-Free Fabrication of Sub-Micrometer Copper Interconnects by Iodine-Catalyzed Chemical Vapor Deposition." *J. Appl. Phys.*, **93**(2), 1257–1261 (2003).

B.C. Baker, M. Freeman, B. Melnick, D. Wheeler, D. Josell, and T.P. Moffat. "Superconformal Electrodeposition of Silver from a $KAg(CN)_2$-KCN-KSeCN Electrolyte." *J. Electrochem. Soc.*, **150**(2), C61–C66 (2003).

T.P. Moffat, D. Wheeler, C. Witt, and D. Josell. "Superconformal Electrodeposition Using Derivitized Substrates." *Electrochemical and Solid-State Letters*, **5**(12), C110–C112 (2002).

D. Josell, B. Baker, C. Witt, D. Wheeler, and T.P. Moffat. "Via Filling by Electrodeposition: Superconformal Silver and Copper and Conformal Nickel." *J. Electrochem. Soc.*, **149**(12), C637–C641 (2002).

Our findings have also been conveyed to the U.S. microelectronics industry, academia, and other national laboratories through more than 15 external presentations in the last year, including an invited presentation at Intel's Portland, Oregon facility. Project publications generated 100+ citations in the past year.

For More Information on this Topic

D. Josell, D. Wheeler, T.P. Moffat (Metallurgy Division, NIST)

Pore Size Distributions in Low-k Dielectric Thin Films from SANS Porosimetry

The microelectronics industry is testing a wide variety of porous low-dielectric constant ("low-k") materials for future use in integrated circuits. To understand low-k thin film properties, a quantitative analysis of pore size distribution is vital. The Electronics Materials group has developed a new approach to this challenging problem based on a small angle neutron scattering (SANS) porosimetry technique. The new technique quantifies pore size distribution and reveals subtle material characteristics inaccessible to other measurement techniques.

Barry J. Bauer and Ronald C. Hedden

As feature size on integrated circuits decreases to below 100 nm, electrical crosstalk, or interference between interconnects, becomes a major obstacle to device performance. A need has arisen to develop improved electrical insulating materials for the next generation of microelectronic devices. Silicon dioxide and fluorosilicate glass, the insulators used in today's devices, have dielectric constants (k) of about 4.2 and 3.7 respectively, but materials with dielectric constants of 2.2 or lower will be needed by 2007. However, it has proven difficult to improve existing materials by changing their chemical structure.

Much of the recent developmental efforts in low-k dielectrics involve production of nanoporous thin films. By introducing tiny air-filled pores into the material, the bulk dielectric constant is lowered because air has a dielectric constant of 1.0. The microelectronics industry is testing a wide variety of porous low-dielectric constant ("low-k") materials, including both organosilicate and organic polymer types. To understand the basis for their physical properties, detailed structural characterization is essential. Specifically, quantitative characterization of the pore size distribution is a critical issue because pore size impacts mechanical, thermal, and barrier properties of the films. Because pore size is very small (< 10 nm) and pore volume fraction is high (0.1 to 0.5), microscopy techniques are generally insufficient for evaluation of pore size distribution.

A new approach to pore size determination combines the established science of capillary porosimetry with a powerful analytical technique, small angle neutron scattering (SANS). Capillary porosimetry is an established experimental technique applicable to determination of pore size distributions. The porous material is exposed to the vapor of a "probe solvent," and pores fill with liquid solvent by capillary condensation. An adsorption isotherm is constructed by measuring solvent uptake as a function of partial pressure. In general, filling of the pores with solvent is size-dependent; the smallest pores fill first as solvent partial pressure is increased. Alternatively, the sample temperature may be varied while solvent partial pressure is held constant. Optical, x-ray, or gravimetric techniques may be employed to measure solvent uptake. Figure 1 shows solvent adsorption curves obtained by specular x-ray reflectivity (SXR) for an organosilicate type low-k material.

A limitation of capillary porosimetry is that pore size is usually not directly measured but is calculated by applying a physical model to the adsorption data. Serious ambiguities result when hysteresis phenomena are observed, which is normally the case for nanoporous materials. In addition, physical models for adsorption may fail when pores are very small, as in the low-k dielectrics. Conventional analysis of capillary porosimetry data, therefore, can provide only qualitative comparisons between low-k materials, not quantitative pore size distributions. However, a great improvement to the technique is possible by using small angle neutron

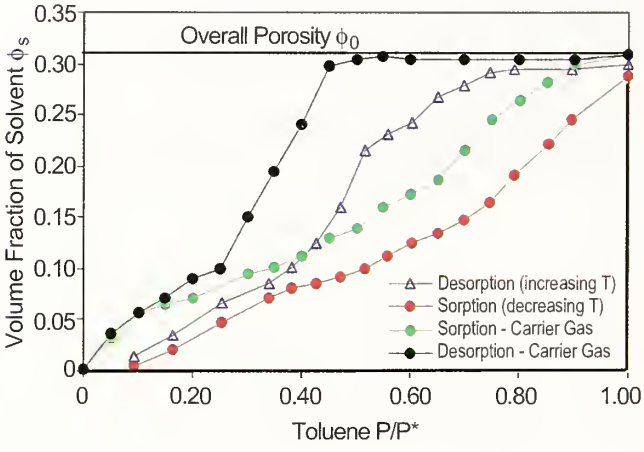

Figure 1: *Solvent adsorption data for an organosilicate low-k dielectric measured by x-ray reflectivity. Porosimetry is conducted by two methods: under isothermal conditions while varying solvent partial pressure in a carrier gas (green, black), or in a saturated solvent atmosphere while varying sample temperature (red, blue).*

scattering (SANS) to observe the adsorption process. By monitoring the pore filling and unfilling with SANS, important characteristics of the pore size distribution can be quantified irrespective of hysteresis phenomena.

To facilitate SANS porosimetry experiments, a programmable atmospheric control device was constructed that uses mass flow controllers to deliver solvent vapor in air to a flow-through sample cell. The partial pressure P of the solvent can be varied from 0.0 (pure air) to P^* (saturated solvent vapor). The sample may also be exposed to solvent vapor at a constant partial pressure P while sample temperature is varied, effectively changing P*.

The first stage of neutron porosimetry is a "contrast match point" determination. The pores are filled with solvent mixtures of variable neutron scattering length density (SLD). The solvent SLD is varied by mixing hydrogen- and deuterium-containing analogs of the solvent. The scattered intensity $I(q)$ from the solvent-filled, porous material depends on the difference in SLD or "contrast" between the solvent and the matrix. The solvent SLD is varied systematically, and the scattered intensity $I(q)$ is measured at each composition. If the material is homogeneous in atomic composition and all of the pores fill with solvent, a contrast match solvent composition exists for which $I(q)$ becomes zero over all q. If the material has inhomogeneities in its atomic composition, or if some of the pores are not filled by solvent ("closed pores"), a contrast match point will not be observed. SANS porosimetry is more applicable to samples with a true contrast match point, as subsequent data analysis is complicated by inhomogeneities.

The second stage of the measurements is porosimetry using solvent vapor of the contrast match composition. SANS data are collected as the partial pressure of the probe solvent is increased (sorption) and decreased (desorption). When pores fill with the contrast match liquid, their SLD matches the sample matrix, so the SANS measurement yields the size of only the "empty" pores. Thus, as solvent partial pressure is increased, pore size is measured for sub-populations of pores of increasingly large size.

If the volume fraction of the solvent in the film is also measured as a function of partial pressure, then average pore size and pore volume fraction are simultaneously known. X-ray reflectivity porosimetry allows such measurement with high precision and is a powerful complement to SANS porosimetry. Figure 2 shows combined results from both techniques: pore size from SANS is plotted vs. empty pore volume fraction from SXR. The data are essentially unaffected by hysteresis phenomena within the limits of uncertainty of the experiment. When all pores are empty, the SANS measurement gives the average pore size for the entire distribution. As pores are filled, the upper end of the pore size distribution is probed because only the larger pores are empty and contribute to $I(q)$ from SANS. For the sample shown in Figure 2, the average pore size is about 60 Å, but the sample contains some pores of 80 Å or larger. By using capillary porosimetry to isolate the scattering from the largest pores, sub-populations of large pores within a low-k material can be readily identified, provided their concentration is high enough to make a measurable change in the scattering. Such information is valuable to the low-k integration effort because large pores are a leading cause of device failure.

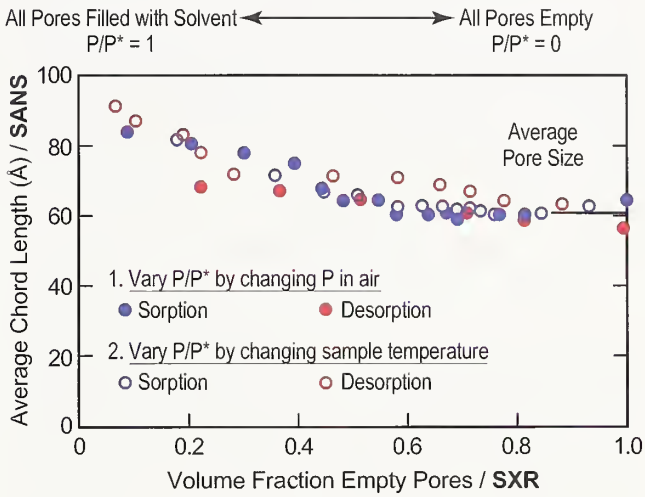

Figure 2: *Size information (average chord length) from SANS porosimetry plotted vs. volume fraction empty pores from x-ray reflectivity. The scattering data contain size information related to the average size of only the empty portion of the pores. As solvent partial pressure is increased from P/P*= 0.0 to P/P*= 1.0 (saturated solvent vapor), pores fill with liquid solvent in order from smallest to largest. As P/P* approaches 1.0, the scattering from the largest pores is probed.*

The SANS porosimetry technique allows characterization of pore size distribution without a need for a physical model for adsorption. SANS porosimetry is perhaps the most quantitative technique available today for characterizing pore size distribution in nanoporous low-k thin films.

For More Information on this Topic

B. Bauer, H. Lee (Polymers Division, NIST); R. Hedden (Department of Materials Science and Engineering, The Pennsylvania State University)

Critical Dimension Metrology of Nanoscale Structures with Small Angle X-ray Scattering

The continued reduction in pattern sizes throughout the semiconductor industry will soon require new metrologies capable of high throughput non-destructive measurements of dense, high-aspect ratio patterns with sub-nanometer resolution. In collaboration with industrial partners, we are developing a metrology based on Small Angle X-ray Scattering (SAXS) to quickly, quantitatively, and non-destructively measure the smallest, or "critical," dimensions expected in the next two technology nodes with sub-nanometer precision. Quantities of interest include critical dimension, pattern sidewall angle, statistical deviations across large areas, and quantitative measures of pattern sidewall roughness. These efforts are driving toward the specification of a laboratory scale device capable of providing pattern dimensions during routine tests of fabrication processes.

Ronald L. Jones and Wen-li Wu

The drive to reduce feature size to the sub-100 nm regime continues to challenge traditional metrology techniques for pattern characterization. Determination of the quality of the patterning process currently depends on the production of test patterns, such as line gratings, and evaluating dimensional control and the number of defects. As pattern sizes decrease, existing metrologies based on scanning electron microscopy and light scatterometry face significant technical hurdles in quantifying pattern dimensions and defects in dense, high-aspect ratio patterns used in modern semiconductor circuitry. There are currently no clear solutions to pattern quality measurement for future technology nodes with dimensions on the order of 30 nm and dimensional control to less than a nanometer.

To address these issues, NIST is developing a transmission x-ray scattering-based method capable of angstrom level precision in critical dimension evaluation over large, (50 x 50) μm, arrays of nanoscale periodic structures. In contrast to light scatterometry, Small Angle X-ray Scattering (SAXS) is performed in transmission using a sub-Angstrom wavelength. With a wavelength more than an order of magnitude smaller than the pattern size, the patterns can be analyzed using methods traditionally employed in crystallographic diffraction. The high energy of the x-ray beam allows the beam to pass through production quality silicon wafers without requiring a specialized sample environment (ultrahigh vacuum). While current measurements utilize the flexibility and wide array of instrumentation available at a synchotron source, initial results and the commercial availability of x-ray sources and detectors suggests the technique is portable to a laboratory scale device.

As shown in the schematic below, the patterned sample is placed in an x-ray beam where the transmitted intensity is measured as a function of the scattering angle, 2θ, on a 2-D detector. The intensity is then fit to models describing the average pattern shape. To save valuable space within the total patterned area, industrial test patterns are typically smaller than (50 x 50) μm. Using a monochromator to define the wavelength and two sets of beam-defining slits, beam footprints of approximately (40 x 40) μm have been successfully demonstrated. In contrast to 1-D techniques such as light scatterometry, the use of a 2-D detector allows the simultaneous characterization of all dimensions for patterns such as vias (arrays of cylinders standing perpendicular to the surface) and via pads (arrays of rectangles). In addition to measuring the pattern dimensions along the substrate plane, measurements at varying sample rotation angles, ω, can be used to reconstruct the average 3-dimensional pattern shape.

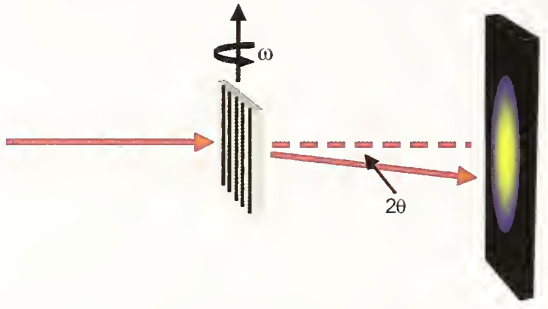

Figure 1: *Schematic of SAXS geometry, showing incident and scattered beams (red lines), sample with pattern oriented at rotation angle ω and 2-D detector (right).*

In collaboration with International SEMATECH, recent SAXS measurements of line gratings have demonstrated the capability of SAXS to measure fabricated patterns of thermally grown oxide with overall dimensions designed for current metrologies. The resulting detector image is a series of diffraction peaks along a single diffraction axis perpendicular to the orientation of the grating. The number of observable diffraction orders is in part determined by the pattern quality. The observation of over 30 orders of diffraction suggests the relatively high quality of these patterns and provides ample data for

high-precision analysis. In addition, the number of observable diffraction orders serves as an immediate measure of pattern quality, termed a SAXS "fingerprint." With a measurement time on the order of a second, dose exposure matrices commonly used to evaluate optical imaging conditions can potentially be evaluated in a matter of minutes.

In addition to the SAXS "fingerprint," quantitative information is obtained through model fitting of the data. In contrast to reflection-based techniques, the models used here are relatively simple. Quantitative measures of the pattern repeat period and the line width are therefore obtained rapidly and precisely. For these samples, SAXS data have provided sub-nanometer precision in both average repeat distance and average line width. The precision of this measurement is in part dictated by the number of observable diffraction orders, which is in turn limited by the instrumental resolution and pattern quality. Ongoing studies will compare these results with measurements from light scatterometry, atomic force microscopy, and scanning electron microscopy.

In collaboration with the IBM T.J. Watson Research Center, the effects of specific types of defects in patterns on the resulting SAXS image are being explored. Shown in Figure 2, a simple model of an ideal line grating captures the main features of the diffraction spots; however, additional information is observed in the 2-D image perpendicular to the diffraction axis. Streaks of intensity emanating from diffraction peaks are visible near the beamstop. These streaks are indicative of deviations from the ideal grating and may provide information about defects such as long wavelength line edge roughness.

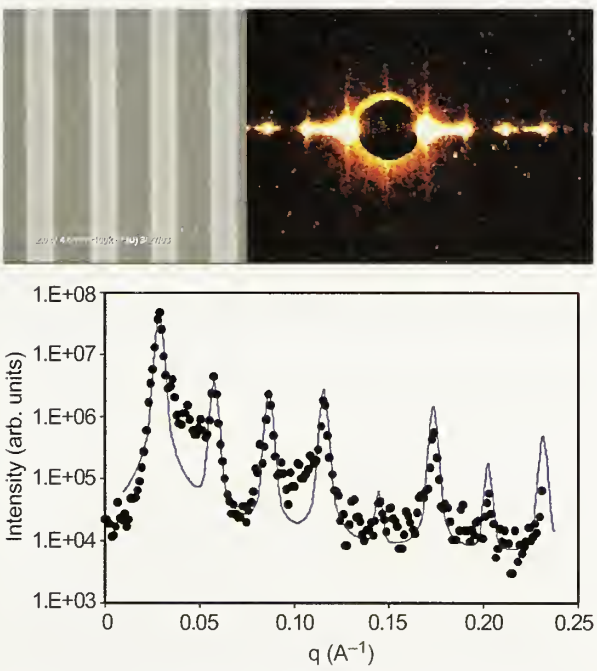

Figure 2: *Top down SEM image (top left) of a photoresist grating on a silicon wafer compared to the resulting 2-D SAXS image (top right). Also shown are the intensities of the diffraction peaks as a function of scattering vector, q ($=4\pi/\lambda \sin\theta$, where λ is the x-ray wavelength) fit with a simple model (solid blue line).*

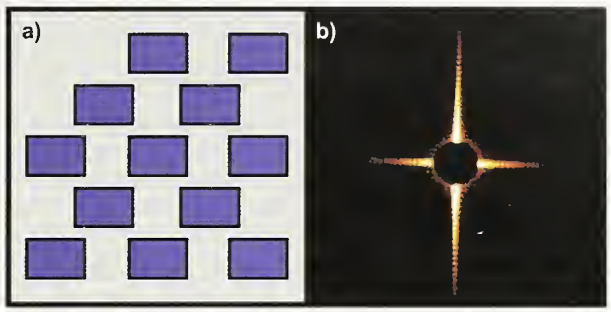

Figure 3: *Schematic of via-pad patterns (a), where the blue rectangles represent etched regions in a low-k film, and (b) the resulting SAXS detector image.*

In addition to precisely measuring dense patterns of etched silicon oxide, the application of SAXS has been demonstrated for a wide range of materials that are currently used or are being explored for use in the microelectronics industry. We demonstrated the capabilities of SAXS on dense patterns of organic photoresist, silicon oxide, and nanoporous low-k samples (detector image from 2-D array of via pads shown in Figure 3). Additionally, measurements on samples of copper-filled, low-k patterns demonstrate the capability to probe multiple component and metallic patterns. Finally, the transmission geometry allows the probing of densely packed structures, whether buried or exposed, providing a potential to measure other nanoscale 3-D structures being explored for future microelectronic devices and photonic crystals.

Continuing efforts will focus on developing quantitative measures of line edge and sidewall roughness, isolating specific types of long-range order defects arising from masks, and reconstructing an average 3-D pattern shape. In addition, further investigations will provide precise specifications for a laboratory scale device capable of similar measurements.

For More Information on this Topic

R. Jones, T. Hu, W. Wu, E. Lin (Polymers Division, NIST); G. Orji, T. Vorburger (Precision Engineering Division, NIST); A. Mahorowala (T.J. Watson Research Center, IBM); G. Barclay (Shipley Co.); D. Casa (Advanced Photon Source, Argonne National Laborotory)

R.L. Jones, T.J. Hu, E.K. Lin, W.-L. Wu, D.M. Casa, N.G. Orji, T.V. Vorburger, P.J. Bolton, G.G. Barclay, *Proc. SPIE* **5038**, 191 (2003).

NEMI–NIST–TMS Workshop on Tin Whiskers: Cause and Effect

This NEMI–NIST–TMS workshop brought together key researchers to compare in detail research that has been done in the area of tin whiskers, and to see if a consensus could be developed on a basic model defining the conditions for whisker formation, or, if not, on the work required to reach such a consensus. The end goal is to provide direction to the electronics industry in developing deposition processes that will assure that long-lifecycle products will not experience catastrophic failure due to whisker growth.

William J. Boettinger and Maureen Williams

Since the mid 1940s, the phenomenon of metallic growths from electrodeposited surface finishes on electronic components has been observed and studied. Electrodeposited surface finishes applied to the component leadframe protect the material from corrosion and improve solderability of the components prior to board assembly. These metallic growths are referred to as whiskers and may form different shapes, as seen in Figure 1.

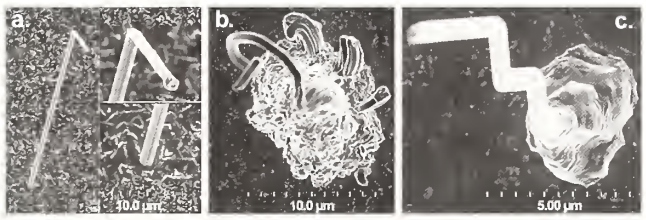

Figure 1: *Three different whisker types from bright Sn coatings; a) Filament with tip and base shown in insert; b) Odd shaped eruption with filimenery growths; c) filament growing from an eruption.*

The most commonly used commercial surface finishes are Tin (Sn) based. Sn whiskers (filament type whiskers are typically 1 µm diameter and several mm long) can grow from the Sn plate and cause electrical shorts and failures. Tin–lead (Pb) alloys have been used extensively for surface finishing of electronic components because Pb was found to be effective in retarding Sn whisker growth and keeping production costs low. Since Pb-free solder alloys have been introduced, electronic manufacturers are seeking a new surface finish technology that will prevent Sn whisker growth without the use of Pb. Whiskers are generally believed to grow to relieve residual stress in electroplated Sn. Figure 2 shows a schematic of compressive stresses in electrodeposited Sn plating resulting in the growth of a Sn whisker. Some of the key factors that have been found to influence Sn whisker growth are: deposit thickness, diffusion, thermal stresses, substrate material, electrolyte type, plating conditions, temperature, humidity, organic and inorganic inclusions, grain size and shape, and interdiffusion barriers. In spite of this wealth of information, a basic understanding of whisker growth and its prevention does not currently exist.

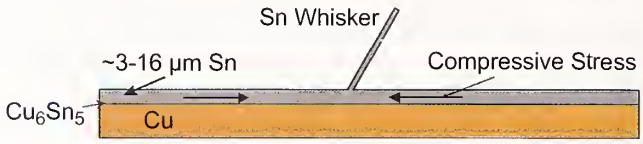

Figure 2: *Schematic of Sn whisker growth from a Sn electrodeposited plating.*

The National Institute of Standards and Technology (NIST), the National Electronics Manufacturing Initiative (NEMI), and The Minerals, Metals & Materials Society (TMS) co-sponsored a one-day workshop, "Tin Whiskers: Cause and Effect," on Sunday, March 2, at the San Diego Convention Center. The event was held in conjunction with the 2003 TMS Annual Conference and Exhibition.

The agenda consisted of four presentations during the morning and round table discussions in the afternoon. The 44 attendees represented a variety of industrial, academic, and government organizations, including Analog Devices, Brocade Communications Systems, Cookson Electronics, Hanyang University, HP, IBM, Intel, KAIST, Kyocera, Los Alamos National Lab, Michigan State, Millenium Chemicals, Motorola, Oak Ridge National Lab, Research in Motion, Sandia National Laboratory, Shipley TI, Sun Yat-Sen University (Taiwan), SUNY at Buffalo, Technic, The Aerospace Corporation, University of Kentucky, and Washington State University. All of the participants contributed to a lively afternoon discussion of the papers presented and current theories.

Stress in Electroplated Sn

Dr. Chen Xu of Cookson Electronics outlined his work on understanding the whisker growth rate and carrying out structural and chemical characterizations of whisker growths. He presented a "whisker index" — a proposal to characterize whiskers and presented data on this factor as a function of various types of Sn plating. He discussed the use of x-ray diffraction (XRD) for measuring stress in Sn plated films, showing the changes in stress as a function of time. His data shows that compressive stress in the film leads to whisker growth, while tensile stress does not.

He presented data to show that a nickel (Ni) under layer will result in tensile stress in the Sn layer, and he saw no whisker growth when a Ni layer was deposited between the Cu and Sn layers.

Spontaneous Growth of Tin Whiskers

Dr. Dong Nyung Lee of the School of Materials Science and Engineering, Seoul National University showed results of microstructure characterization using SEM techniques, including angle of growth, and pole figures. To release the compressive stress in the tin film, tin whiskers grow from the grain whose surface oxide is sheared. The whisker growth is controlled by the expansion of prismatic dislocation loop on the slip plane by climb, that is, by means of the operation of the Bardeen–Herring dislocation source. Whisker growth continues until the stress is relieved.

Tin-Whisker Microstructural Analysis

Dr. George T. Galyon of the IBM Server Group provided a critical analysis of the literature outlined in his *Annotated Sn Whisker Bibliography*, noting that there appear to be necessary conditions for whisker formation (*i.e.*, stress) that are not always sufficient to explain the overall phenomena. He provided a great deal of information on the use of the Focused Ion Beam (FIB) tool in examining whiskers. Very little, and only recent, work has been reported using this new tool, and it seems to provide considerable additional insight into whisker structures. His observations indicate that whisker growth is the result of a recrystallization of the tin at the base of the whisker resulting in additional material pushing the whisker out of the film.

Focused Ion Beam, Transmission Electron Microscopy, and Synchrotron Radiation

Dr. King N. Tu, of the Department of Materials Science and Engineering at UCLA, performed studies on tin whiskers with focused ion beam (FIB) imaging, cross-section transmission electron microscopy (XTEM) observation, and synchrotron radiation (SR) micro-diffraction analysis. Morphology of whiskers and orientation relationship between a whisker and grains in the tin plating has been studied by FIB and XTEM. A large amount of precipitates in the grain boundaries were observed. The precipitation of Cu_6Sn_5 intermetallic is believed to maintain the driving force for spontaneous whisker growth.

Discussion Summary

Discussions established that Sn whiskers are caused by compressive stress in the Sn plated film, and that material somehow moves through the grain boundaries to form a whisker. Whiskers grow from material deposited at the base of the whisker. The formation of Cu_6Sn_5 intermetallics in the Sn grain boundaries may contribute to the growth of a compressive stress. The whisker may take advantage of weakness in the oxide film to erupt.

While no specific mechanism for Sn whisker growth was established, several questions were posed. Some of these questions included:

- Why is recrystallization of Sn necessary for whisker growth?
- What is the mechanism by which the Sn is transported to the whisker base?

Discussions also determined several areas that require further study to determine the growth mechanism:

- The role of Pb in suppressing whisker formation; the role of a surface oxide layer;
- The role of texture;
- The role of impurities; and
- The role of a diffusion barrier.

An understanding of the details of the nucleation process is also needed. The most important conclusion was that further systematic experimental work must be done to establish the growth mechanism.

Currently at NIST, efforts are focused on analyzing the average stress relaxation in electrodeposited films as function of time. These experiments concentrate on *in situ* stress measurements during the plating process and post-plating. Additional experimental work is planned in collaboration with NEMI members.

"I consider your [NIST Metallurgy Division] group a key asset to industry in making these decisions on the soundest possible scientific basis. There is no comparable body of expertise anywhere in the world that matches that found in your group."

Dr. George T. Galyon
(IBM) — Chairman, NEMI
TinWhisker Modeling Committee

For More Information on this Topic

W.J. Boettinger, M. Williams (Metallurgy Division, NIST); R. Gedney (NEMI); K.-W. Moon (University of Maryland)

Crystal Chemistry of Novel Wireless Dielectrics: Bi-Zn-Nb-O Pyrochlores

The primary technology drivers for wireless consumer devices include miniaturization, reduction of component part count, and increased functionality. Multilayer ceramic integrated circuits manufactured using low-temperature co-fired ceramic technology provide a viable solution to this challenge. Recently, bismuth-based pyrochlores have been recognized as attractive candidates for capacitor and high-frequency filter applications in multilayer structures co-fired with metal electrodes. However, understanding of the dielectric behavior of these materials has been impeded by the absence of detailed structural information. In the present study, we conducted a detailed analysis of the cubic pyrochlore-type compound $Bi_{1.5}Zn_{0.92}Nb_{1.5}O_{6.92}$ to establish the details of its crystal chemistry and the structural origin of its dielectric response.

Igor Levin

Ternary oxides in the Bi_2O_3-ZnO-Nb_2O_5 (BZN) system exhibit (Figure 1) high dielectric constants (ε), relatively low dielectric losses, and compositionally tunable temperature coefficients of capacitance (τ_c). Such properties, combined with sintering temperatures of less than 950 °C, render these materials as attractive candidates for capacitor and filter applications in multilayer structures co-fired with silver electrodes. This system features two structurally distinct ternary compounds, $Bi_{1.5}Zn_{0.92}Nb_{1.5}O_{6.92}$ ($\varepsilon \approx 145$, $\tau_c \approx -400\times10^{-6}$/°C) and $Bi_2Zn_{2/3}Nb_{4/3}O_7$ ($\varepsilon \approx 80$, $\tau_c \approx +200\times10^{-6}$/°C), exhibiting very dissimilar dielectric properties. Since the two compounds exhibit opposite signs of τ_c, their mixture yields temperature-compensated ceramics.

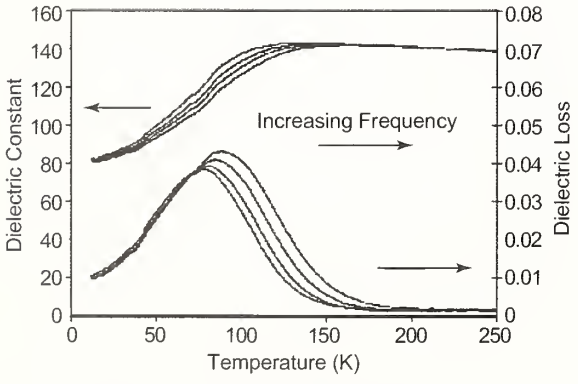

Figure 1: *Dielectric response of pyrochlore-type $Bi_{1.5}Zn_{0.92}Nb_{1.5}O_{6.92}$. (Courtesy of C. Randall and J. Nino, PSU.)*

$Bi_{1.5}Zn_{0.92}Nb_{1.5}O_{6.92}$ ceramics exhibit a low-temperature dielectric relaxation, which has been attributed to a dipolar glass-like mechanism, while no such behavior is observed for $Bi_2Zn_{2/3}Nb_{4/3}O_7$ in the same temperature range.

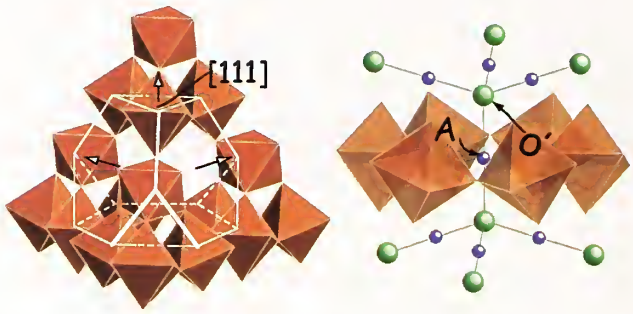

Figure 2: *Illustrations of the pyrochlore structure. Pyrochlores are often described by the formula $B_2O_6{\bullet}A_2O'$, which emphasizes that the structure is built of two interpenetrating networks: $[BO_6]$ octahedra sharing vertices form a three-dimensional network based on a diamond net (left), which results in large cavities occupied by the O′ and A atoms, themselves forming a second cuprite-like A_2O' tetrahedral net (right).*

Despite growing technological interest in these ceramics, their crystal chemistry and the origin of their dielectric behavior have remained uncertain. The compound $Bi_{1.5}Zn_{0.92}Nb_{1.5}O_{6.92}$ was reported to exhibit a cubic pyrochlore structure (Figure 2), $A_2B_2O_7$, implying that the Zn ions occupy both A- and B-sites. However, in the absence of detailed structural/compositional data, the presence of rather small Zn ions on the eight-fold coordinated A-sites remained highly controversial because the ionic radius of Zn falls outside the known limits of structural stability for pyrochlores. The other compound, $Bi_2Zn_{2/3}Nb_{4/3}O_7$, according to our recent work, was found to adopt a monoclinic zirconolite-like arrangement. The zirconolite structure, which, like pyrochlore, can be described as an anion-deficient fluorite-derivative, features a distinctly different type of cation arrangement on the metal sites. In the present work, we conducted a detailed structural analysis of the cubic pyrochlore $Bi_{1.5}Zn_{0.92}Nb_{1.5}O_{6.92}$ to elucidate its crystal chemistry and the origin of the dielectric relaxation.

Electron diffraction patterns from single grains of $Bi_{1.5}Zn_{0.92}Nb_{1.5}O_{6.92}$ were consistent with both a pyrochlore-type unit cell and symmetry. However, several reflections (*e.g.*, 442) observed in the experimental electron, x-ray, and neutron powder diffraction patterns, although accountable by the

Fd3m symmetry, violated special reflection conditions for the 8*b*, 16*c*, 16*d*, and 48*f* sites occupied in the ideal arrangement; these observations suggested that some of the atoms are displaced to lower symmetry positions. Indeed, Rietveld refinements using neutron data confirmed appreciable distortion of the A-site environment that occurs to accommodate the bonding requirements of the A-cations (Figure 3). This distortion is realized through (i) displacements of both A-cations and O′ anions from their ideal high symmetry positions (16*d*-A, 8*b*-O′), and (ii) local tilting of [BO_6] octahedra. A combination of the best fit and most reasonable values of displacement parameters were obtained by placing both A and O′ ions on the 96*g* (*x*,*x*,*z*) positions. Similar positional parameters were obtained at both 298 K and 12 K, suggesting that the displacements are static in nature. In the disordered model, each A cation is randomly distributed over six sites, which are displaced from the ideal 16c positions approximately along the three <112> directions perpendicular to the corresponding O′-A-O′ link. The displacements of the A-cations are confined to the {111} layers and result in shortening of three-out-of-six A-O bonds. The displacements of O′ ions occur along all six <110> directions, so that each O′ ion is statistically distributed over 12 sites.

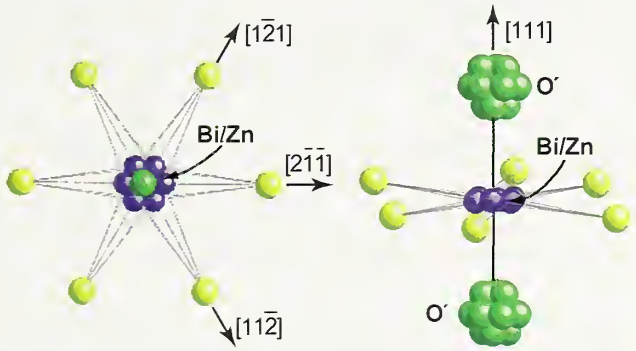

Figure 3: *Nearest-neighbor environment indicated by the refinement results for the A = (Bi/Zn) cations in the BZN pyrochlore. Yellow and green spheres represent O and O′ atoms, respectively, while blue spheres correspond to the A-cations. Left: View along <111> direction with six-randomly occupied A-cation positions indicated by blue spheres. The O′ atoms are shown in the ideal positions for clarity. Right: View along the direction nearly perpendicular to the <111>. The displaced positions of both the A- and O′ atoms are indicated.*

The bond strain about the A-sites is minimized when both O′ ions in the O′-A-O′ link move toward the corresponding {111} layer; these A-sites are expected to be occupied by Zn. Three other O′-A bonds for the same O′ ion will be stretched so that those A-sites are likely to be occupied by Bi. Because no superstructure reflections were observed, any such structural correlation must be short-range in nature. Crystal-chemical considerations suggest local ordering in which each O′ ion is bonded to three Bi and one Zn cations; in such configurations, the bonding requirements of both Zn and Bi can be met. Electron diffraction patterns (Figure 4) revealed weak, yet well-structured, diffuse scattering which can be attributed to such short-range ordering of Bi and Zn on the A-sites.

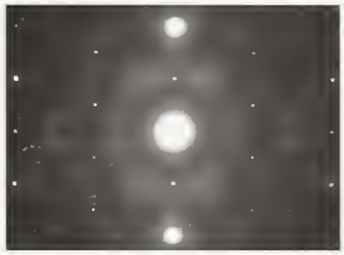

Figure 4: *High-index zone axis electron diffraction pattern from the pyrochlore $Bi_{1.5}Zn_{0.92}Nb_{1.5}O_{6.92}$ reveals well-structured diffuse scattering likely associated with local ordering of Bi and Zn.*

Studies of $Bi_{1.5}Zn_{0.92}Nb_{1.5}O_{6.92}$ using far-infrared spectroscopy, conducted by S. Kamba at the Institute of Physics in Prague, indicated that the lowest frequency O′-A-O′ bending mode provides the strongest contribution to the dielectric constant while the contribution of the O-A-O bending is also significant. Both types of bending resemble those produced by the presently identified static displacements of the A, O′ and O atoms; therefore, these displacements are expected to have a strong effect on the dielectric response of the cubic pyrochlore-type compound. Thus, the displacive disorder in the A_2O' network most likely is the origin of the "glass-like" dielectric behavior observed for $Bi_{1.5}Zn_{0.92}Nb_{1.5}O_{6.92}$.

These studies of cubic pyrochlore-type $Bi_{1.5}Zn_{0.92}Nb_{1.5}O_{6.92}$ have established a new crystal–chemical mechanism for the accommodation of small cations such as Zn on the A-sites of the pyrochlore. This new principle has been applied to interpret the structural behavior of other new pyrochlore compounds in the Ca-Ti-Nb-O and Ca-Ti-Ta-O systems. These phases were found to contain a mixture of Ca and Ti on the A-sites, disordered displacements of Ti and O′ atoms, and, also, dielectric relaxation similar to that observed for the cubic Bi-Zn-Nb-O pyrochlore.

For More Information on this Topic

Igor Levin (Ceramics Division, NIST)

I. Levin, T.J. Amos, J.C. Nino, T.A. Vanderah, C.A. Randall, and M.E. Lanagan. "Structural Study of an Unusual Cubic Pyrochlore $Bi_{1.5}Zn_{0.92}Nb_{1.5}O_{6.92}$." *J. Solid State Chem.*, **168** [1], 69–75 (2002).

I. Levin, T.J. Amos, J.C. Nino, T.A. Vanderah, C.A. Randall, M.E. Lanagan, and I.M. Reaney. "Crystal Structure of Compound $Bi_2Zn_{2/3}Nb_{4/3}O_3$." *J. Mater. Res.*, **17** (6), 1406–1411 (2002).

Biaxial Stress Dependence of Raman and Photoluminescence Lines in $Al_xGa_{1-x}As$

Device manufacturers in the optoelectronics and microelectronics industries have expressed the need for a measurement technique to evaluate local residual stresses in thin film systems. In response, this project seeks to calibrate biaxial stress-induced peak shifts in the first order Raman and photoluminescence (PL) lines of $Al_xGa_{1-x}As$ as functions of both stress and composition (x) to provide a set of tools that can simultaneously determine composition and biaxial stress state. While the calibrations are specific to $Al_xGa_{1-x}As$, the approach is expected to be generally applicable to other semiconductor systems.

Grady S. White and Albert J. Paul

Layered structures of ternary semiconductor compounds, *e.g.*, $Al_xGa_{1-x}As$, are routinely used in optoelectronics as light sources and detectors. The wavelengths at which these devices perform, as well as their mechanical and electronic stability, are functions of the stress (strain) under which they operate. Similar semiconductor ternary compounds are used in the microelectronics industry and are subject to the same stress-driven effects. The stresses, generated during processing, are inherent in the devices and are normally predicted by design models. However, there is currently no way for the accuracy of the models to be confirmed experimentally. The goal of this project is to develop a suite of tools, consistent with those used in industry, that can measure local stresses for model verification.

Photoluminescence (PL) is widely used in the U.S. optoelectronic and microelectronic industries to monitor thin film composition in multilayer devices. Because the same instrumentation can be used for both PL and Raman measurements and because Raman peak positions are known to be stress sensitive, these two techniques were chosen as developmental probes for simultaneously monitoring film stress and composition. The critical question addressed is whether a combination of the two techniques allows separation of stress-induced peak shifts from composition-induced peak shifts, thereby allowing simultaneous evaluation of both stress and composition.

For this study, $Al_xGa_{1-x}As$ films with x = 0.2, 0.5, 0.8, and 0.9 were deposited by molecular beam epitaxy on commercial 655 μm thick, 75 μm diameter undoped GaAs substrates. The deposition temperature was 600 ± 5 °C and the film thickness, in each case, was nominally 3 μm. Bulk x = 0 specimens were cleaved from a polished, undoped, GaAs substrate, 500 μm in thickness and 50 mm in diameter. All specimens were oriented with the (100) direction normal to the plane formed by the specimen surface. Squares 11 mm x 11 mm were cleaved from the wafers and placed into a biaxial loading rig in the optical path of a commercial micro-Raman system.

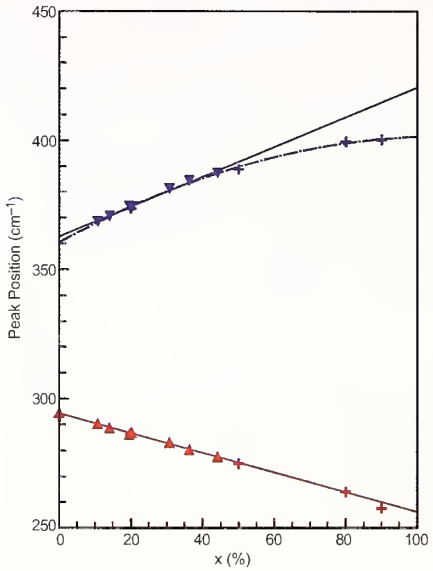

Figure 1: *Unstressed Raman peak positions of GaAs-like (lower) and AlAs-like (upper) peaks as function of x. Triangles and "+" symbols represent two sets of specimens.*

First order Raman spectra of $Al_xGa_{1-x}As$ ($0 < x < 1$) consist of both a GaAs-like line and an AlAs-like line. Figure 1 shows the peak position as a function of x for both of these lines in the absence of stress. The GaAs-like line is linear across the entire composition range, whereas the AlAs-like line is clearly nonlinear and is well described by a quadratic expression ($R^2 > 0.99$).

Data in Figure 2 were obtained from the GaAs-like line of two x = 0.5 specimens. The behavior shown in Figure 2 is typical of the behavior at all compositions for both the GaAs-like and the AlAs-like peaks. Peak shifts are linear with stress, and the peak position decreases with increasing stress. Error bars in all of the figures represent the 95 % Confidence Level.

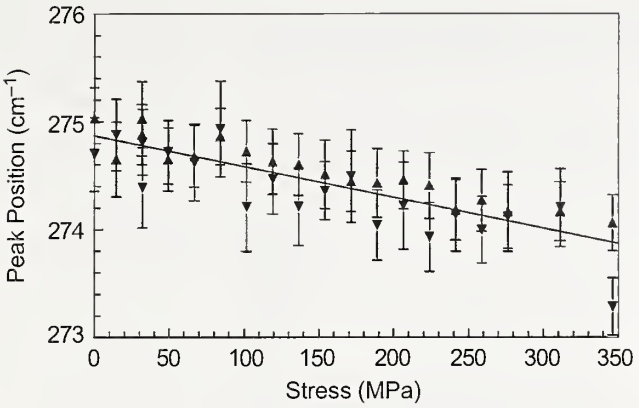

Figure 2: *Peak shift of GaAs-like peak; x = 0.5. The upward and downward triangles represent data taken from two different specimens.*

Figure 3 shows the change in peak position/stress for both Raman lines as a function of composition. Within the precision of the Raman measurements, the stress sensitivity of both lines is independent of x. However, the AlAs-like line shifts almost 50 % more for a given stress than the GaAs-like line. Figures 2 and 3 show that while the phonon energy of both the GaAs-like and the AlAs-like peaks depend strongly upon the relative amounts of Ga and Al in the unit cells, the change in energy with the application of stress is essentially independent of the Ga/Al ratio.

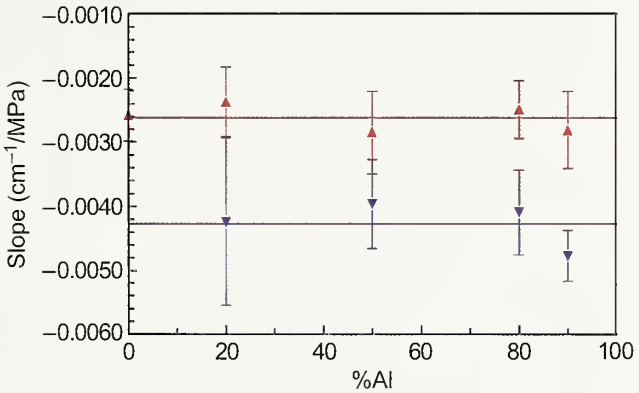

Figure 3: *Slopes (i.e., peak position/stress) of Raman lines as a function of composition: GaAs-like peak (top) and AlAs-like peak (bottom).*

In contrast to the Raman lines, the PL peak shift with stress (Figure 4) shows strong composition dependence for the direct electron transition (x < 0.5). For x = 0.8 and 0.9, the PL spectra are more complicated and result from indirect transitions. The peak positions in this region, while still dependent on x, are essentially independent of stress. The values shown in Figure 4 for x = 0.8 and 0.9 are averages of the multiple peaks composing the PL at those compositions. However, none of the individual peaks deviates substantially from the average values shown in Figure 4. At x = 0.5, the PL is also indirect. However, at that composition, the PL spectrum consists of several peaks that are essentially independent of stress (upper point in Figure 4) and one peak that is stress dependent (lower point in Figure 4).

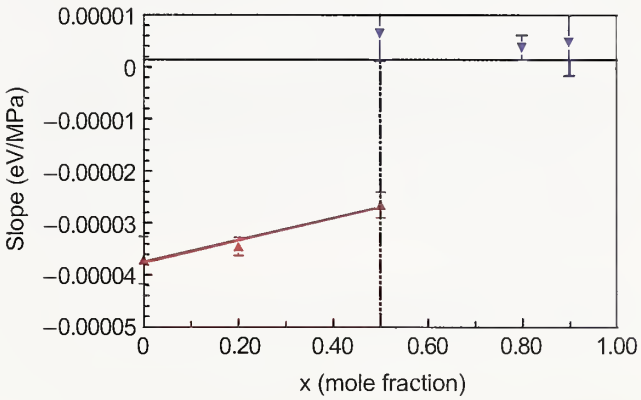

Figure 4: *Slopes (i.e., peak position/stress) of PL lines as a function of composition. In the left side of the figure, PL results from direct transition; in the right side, PL results from indirect transition.*

Because both the Raman and PL spectra are functions of stress and composition, the combination of measurements can be used to solve for composition and biaxial stress state simultaneously. Even for x > 0.5, where the PL is independent of stress, the measured composition dependence of the PL lines coupled with the stress and composition dependence of the Raman lines permits both composition and stress to be determined. Because both the GaAs-like and the AlAs-like Raman line positions have been calibrated for both stress and composition, there are three, rather than two, peaks that provide information regarding stress and composition. The existence of the third peak provides a tool for self-consistency checks on the values obtained.

A manuscript, *Biaxial Stress Dependence of the GaAs-Like and AlAs-Like Raman Lines in $Al_xGa_{1-x}As$,* by G.S. White, A.J. Paul, K.A. Bertness, and A. Roshko that describes the Raman measurements in detail, has been submitted for publication.

For More Information on this Topic

G.S. White, A.J. Paul (Ceramics Division, NIST); K.A. Bertness, A. Roshko (Optoelectronics Division, NIST)

Artifacts in Ballistic Magnetoresistance Measurements

Magnetic sensors play a central role in many important technologies ranging from data storage to health care to homeland security. A common need among these technologies is higher sensitivity and smaller size. Advances in the past year in the Ballistic Magnetoresistance (BMR) effect appeared to provide enormous progress in sensitivity in nanoscale devices. The scientific press reported it as one of the major discoveries of the year. Unfortunately, it appears to be wrong. Experiments at NIST have found that several simple artifacts can account for the results. NIST is taking a leading role in designing artifact-free metrology to provide reliable data to the magnetic sensor industry.

William F. Egelhoff, Jr.

Magnetic sensors play a central role in many important technologies. To name just a few, computer hard disk drives use magnetic sensors to read stored data (Figure 1), magnetoencelophalography uses magnetic sensors to image brain wave activity, and bio-hazard detectors use magnetic sensors to detect magnetic beads bio-tagged for anthrax, botulism, cholera, and other pathogens.

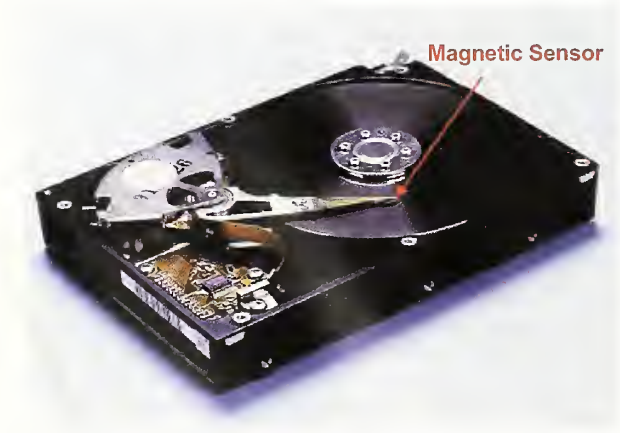

Figure 1: *Computer hard disk drives use a magnetic sensor to read data.*

A common need among these technologies is higher sensitivity and smaller size. With higher sensitivity and smaller size, more data could be stored on a hard disk, higher resolution imaging of brain activity would be possible, and earlier warnings of bio-contamination could be given.

Currently, the Giant Magnetoresistance (GMR) effect is used for the best small-scale sensors. A GMR sensor can, at best, exhibit a ≈ 15 % change in electrical resistance in response to a magnetic field. Shock waves went through the magnetic-sensor community in 2003 when a value for the Ballistic Magnetoresistance effect (BMR) of 100,000 % was published and a value of 1,000,000 % was reported at a major scientific conference.

Understanding these results suddenly became a high priority for the magnetic-sensor community. For example, Seagate, the world's leading hard-disk drive manufacturer, sent Dr. Erik Svedberg, a physicist in its research labs, to work with us half-time in 2003 to investigate BMR. Seagate selected to work with NIST because we already had a strong program in place to investigate BMR and a network of collaborators that included those groups reporting the high BMR values. NIST had initiated the BMR research program prior to these reports because earlier less-sensational reports of BMR looked promising but faced a number of problems. BMR samples had poor reproducibility, poor stability, and poor reliability. The fabrication techniques were poorly understood, and there was no theory to explain the magnitude of the BMR effect. It was felt that NIST might help with what is often a long, hard road from a laboratory demonstration of a concept to a commercially successful device.

As the NIST program developed over the past two years, it became clear that other labs were able to achieve much higher BMR values, some in the 100 % to 700 % range, while NIST results rarely exceeded 10 %. The trend accelerated in 2002 as these other labs began reporting results of 3,000 % to 10,000 %. These BMR values were reported as major discoveries in *Science*, *Science News*, and *Physics News*.

In late 2002 and early 2003, scientists from these other labs visited NIST to demonstrate how they achieved these results. NIST staff analyzed the experiments and found them to be subject to a variety of artifacts that can mimic BMR. The small BMR values that NIST had measured were directly attributable to more careful experimental design that excluded the artifacts.

The most common artifact is a result of magnetostriction, in which the length of a magnetic wire changes length in a magnetic field. Figure 2 illustrates the geometry that produced some of the sensational effects attributed to BMR. Two Ni wires are brought together with a gap of ≈ 20 μm. The gap is bridged by electrodepositing Ni in a way that forms a nanocontact with one of the Ni wires. This nanocontact is thought to have dimensions on the order of 10 nm. When a magnetic field is applied along the axis of one of the wires, a sharp increase in the electrical resistance

of the nanocontact is observed, as illustrated in the inset in Figure 2. The results were interpreted as BMR assuming that the magnetic field was magnetizing the two sides of the nanocontact in opposite directions and the resulting magnetic domain wall impeded the flow of electrons, thereby increasing the measured resistance.

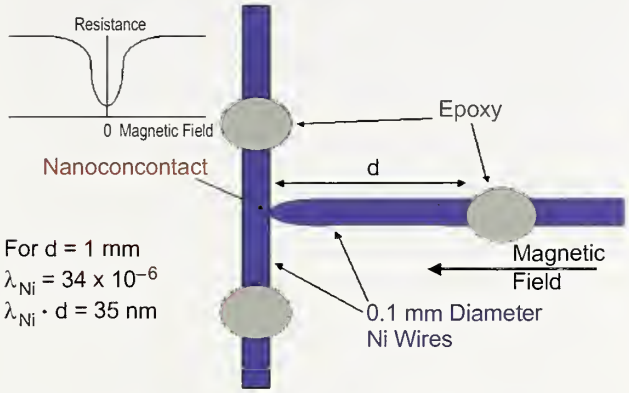

Figure 2: *An illustration of the geometry used to generate sensational apparent BMR values.*

A simpler explanation accounts for the result: the magnetic field also makes the Ni wire shorter. Using the magnetostriction constant λ for Ni and the length of free wire, the calculated shortening is 35 nm. This distance is enough to stretch and severely deform a 10 nm nanocontact, increasing its electrical resistance. In fact, in experiments at NIST using electrochemical techniques, it was possible to break and reform nanocontacts thus giving what would correspond to infinite BMR.

Further experiments at NIST using alloy wires whose composition is tailored to have a magnetostriction constant of zero showed no resistance change in a magnetic field. These wires were magnetic and should exhibit BMR if the effect was as claimed, casting further doubt on the high values reported.

Another approach investigated at NIST involved replacing the Ni wires with Ni thin films deposited on wafers. The strength of bonding between the Ni and the wafer anchored the Ni films and suppressed the shortening effect. In this geometry, the nanocontact showed no resistance change, further supporting the conclusion that the high BMR values were not true BMR.

When informed about the NIST results, one of the other labs responded with a method to produce the high BMR values in magnetic nanocontacts electrodeposited at an unusually large voltage on wafers. NIST examined the techniques and found that the unusually large deposition voltage did not produce a solid contact. Instead, the deposit consisted of loosely assembled magnetic particles. When a magnetic field was applied, a compaction of the powder could be observed in a microscope. The small magnetic particles, upon becoming magnetized in the same direction, were clumping together under the magnetostatic attraction, as illustrated in Figure 3.

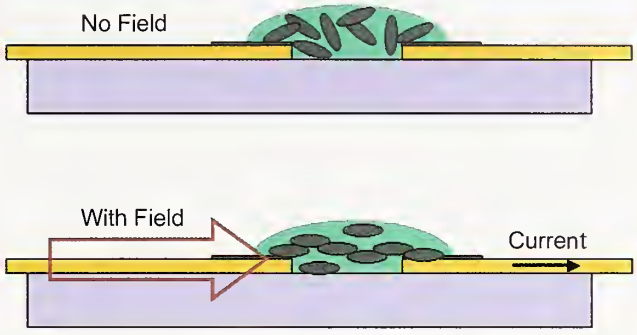

Figure 3: *An illustration of how magnetostatic forces cause magnetic particles to clump together to create conducting paths.*

In samples made this way, the no-field case was the high resistance state, and the with-field case was the low resistance state. When the particles clumped together, they created additional current-carrying paths to lower the electrical resistance. There was no evidence of anything resembling true BMR in these samples.

A preliminary report of these artifacts was presented at the March Meeting of the American Physical Society in 2003. A more comprehensive report of the work will be presented at the Magnetism & Magnetic Materials Conference in January 2004.

Experiments are continuing at NIST to put BMR on a firm scientific foundation. Although a conclusive answer is not available at this point, the results, so far, suggest that there may be a small BMR effect but not one that is large enough to be of great interest to the magnetic-sensor community. NIST's work on this topic is likely to be completed early in FY04.

"The technical challenges facing the data storage industry in the next 10 years are so broad and so deep that the industry cannot do it alone. We need researchers like you here at NIST to help us."

Dr. Sining Mao
Senior Manager, Recording Heads Division, Seagate Technology

For More Information on this Topic

E. Svedberg (Seagate); N. Garcia (CSIC, Madrid); H. Chopra (SUNY-Buffalo); R. McMichael, T. Moffat, J. Mallett (Metallurgy Division, NIST); M. Stiles (Electron and Optical Physics Division, NIST); C. Powell (Surface and Microanalysis Science Division, NIST)

Modeling Dynamics, Damping and Defects for Perpendicular Magnetic Recording Media

In its accelerating march toward ever higher recording densities, the hard disk drive industry is moving toward perpendicular recording, where the magnetization of the written bits is directed perpendicular to the disk surface. One of the metrology needs generated by the shift to perpendicular recording is the characterization of inhomogeneity in the media. This article describes our development of models that enable measurement of inhomogeneity in perpendicular media by ferromagnetic resonance.

Robert D. McMichael

One of the growing metrology needs of the hard drive industry is the ability to characterize the new generation of perpendicular recording media, where the information is stored as magnetic bits magnetized perpendicular to the disk surface. To store these bits, it is desirable to have media with small, nearly decoupled grains with strong, uniform anisotropy and easy axes directed along the disk normal. Typical grain sizes in the new media are approximately 10 nm.

Characterization of the average properties of perpendicular media is routinely accomplished by magnetometry. However, there is a significant need for information about the inhomogeneity of perpendicular media, particularly the angular easy axis distribution and the distribution of anisotropy fields. Inhomogeneity of the media impacts the bit writing process, analysis of bit stability, and media noise in the read process.

Information about the dispersion of the crystallographic axes can be obtained from x-ray diffraction, but magnetic coupling may force two crystallographically distinct grains to behave as a single magnetic grain, so a purely magnetic measurement of the dispersion angle would be more closely related to the performance of the media.

For variations in the anisotropy field, the only estimates currently available are based on TEM compositional analysis coupled with anisotropy studies on bulk materials. Here again, a direct, purely magnetic measurement would give a clearer indication of the magnetic performance of the media.

The new perpendicular media, with aligned anisotropy axes, is much better suited to ferromagnetic resonance measurements than longitudinal media. Ferromagnetic resonance is a peak in the transverse susceptibility at a frequency that corresponds to precession of the magnetization about its equilibrium orientation. The width of the ferromagnetic resonance peak, or "line width," is the combined effect of damping and inhomogeneity. While there are well-established models for damping, better models of inhomogeneity were needed for interpretation of line width data.

Through our modeling the dynamics of inhomogeneous films, we have laid the theoretical support needed for interpretation of line width data to obtain inhomogeneity information on magnetic thin films.

Previously, there were two known models of ferromagnetic resonance line broadening by inhomogeneity: the "local resonance" model and the "two-magnon" model. The local resonance model assumes that interactions are not important, and the line width is therefore a direct measure of the inhomogeneity strength. The "two-magnon" model includes interactions but, because it is a result of perturbation theory, is limited to weak inhomogeneity. The two-magnon linewidth depends quadratically on the inhomogeneity strength. The models give very different results, but both models have been successfully used to describe separate sets of linewidth data.

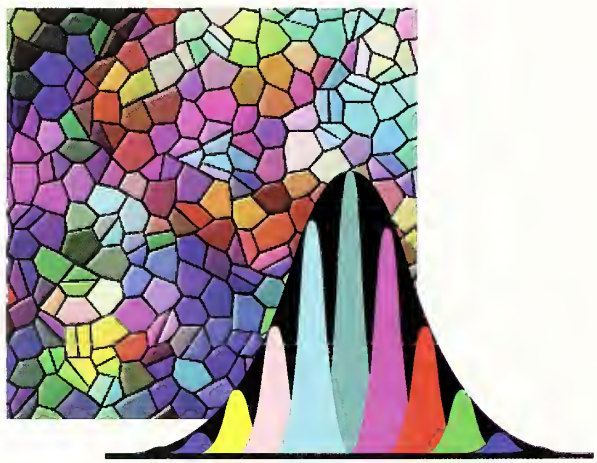

Figure 1: *In the absence of interactions, inhomogeneity leads to local resonances at a distribution of frequencies, leading to a broadened resonance line. Interactions cause narrowing of the envelope peak described by the two-magnon model.*

To understand the relationship between the local resonance and two-magnon models of line width, we modeled a series of inhomogeneous films with different grain sizes and different levels of inhomogeneity, and we computed the eigenmodes of the magnetization

motion (Figure 1). We found that the behavior of the magnetization dynamics depends on the relative strengths of the interactions and the inhomogeneity. For a uniform film, the eigenmodes are spin waves ("magnons" in quantum mechanics), and inhomogeneities or strong interactions cause mixing of the spin wave modes in agreement with the two magnon model. For strong inhomogeneities relative to interactions, the dynamics were localized on individual grains in agreement with the local resonance model. These results are summarized in Figure 2, where small grain sizes correspond to strong intergranular interactions, and large grains correspond to weak interactions. These results unify the local resonance and two-magnon models.

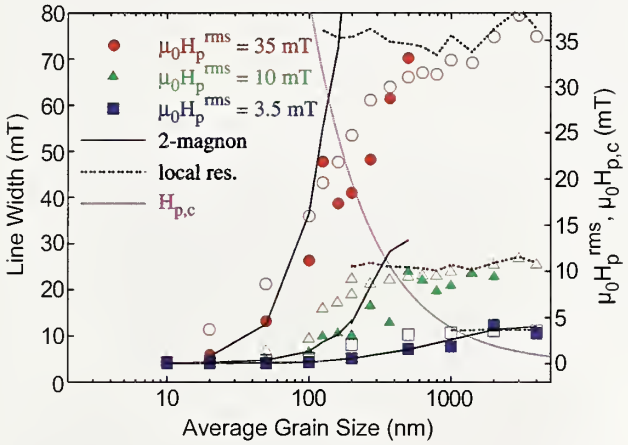

Figure 2: *Line widths as a function of grain size in a Permalloy film calculated by eigenmode analysis for three random field strengths H_p. (Open and closed symbols are for two methods of computing line width from the eigenmode spectrum.) The line width transitions smoothly from the local resonance model for large grains (weak interactions) to the two-magnon model when grains are small. The pink line indicates where interactions and inhomogeneity are roughly equal.*

The full eigenmode analysis takes a significant amount of computation time, making it a poorly suited technique for data fitting. However, the results in Figure 2 suggest a simple first approximation; for a given combination of microstructure and inhomogeneity, the lesser of the two-magnon model and the local resonance model is likely to be valid, except in the range where they are similar.

Figures 3 and 4 show two-magnon and local resonance line width calculations for perpendicular media with thickness 15 nm and grain size 10 nm with an average anisotropy field of 1.4 T (14 kOe). In these figures, the top diagram portrays the local resonance result, the green curve is the two-magnon model with dipolar interactions only, and the blue and pink curves are for fractional and full exchange coupling. For the given inhomogeneity strengths, the two magnon model results are expected to be a good approximation to the line width, but for larger values of inhomogeneity, the two magnon results will exceed the local resonance values and the local resonance results would be valid.

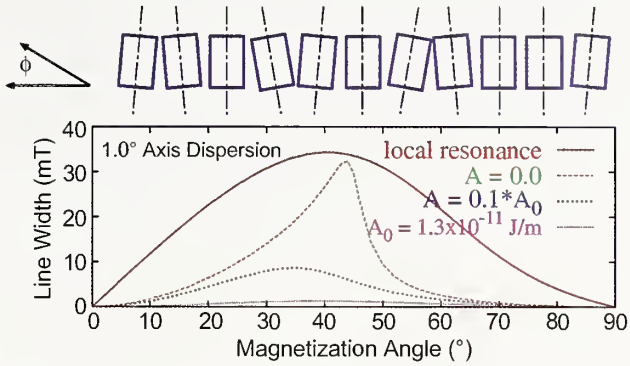

Figure 3: *Local resonance and two-magnon line widths resulting from tilting of the easy axis directions in perpendicular recording media with 10 nm grains. Two magnon results are calculated for three values of exchange coupling.*

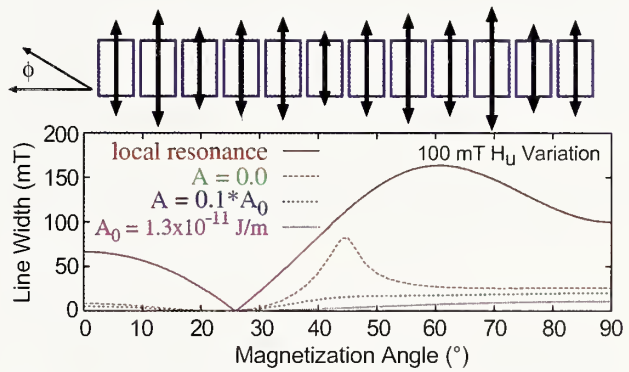

Figure 4: *Local resonance and two-magnon line widths resulting from anisotropy variations in perpendicular recording media with 10 nm grains. Two magnon results are calculated for three values of exchange coupling.*

These results show that the ferromagnetic resonance line width can be a sensitive probe of inhomogeneity in perpendicular recording media with the ability to differentiate damping, c-axis dispersion, and anisotropy variations. For weak inhomogeneity, the two-magnon model becomes valid, and the line width can also provide information about exchange coupling.

A ferromagnetic resonance apparatus with the frequency and field ranges necessary to measure perpendicular media is in the design phase.

For More Information on this Topic

R.D. McMichael, W.F. Egelhoff, Jr. (Metallurgy Division, NIST)

R.D. McMichael, D.J. Twisselmann, and A. Kunz. *Phys. Rev. Lett.*, **90**, Art. No. 227601 (2003).

Nanoscale Measurement of the Amount of Complex Hydrocarbon Molecules on Magnetic Hard Disks

The requirement for protection in the head-disk interface is rising. In order to reach 1 Terabit/in^2 areal density and double the data transfer rate, the spacing between the head and disk is shrinking to 3.5 nm at a flying speed approaching 40 m/s. Occasional contacts will test the shear strength of the molecular layer on top of the carbon overcoat. Current lubricant molecules are alcohol-functionalized perfluoropolyether which are inert and oxidatively resistant but lack solubility and surface bonding strength. Alternative molecules such as multiply alkylated cyclopentanes are being considered to improve protection. In order for any alternate molecules to be used, the average molecular thickness on a hard disk surface needs to be measured accurately at 10Å ± 1Å. We have developed a unique master calibration technique that, for the first time, is able to accurately determine the average molecular thickness of a complex hydrocarbon mixture on magnetic hard disks.

Richard Gates, Charles Ying, and Stephen Hsu

The Information Storage Industry Consortium (INSIC) has set a goal of reaching 1Tbit/in^2 areal density by 2006 with a concurrent increase in data transfer rate approaching 100 Gbit/s. This translates to an extraordinarily ambitious technical goal of a 10-fold increase in capacity in four years. To reach that goal, the flight height and the carbon overcoat thickness need to be reduced to 3.5 nm and 1 nm respectively. Since the disk is protected by the thickness of the carbon overcoat and 10Å of lubricant molecules, alternative carbons and lubricant molecules are needed to provide the same degree of protection with one-fifth the amount of lubricant and overcoat.

Under the proposed new design, head-disk interface contacts are inevitable due to reduced flight height, waviness of the disk, and rotational wobble. One of the key characteristics that has been identified for protective molecules is the adhesive strength to resist high shearing action. A typical solution in this case would be to add strongly surface-bonding molecules to the lubricant as additives. The current disk lubricant, a functionalized perfluoroalkyl ether, has limited solubility. Therefore, hydrocarbon molecules with extremely low volatility characteristics are needed. Multiply alkylated cyclopentane is one such molecule.

Current industrial practice of measuring the thickness of perfluoroalkyl ether on a hard disk surface (tip to valley distance from 15 Å to 25 Å) relies on a cross calibration between fourier transform infrared spectroscopy (FTIR) and x-ray photoelectron spectroscopy (XPS) on CF2 bonds which is symmetrical and sharp. For complex hydrocarbons, there are multiple peaks interrelated at different frequencies, and there is no established technique for such measurement.

The measurement of "average film thickness" needs to be defined. The lubricant molecules are a complex mixture of isomers with different molecular weights. The surface is atomically rough, and the coverage is below the full "monolayer" level. Nano- and microscale aggregations undoubtedly take place, and the distribution of molecules across the surface hills and valleys is not known. Recent data from UC Davis tend to support this observation. High-frequency modulation atomic force microscopy (AFM) was used to image the surface, and from these data, elasticity information can be extracted. Figure 1 relates the topographic image with elasticity of a hydrocarbon covered hard disk surface. The bottoms of the valleys show higher hardness suggesting that the hydrocarbon molecules do not reside at the bottom of the valleys.

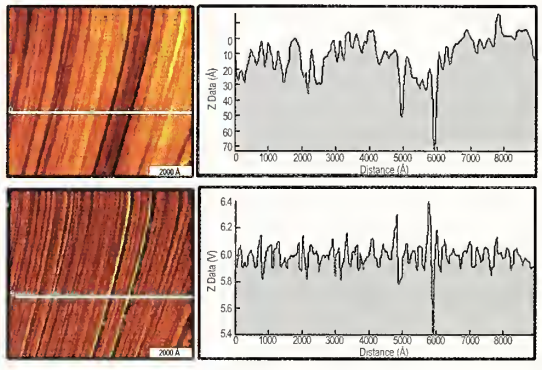

Figure 1: *AFM topographic images and elasticity data.*

Detection and measurement of a one nanometer thick complex molecular layer on a rough surface taxes the detection limits of analytical instrumentation. We first used FTIR and a modified XPS technique. The modified XPS technique scanned the surface twice: once without lubricant coverage and once with lubricant coverage. The decrease of x-ray photoelectron signal intensity from the molecule coverage was used to estimate film thickness. Unfortunately, the carbon overcoat thickness was found to vary along the radial direction of the disk. Depending on the specific batch of disks tested, the variation could be as much as 5 %–10 % from the inside radius to the outer edge of the disk. Hence, this measurement technique is insufficient to measure the "molecular thickness" as required by industry to control the process.

We tried various techniques such as AFM scratching, ellipsometry, and x-ray reflectivity (XRR). The latter technique has difficulty with surface roughness and the fact that the average film thickness is below the peak-to-valley distance. For AFM, the molecules wet the tip. Ellipsometry data at this range have large scatter. So the conclusion is there is no acceptable technique to measure such "film thickness" of a complex hydrocarbon molecular mixture to the industrial specification of 10 Å ± 1 Å.

To develop a solution to this industrially important issue, we created a master calibration sample approach. Basically we deposit a known (gravimetrically) solution on a disk with a barrier film surrounding a known area and allow the solvent to evaporate under controlled conditions. The resulting "film thickness" can then be used to calibrate various instruments. The challenges are uniform distribution of molecules across the area, containment of fluid, meniscus forces, and evaporation rate control.

Figure 2: *Confined lubricant solution on a hard disk.*

Initially, this approach was attempted with liquid–phase samples; however, under these conditions, evaporation and meniscus forces lead to uncontrolled lubricant film uniformity. This was solved by evaporating the solvent from the mixture while it is in the solid state. The solution is placed within the barrier (Figure 2) and rapidly frozen using liquid nitrogen. Then the solvent is slowly removed by evaporation into an inert gas at –10 °C.

By controlled slow evaporation of solvent directly from a solid frozen state, we avoid the meniscus and surface tension forces which tend to create non-uniformity of the liquid mass. A pseudo "sublimation" process is created. In this way, uniform signal detection by FTIR confirms that the distribution of molecules across the area is less than 5 % at less than full monolayer coverage. Using this new technique, a series of "film thickness calibration standards" was created (see Figure 3).

A series of three master calibration samples was prepared and submitted for XPS photoelectron attenuation analysis. The very small variation of XPS intensity across the disk surface indicated that film uniformity was quite good, varying by less than 5 %. A correlation plot of XPS estimated thickness versus master calibration target thickness (Figure 4) yielded a straight line, but the slope was not 1.0 (referenced in red). This indicates that the XPS attenuation technique has an inherent bias due to inaccurate assumptions in the model used in the analysis. The observation that the slope of the XPS versus target thickness correlation is 0.6 indicates that the initial XPS attenuation technique was underestimating the hydrocarbon film thickness by about 40 %. The effect has been attributed to the difference in density between the hydrocarbon and carbon overcoat. Utilizing this information, the model was refined to accommodate this effect.

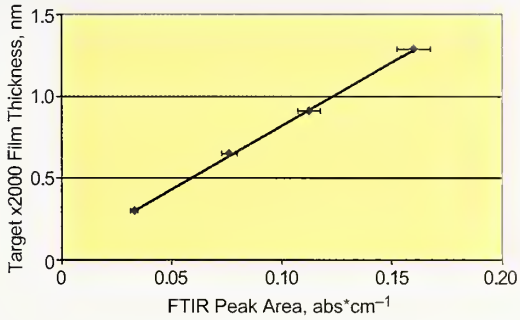

Figure 3: *Calibration curve relating FTIR signal to known hydrocarbon film thickness determined gravimetrically. Error bars are one standard deviation.*

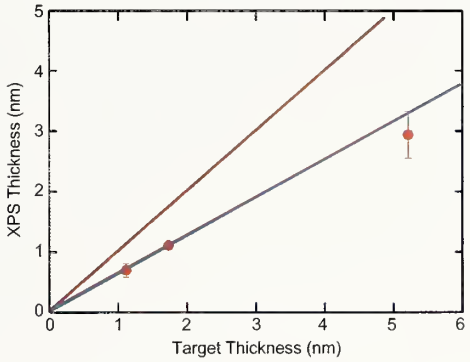

Figure 4: *XPS signal calibration for known hydrocarbon film thickness. Error bars are one standard deviation.*

A calibration method for nanometer-scale complex hydrocarbon films on an engineering surface has been developed. The method is based on gravimetric solution preparations and utilizes a novel freeze-evaporation technique to extract the carrier solvent while leaving a uniform film of complex hydrocarbon on the surface. The method can be applied to a variety of surfaces and offers the potential for calibrating many different analytical techniques for their ability to measure thickness of complex hydrocarbons.

For More Information on this Topic

S. Hsu (Ceramics Division, NIST)

Projects in Materials for Micro- and Optoelectronics

Characterization of Porous Low-k Dielectric Constant Thin Films

NIST is working to provide the semiconductor industry with unique on-wafer measurements of the physical and structural properties of porous thin films important to their use as low-k dielectric materials. The methodology utilizes several complementary experimental techniques to measure the average pore and matrix morphology. Pore size distributions are calculated by x-ray reflectivity and neutron scattering porosimetry. Methods have been developed to measure closed pore content and matrix morphology in films having complex structures with any morphological type.

Barry J. Bauer

The next generation of integrated circuits will require feature sizes that demand new low-k interlayer dielectric materials. To address problems with power consumption, signal propagation delays, and crosstalk between interconnects, dielectric constants need to significantly decrease. The primary approach to low-k dielectric materials is the introduction of nanometer scale pores into a solid film to lower its effective dielectric constant. While these modifications change the dielectric constant favorably, other important parameters such as physical strength and barrier properties will also change, often in an unfavorable way. Characterization of the pore structure is crucial to the development of new dielectric materials, and new measurement methods are necessary.

NIST provides low-k characterization using a combination of small angle neutron scattering (SANS), high-resolution x-ray reflectivity (HRXR), and ion scattering techniques. These measurements are performed directly on films supported on silicon substrates so that processing effects can be investigated. New methods are required, however, to provide more detailed information necessary to complete the product development.

This year, we have continued our efforts on characterization of current industrially relevant materials primarily through International SEMATECH, a consortium of microelectronics companies, but also through other industrial partners. The technological roadmap has progressed to a decision point at which materials will be chosen for the next step: the integration of low-k materials into complex circuits. NIST has provided a considerable body of data to make this choice possible.

To advance the measurement capabilities, we have perfected new techniques for more thorough and accurate film characterization. Work has been completed on a small angle neutron scattering (SANS) technique and instrumentation for measurement of films that have been infused by mixtures of normal solvent and the same solvent in which the hydrogens have been replaced by deuterium (see Figure 1). The match point measures where the neutron contrast matches that of the wall material. By filling the open pores with contrast match fluids, SANS reveals the closed pore content and size. The relative open and closed pore content is becoming increasingly important to low-k applications. The same instrumentation has been used to determine the uniformity of the wall material with respect to remnants of porogen that remain after incomplete thermal treatment.

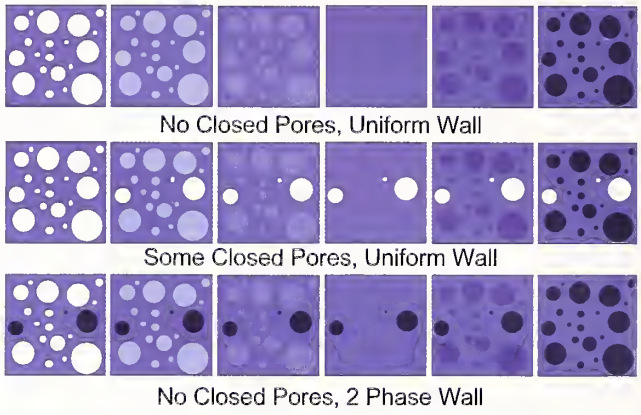

Figure 1: *Schematic illustrating different sample characteristics that can be distinguished using SANS contrast match techniques.*

This year, several projects have been completed in response to industry needs. SANS has been used to measure the size and volume fraction limits of damaging "killer" pores in collaboration with Dow Chemical. X-ray reflectivity has been used to measure the effects of plasma treatment on film density profiles in collaboration with Axcelis. The pore formation process was quantified to connect pore size distributions of the formed pores with pore size distributions of the porogen used to generate the pores in collaboration with Dow Chemical. A new method of calculating pore size distributions from SANS data has been demonstrated.

Contributors and Collaborators

H. Lee, R. Hedden, C. Soles, M. Silverstein, D. Liu, W. Wu (Polymers Division, NIST); C. Glinka (Center for Neutron Research, NIST); J. Iacoponi, Y. Liu (International SEMATECH); B. Landes (Dow Chemical); C. Waldfried, O. Escorcia (Axcelis); B. Hwang, W. Gray (Dow Corning)

Polymer Photoresists for Next-Generation Nanolithography

Photolithography, the process used to fabricate integrated circuits, is the key enabler and driver for the microelectronics industry. As lithographic feature sizes decrease to the sub 100 nm length scale, significant challenges arise because both the image resolution and the thickness of the imaging layer approach the macromolecular dimensions characteristic of the polymers used in the photoresist film. Unique high-spatial resolution measurements are developed to reveal limits on materials and processes that challenge the development of photoresists for next generation sub-100 nm lithography.

Eric K. Lin

Photolithography is the driving technology used by the microelectronics industry to fabricate integrated circuits with ever decreasing sizes. In addition, this fabrication technology is rapidly being adopted in emerging areas in optoelectronics and biotechnology requiring the rapid creation of nanoscale structures. In this process, a designed pattern is transferred to the silicon substrate by altering the solubility of areas of a polymeric photoresist thin film through an acid catalyzed deprotection reaction after exposure to radiation through a mask. To fabricate smaller features, next generation photolithography will be processed with wavelengths of light requiring photoresist films less than 100 nm thick and dimensional control to within 2 nm. Material, interface, and transport issues arise when fabricating structures over these length scales. To date, the materials and processes needed to fabricate sub-100 nm features have not been selected because of increasingly challenging technical issues.

To advance this key fabrication technology, we work closely with industrial collaborators to develop and apply high-spatial resolution and chemically specific measurements to understand changes in material properties, interfacial behavior, and process kinetics at nanometer scales that can significantly affect the patterning process.

This year, we have applied and enhanced unique measurement methods to provide structural measurement of fabricated nanoscale structures and new insight and detail into the complex physico–chemical processes used in advanced chemically amplified photoresists. These methods include x-ray and neutron reflectivity (XR, NR), small angle neutron and x-ray scattering (SANS, SAXS), incoherent neutron scattering (INS), near-edge x-ray absorption fine structure spectroscopy (NEXAFS), combinatorial methods, nuclear magnetic resonance (NMR), quartz crystal microbalance (QCM), Brillouin light scattering (BLS), fluorescence correlation spectroscopy (FCS), and atomic force microscopy (AFM).

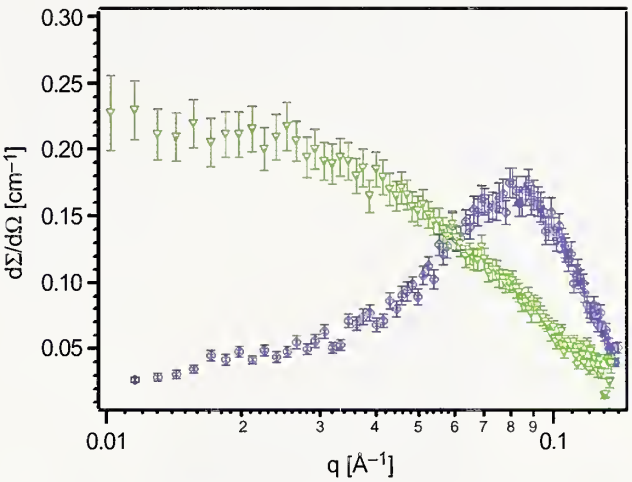

Figure 1: *SANS data from a model photoresist polymer in organic solvent (green) and aqueous base developer (blue). The peak in the blue curve shows electrostatic effects on the chain conformation not present in the organic solvent.*

Accomplishments for this past year include: advancements in critical dimension measurement with SAXS (see highlight); identification of polyelectrolyte effects in photoresist dissolution (see Figure 1) and their impact on the resolution of the structure; direct measurement of surface segregation of a fluoropolymer blend component to the surface of the resist film impacting its dissolution behavior; identification of key anti-reflection coating (ARC) components responsible for profile control problems at the ARC-resist interface; correlation of polymer local dynamics with transport of water and photoacid diffusion showing the effect of confinement on resist processing parameters; and the first measurement of the shape and form of the 3-D deprotection volume from the reaction-diffusion of dispersed photoacids, a key variable in model predictions of the roughness or resolution of photoresists.

Contributors and Collaborators

C. Soles, W. Wu, R. Jones, V. Prabhu, C. Wang, E. Jablonski, B. Vogt, M. Wang, N. Noda, F. Starr, P. McGuiggan, D. VanderHart, C. Chiang (Polymers Division, NIST); D. Fischer, S. Sambasivan, (Ceramics Division, NIST); S. Satija, C. Glinka (NCNR, NIST); D. Goldfarb, K. Temple, A. Mahorowala, M. Angelopoulos (IBM T.J. Watson Research Center); B. Trinque, S. Burns, C. Willson (University of Texas at Austin); R. Puligadda, Y. Wang, C. Devadoss (Brewer Science)

Dielectric Measurements of Polymer Composite Films in the Microwave Range

Polymer composite materials with enhanced electromagnetic properties have been identified by the industry as essential for advancing miniatnrization and fnnctional performance of high-speed electronics. This project develops dielectric metrology specific to the needs of the electronics industry for embedded passive materials and devices. The current focns is on the measurement of permittivity at microwave freqnencies and impedance at high AC voltages. These nnique measnrements enable the identification of the key structural attribntes that control the properties of organic resins filled with electronic modifiers.

Jan Obrzut

In recent years, a broadband technique has been developed successfully as a standard test method that enables dielectric measurements at microwave frequencies. The technique is based on the observation and theoretical analysis of the fundamental mode propagating at high frequencies in thin-film dielectrics that terminate a coaxial air-filled transmission line. This year, we applied 3D numerical simulations of the electromagnetic field to improve understanding of the measurement and enabled an extension to frequencies up to 12 GHz. The numerical simulations were used to identify and quantitatively analyze the residual inductance of the film specimens. For high-k materials with a high capacitance density, even small residual inductance can cause resonant oscillations, which leads to systematic uncertainties in the measured permittivity. Results from the numerical simulations helped formulate a closed-form expression for the input impedance of complex thin-film materials that is accurate up to 12 GHz. Broadband dielectric measurements of high-k composite materials that are of interest to bio- and nanotechnology and microelectronics are now possible and at previously inaccessible frequencies.

In partnership with IPC, we initiated a standard test method development and chaired the IPC-D-37d test method subcommittee for Embedded Passive Devices. We guided the design of the test protocol and made arrangements with co-sponsoring member companies for round robin evaluation. The committee forum has recognized NIST for being the leading laboratory in the characterization of high-k materials and for effectively addressing the standardization needs of the emerging electronic packaging technologies.

A suitable testing procedure has been demonstrated for unambiguous determination of dielectric properties at high AC voltages. The specimen voltage and current are determined as complex quantities from the corresponding time resolved voltage waves. The new testing procedure represents a compatible extension of the existing standard test method but is better suited for capacitive and/or resistive thin-film materials. It was found that embedded passive materials do not exhibit a constant impedance characteristic, as in conventional dielectrics, but, rather, their impedance sharply decreases with increasing voltage. This change in impedance could not be detected by the conventional test methods.

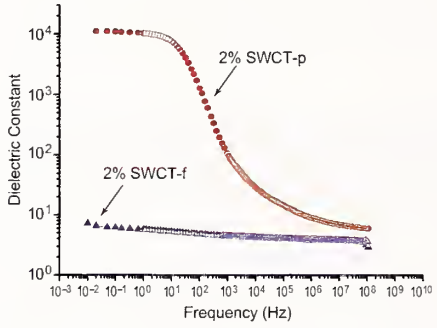

Figure 1: *Dielectric properties as a function of frequency for normal and functionalized nanotubes in PMMA.*

Our unique capability to measure the dielectric relaxation time in the sub-nanosecond regime and the relaxation strength for a wide range of dielectric permittivity values is used to quantify dispersion, alignment, and structure in nanostructured composite materials. Figure 1 shows the dielectric properties of two composites containing a 2 % mass fraction of single wall carbon nanotubes (SWCT) dispersed in poly(methyl methacrylate) (PMMA). The SWNTs were surface-modified to affect dispersion and coupling.

Functionalized nanotubes, SWCT-f, showed an increase in the dielectric constant and can be rationalized based on the log mixing-rule law. In contrast, adding purified SWCT (SWCT-p) to PMMA increases the dielectric constant by 3 orders of magnitude. Small angle neutron scattering data indicate that this formulation exhibits a preferential coupling within the dispersed phase where a small amount of modifier causes a large enhancement in the properties of the mix. These results can be utilized in advanced engineering of plastic composites to obtain enhanced structural, optical, thermal, and electronic properties.

Contributors and Collaborators

A. Anopchenko, K. Kano, (Polymers Division, NIST); B. Rust (Mathematical and Computational Sciences, NIST); R. Croswell (Motorola); D. McGregor (DuPont); H. Wang (Michigan Technical University); K. Winey, J. Fischer (University of Pennsylvania)

Electronic Packaging and Components: Packaging Reliability

We are developing methods to examine materials and interfaces in electronic packaging applications and elucidate the damage mechanisms. Our current focus is on advanced packaging structure, embedded passive materials, and thin metal films using thermal microscopy to measure heat flow and thermal properties on increasingly smaller size scales.

Andrew Slifka

Technical Description

The microelectronics industry is moving toward higher density components of smaller size using less expensive materials. One move in this direction is the advent of embedded and integrated passive components in printed circuit boards (PCBs). These organic-based PCBs can have a large coefficient of thermal expansion (CTE) in comparison with many materials found in proximity. This CTE mismatch can reduce the reliability of electronic packaging systems by causing localized stress.

In addition, thermal issues are becoming increasingly important as size decreases and functionality increases. Applications in the microelectronics industry would include heat removal and interconnects.

We are investigating the damage induced from CTE mismatches between organic materials, organics and metals, and organics and ceramics to determine the initiation of damage and the ultimate failure mechanisms in these systems. Thermal microscopy is used to measure changes in interfacial thermal resistance in order to detect the onset of thermomechanical damage at that interface before any surface manifestation is visible.

We are developing new measurement methods using scanned-probe microscopy (SPM) in order to characterize packages and measure thermal conductivity of thin films at increasingly smaller size scales.

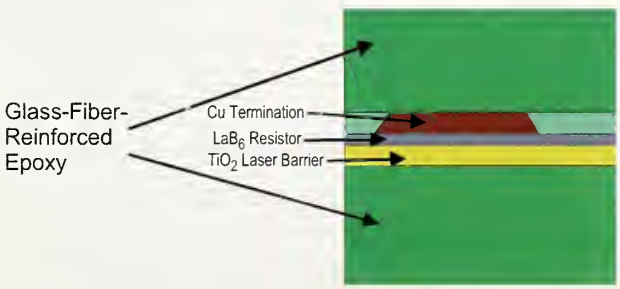

Figure 1: *Schematic of an industrial embedded resistor sample.*

Accomplishments

We are continuing measurements on industrial embedded resistors (Figure 1), making comparative measurements between the SPM thermal system and the IR microscope. We have purchased a new IR microscope that has better accuracy than our old system, but the measurement protocol has remained the same.

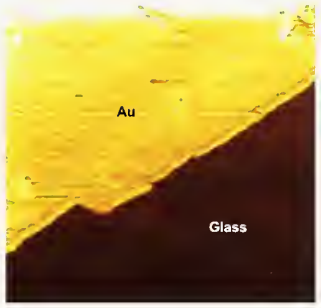

Figure 2: *Thermal SPM image of a 150 nm gold film on glass.*

We have begun measurements of films using thermal SPM in a mode that uses the probe tip as a point-source heater, which is kept at a constant temperature because the probe tip is a resistive element in a Wheatstone bridge circuit. Heat from the probe tip is conducted into the sample, and as a film becomes thinner, heat loss from the probe tip is due more to the substrate rather than to the film. Dr. K. Cole has developed a theory that accounts for this film effect. We have been making preliminary measurements using various thicknesses of gold films on different substrates and comparing the theory to our measurements. Figure 2 shows a 150 nm thick gold film on a glass substrate. We will add interfacial modifications to the samples and to the theory in order to make the measurement method applicable to films used in industry. In addition, we have been using this measurement method on diamond-like-carbon (DLC) films. These industrial films are made from a polymer precursor, which allows easy and inexpensive coating onto various substrates. The thermal conductivities of these films, and how they compare to conventionally processed DLC films, is being investigated.

Contributors and Collaborators

John Felten (DuPont Technologies Research, Triangle Park, NC); Richard Snogren (SAS Circuits, Inc., Littleton, CO); Dr. Kevin Cole (University of Nebraska); Charles Partee (Cenymer Corporation, Longmont, CO)

Electronic Packaging and Components: Acoustic Loss in Piezoelectric Crystals

Langasite, langatate, and langanite are piezoelectric materials that show promise of providing characteristics superior to quartz for a variety of electronic oscillator and filter applications. The acoustic loss of these crystals is being studied in our laboratory to identify and quantify the dominant physical mechanisms that degrade performance. Through this work, the project seeks to provide guidance to other researchers in minimizing the acoustic loss and determining the most promising material to pursue among this group of compounds.

Ward Johnson and Sudook Kim

Technical Description

Langasite ($La_3Ga_5SiO_{14}$) and its isomorphs, such as langatate ($La_3Ga_{5.5}Ta_{0.5}O_{14}$) and langanite ($La_3Ga_{5.5}Nb_{0.5}O_{14}$), have attracted significant attention in recent years as materials for improved electronic oscillators and filters. The advantages of these crystals over quartz include lower acceleration sensitivity; higher piezoelectric coupling, which enables devices to be made smaller; and higher Q, which reduces phase noise and enables higher-frequency operation. These materials also have no phase transition below the melting point, which allows devices to be operated at high temperatures and provides the potential of producing large-diameter wafers (for surface-acoustic-wave devices) more easily and cheaply than with quartz.

The acoustic loss Q^{-1} in langasite, langatate, and langanite at ambient temperatures has been found to vary significantly between specimens, even when taken from the same crystal boule. This research project has provided information on the physical sources of these variations in each of these materials through measurements of Q^{-1} as a function of temperature T and frequency.

Accomplishments

Measurements of the acoustic loss of trapped resonant modes of Y-cut plano-convex disks of langasite, langatate, and langanite were performed between 100 K to 740 K. Figure 1 shows an example of measurements on langasite with the minimum value of measured Q^{-1} ($Q^{-1}{}_{min}$) subtracted. $Q^{-1}{}_{min}$ occurs near the lowest measured temperature, 100 K, and is ~1 x 10^{-6} at each frequency. Anelastic relaxation peaks appear on top of a background that increases with an approximate Arrhenius temperature dependence. These features are similar to those observed in langatate and langanite.

Activation energies determined from the peak positions of the lowest-temperature relaxations in langasite and langatate (assuming a Debye form) are 0.34 ± 0.05 eV and 0.25 ± 0.03 eV, respectively, which are typical of point-defect relaxations. The lower value of the activation energy in langatate causes the peak to appear at lower temperatures. This difference may provide an explanation for results in the literature that show the room-temperature Q to be generally higher in langatate than in similarly grown and fabricated langasite.

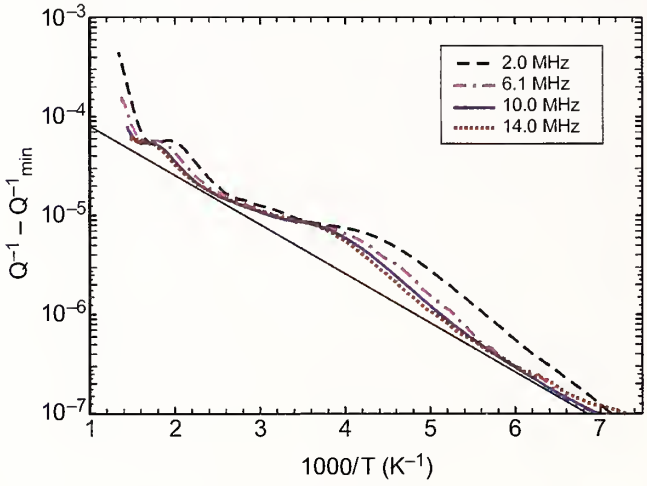

Figure 1: *Q^{-1} versus 1000/T of a langasite specimen with the minimum Q^{-1} at each frequency ($Q^{-1}{}_{min}$) subtracted.*

The ultimate limit of the Q in piezoelectric crystals is determined by phonon–phonon interactions (Akhieser mechanism), which produce a loss that is proportional to frequency and weakly dependent on temperature above ambient temperatures. The results shown in Figure 1 and similar results for langatate and langanite show no evidence for such a contribution to Q^{-1}. The lack of an obvious intrinsic contribution suggests that the maximum attainable Q of these materials may be significantly higher than values reported thus far in the literature.

Contributors and Collaborators

Robert Smythe (Piezotechnology, Inc.); Satoshi Uda (Tohoku University)

(This project was partially supported by a grant from the U.S. Army Research Laboratory.)

Micrometer-Scale Reliability: Mechanical Behavior of Thin Films

Measurement methods and materials data are needed for the design of interconnect structures in high-performance integrated circuits. These micro- and nanometer-scale thin films are formed by physical vapor deposition; their microstructures, and hence their mechanical properties, are quite different from those of bulk materials of the same chemical composition. While the general principles of conventional mechanical testing are applicable to thin films, special test equipment and techniques are required. The ultimate goal of this project is to characterize the exact materials used in IC fabrication, at their proper size scale.

David T. Read

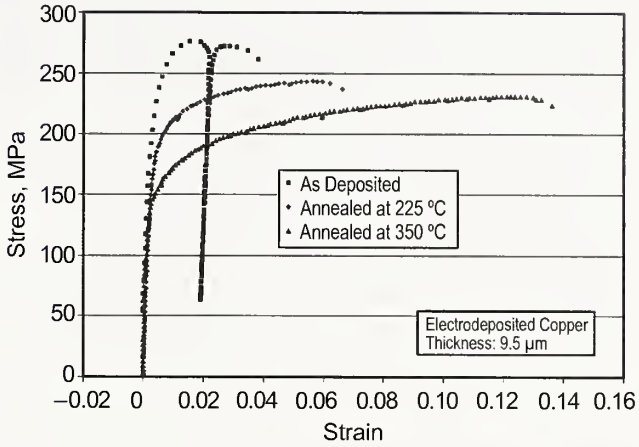

Figure 1: *Stress–strain curves for thick electrodeposited copper.*

Interconnect structures in advanced integrated circuits carry power, signals, and heat from the transistors to the outside environment. These structures consist of multiple layers of thin films of conductors and dielectrics with barrier and adhesive layers. These thin films are an essential component of all advanced electronic devices, and similar materials are used in a variety of other applications, such as reflective coatings. Industry is aggressively pressing new materials into service, reducing the size scale of the structures, and requiring more functionality, including mechanical functionality, from all components of their structures. Design of reliable structures relies on quantitative numerical modeling, which requires accurate material property data. Because the films are formed by physical vapor deposition, their microstructures, and hence their mechanical properties, are quite different from those of bulk materials of the same chemical composition. Techniques for measuring the mechanical behavior of thin films are being developed and applied.

The objectives of this project are:

- To develop experimental techniques to measure the mechanical properties of thin films, in specimens fabricated and sized like materials used in actual commercial devices;
- To relate the mechanical behavior of thin films to microstructure;
- To extend test techniques from their present level (1 µm thick, 10 µm wide) to smaller specimens that are similar in size to the conductive traces used in contemporary VLSI circuits (widths of 0.1 to 1 µm).

In previous years, we reported properties of aluminum, polyimide, and polysilicon films at room temperature, including the special techniques developed to produce and test the specimens. This year, we obtained copper films from an industry collaborator and also developed procedures to electrodeposit copper films in-house for comparison. The thicknesses ranged from 1 to 10 micrometers thick. Photolithography of copper is a challenge which industry has worked around by implementing the damascene process. We used photolithography to make specimens up to 20 micrometers wide from the thicker copper electrodeposits, and our standard 10-micrometer-wide specimens from the thinner films, but making testable specimens was a big part of the effort of this project.

As part of this collaboration, nanoindentation data were also obtained on one series of films. While it is clear that nanoindentation can characterize the general mechanical robustness of a material, the quantitative correlation between nanoindentation data and microtensile data has not been established. In this study, our collaborators performed nanoindentation tests and applied the relatively new procedure of measuring the size of the plastic zone around the indentation with an atomic force microscope (AFM). The yield strengths that they obtained matched up well with the microtensile data shown here.

Contributors and Collaborators

Y.-W. Cheng, J.D. McColskey, R.R. Keller, R. Geiss (Materials Reliability Division, NIST); R. Emery, F. Hua, T. Scherban (Intel)

Micrometer-Scale Reliability: Stress Voiding and Electromigration

Reliability of the small-scale materials that make up advanced chip-level interconnect systems is not readily predictable by extrapolating known behavior for larger scale materials. We concentrate on studies of the failure mechanisms associated with thermal and electrical stressing, which limit performance in a variety of structures with constrained dimensions. Emphasis is placed on the roles of localized stress and variations in microstructure. We perform basic studies on aluminum-based interconnects, as well as measurements on advanced sub-100 nm systems comprising copper or silver.

Robert R. Keller and Roy H. Geiss

Stress voiding (SV) and electromigration (EM) remain as two primary reliability-limiting phenomena in chip-level interconnects, especially with the largely unexplored behaviors of copper/low-k systems. Both phenomena depend sensitively on the mechanical behavior of the metal and dielectric. Failures take the form of surface topography development and void formation, and can lead to open or short circuits. Our earlier work demonstrated that even small variations in localized microstructure can have large impacts on these types of failure.

This year, we have made significant progress in documenting the damage processes leading to failure from low-frequency, high-current-density AC stressing. The tests simulate the type of thermomechanical fatigue that can occur during a device's operational lifetime, due for instance to power cycling, energy saving schemes, and to application-specific thermal fluctuations. Fatigue, in this case, takes place because of cyclic Joule heating in the metal and because of a mismatch between thermal expansion coefficients of the metal and the substrate and/or passivation. Characterization, at present, primarily takes the form of orientation mapping by electron backscatter diffraction (EBSD).

Quasi *in situ* testing of an Al-1Si line revealed an evolution of grain size and orientation during 100 Hz testing at 12 MA/cm^2, as shown in Figure 1. The sequence shows the evolution of surface roughness, grain size, and crystal orientation during five minutes of stressing. Notable is the tendency for surface slip band offsets to form in larger grains. Their severity increased in grains that showed significant growth, such as the one on the left end of the EBSD maps. Other notable observations indicated that many grains changed their orientations during stressing, primarily those that also exhibited growth. This is seen in Figure 1 by the color maps on the right, indicating changes in transverse orientation; we note that virtually every grain maintained a surface normal of (111) throughout testing. The transverse orientation changes, however, led to an increasing number of grains with higher resolved shear stresses, assuming primary loading longitudinally. Such orientation changes facilitate roughness formation by allowing more dislocation slip activity. This particular line failed in 340 seconds, with an open circuit forming several micrometers away from the region shown above.

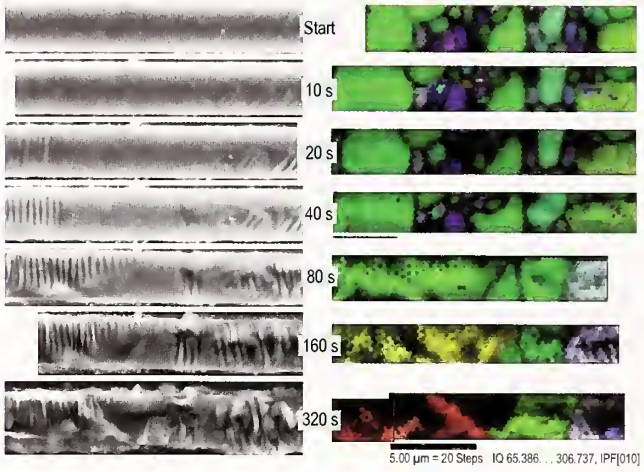

Figure 1: *SEM images and EBSD maps showing damage evolution during five minutes of severe AC stressing in Al-1Si.*

Our work on this long-term project appears to have significance in the three- to five-year timeframe for other researchers, as evidenced by a jump in non-self-citations in the peer-reviewed literature. As an example, for four papers published between 1996 and 1999, we were cited just two times within two years of publishing, but 22 times in 2001 and 2002.

Ongoing work includes more detailed TEM-based studies of the AC-induced damage. We are also measuring electrical and electromigration properties of extremely narrow lines of copper and silver fabricated by novel electrodeposition methods.

Contributors and Collaborators

Y.-W. Cheng (Materials Reliability Division, NIST); D. Josell, T. Moffat (Metallurgy Division, NIST); C. Witt (SEMATECH); R. Mönig, C. Volkert (Max–Planck–Institut für Metallforschung)

Micrometer-Scale Reliability: Bridging Length Scales

We have developed a multiscale model for nanostructures in solids. The model relates the physical processes at the interatomic level to measurable lattice distortions at the nanometer level and macroscopic stresses and strains. The model links the subnano (interatomic), nano (nanostructures), and macro length scales by integrating the powerful techniques of molecular dynamics, lattice-statics Green's function, and continuum Green's functions.

David Read and Vinod Tewary

Technical Description

Mathematical modeling is a very important tool for understanding the mechanical behavior of nanomaterials and for research and design of devices based upon nanostructures. A nanostructure needs to be modeled at the following scales: (i) the core region of the nanostructure (sub nanometer) where the nonlinear effects may be significant; (ii) the region of the host solid around the nanostructure (nanometer); and (iii) free surfaces and interfaces in the host solid (macro). A nanostructure causes lattice distortion in the host solid that manifests as strain throughout the solid. The strain is essentially a continuum-model parameter whereas the lattice distortions are discrete variables that must be calculated by using a discrete lattice theory. Hence, one needs a multiscale model that relates the discrete lattice distortions at the microscopic scale to a measurable macroscopic parameter such as strain.

Conventional models of nanostructures are based upon either the continuum theory, which is not valid close to the defect, or molecular dynamics (MD) that is CPU intensive and usually limited to small crystallites, which may introduce spurious size effects. We need a computationally efficient multiscale model that links the length scales from subnano to macro and can be used on an ordinary desktop. Such a model will be a valuable tool for research and engineering designs.

Our model is based upon the lattice-statics Green's function (LSGF) that reduces asymptotically to the continuum Green's function (CGF). However, the response of the solid containing a nanostructure is given by the defect GF that does not reduce to the CGF. The defect GF ($\mathbf{G}^*$) is related to the perfect LSGF ($\mathbf{G}$) through the Dyson integral equation:

$$\mathbf{G}^* = \mathbf{G} + \mathbf{G}\Delta\Phi\mathbf{G}^*.$$

Using the Dyson equation, we can write the response of the defect lattice as a product of an effective Kanzaki force and $\mathbf{G}$,which links the perfect LSGF and the CGF.

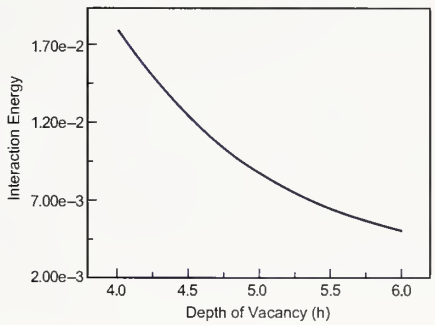

Figure 1: *Interaction energy (eV) between a vacancy and the free surface in Cu (h in units of a=1.807 Å).*

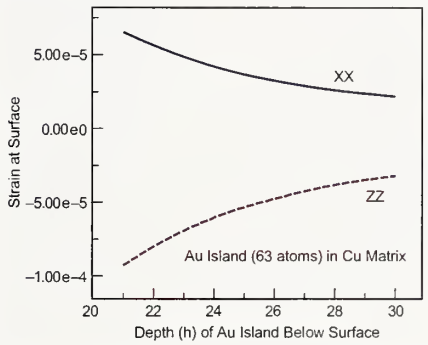

Figure 2: *Strains at the free surface due to a gold nanoisland in Cu.*

Accomplishments

We have developed a multiscale Green's-function (MSGF) method that integrates LSGF and CGF and applied it to model point defects in metals and semiconductors. This method is suitable for a weak defect such as a vacancy. For modeling nanostructures and other strong defects, we have integrated this method with modified MD in the core of the nanostructure. This integration makes our model truly multiscale by seamlessly linking length scales ranging from the subnano to the macro. Our model accounts for the nonlinear effects in the core of the nanostructure, and it provides a fast algorithm for modeling a large crystallite. It takes only a few CPU seconds to calculate the LSGF for a million-atom model on a standard 3 GHz desktop.

Contributors and Collaborators

R.R. Keller, B. Yang (Materials Reliability Division, NIST); E. Pan (Akron University)

Micrometer-Scale Reliability: Molecular Dynamics

It is widely anticipated that applications of nanomaterials will enable major advances in technology in a variety of fields, including sensors, high-strength materials, medicine, and others. Computer simulations seem to offer a path to quantitative understanding of the behavior of nanoscale materials. The form and parameters of the interatomic forces may turn out to be the most concise and useful representation of materials measurement results. Atomistic simulations are widely used to interpret nanoscale phenomena at the boundary between mechanics and chemistry and to support the plausibility of proposed devices. We are developing the capability to use molecular dynamics simulations to interpret our own measurements, and to assess the accuracy of proposed interatomic potentials.

David T. Read

Various approaches to simulating atomic interactions have been reported. The **first principles** approach uses *quantum mechanical* models of nuclei and electrons. Even though this approach typically includes only the valence electrons, it can only handle a few tens of atoms. Recently, in an innovative study, the first principles approach was used to search for new superalloys.

The **molecular mechanics** approach, widely used for organic molecules such as proteins, requires explicit assumptions about atomic bonding, specifically, a list of which atoms are bonded to which other atoms. The bonds are represented by force laws, and the configuration of complex molecules can be studied. Different force laws may be used for certain types of atoms, depending on the chemical environment. For instance, the carbon–carbon force law in diamond may be different from that in graphite.

Molecular dynamics (MD) treats atoms or molecules as particles that follow *Newton's laws* of mechanics. The particles interact with a prescribed force law, which depends only on the chemical identity of the interacting atoms. The force laws are derived empirically, and the parameters are selected by fitting to measured properties, such as the elastic constants, the vacancy energy, the energy of sublimation, phonon frequencies, and others. This approach can treat solids, liquids, or gases, and can model melting temperatures and equilibrium crystal structures.

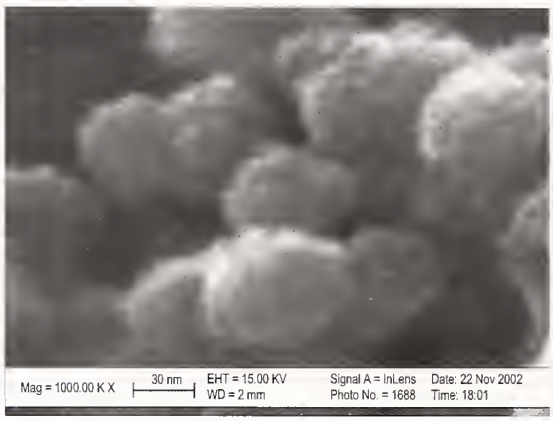

Figure 1: *Scanning electron microscope image of the surface of a copper electrodeposit at a magnification of 1 million.*

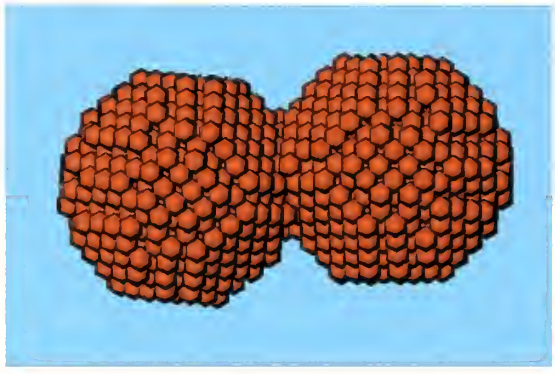

Figure 2: *MD simulation of agglomerated spheres of copper atoms, but with many fewer atoms than the actual structures.*

The many-body potential, introduced in the 1980s, provided some key triumphs of physical insight into the behavior of metals. It allowed quantitative treatment of surface reconstruction, observed in some pure metals under controlled conditions; it allowed understanding of the Cauchy inequality among the elastic constants of metals; and it allowed reasonable values of the energy of a vacancy. Starting in the latter 1980s, Tersoff introduced his potentials for modeling silicon. His innovation was to introduce the dependence of energy on bond angles into molecular dynamics. Even now, MD potentials have been introduced for only a small fraction of possible combinations of atoms. Generally, potentials are available for important and commonly used materials, but not for exotic combinations.

Contributors and Collaborators

J. Rifkin (University of Connecticut; author of MD program used)

Micrometer-Scale Reliability: Solder Reliability

Because of the environmental hazards of lead, the electronics industry is replacing lead–tin eutectic solders with lead-free solders. In doing so, they have created a need for material properties data of the new lead-free solder compositions. Efforts have been made to standardize the collection of the data and disseminate it. A test method has been developed to measure the mechanical properties that uses specimens on the same size scale as that of the solder structures used in industry.

Timothy P. Quinn

Background

Industry groups have pointed out the need for material property data for the new lead free compositions of solder which includes pooling the data that already exists and filling the critical holes in the data especially at low strain rates.

Most of the data that are available for all solders come from specimens that are very large (on the order of millimeters) compared to the solder structures themselves (on the order of hundreds of microns). As the solder structures (solder balls for flip chip packages, for example) become smaller (~150 mm), their dimensions approach the dimensions of the phases in the solder itself. The assumption of a homogeneous material used to analyze the stresses in the structure is challenged. To study this interaction, we have therefore started testing samples that are on the same size scale as current solder structures.

Accomplishments

The long history in the use of current lead-based solders means that these data sets are quite complete and widely available. The modelers and production engineers need equally complete sets of data on the various lead-free alternatives, so they can make informed decisions for their production applications. Researchers are rapidly developing corresponding data on lead-free alloys, but the data are widely distributed among the various technical journals and proceedings. We assisted the National Electronics Manufacturing Initiative (NEMI) efforts by developing a database of properties on the three most common lead-free compositions. Once we had a reasonable base, we published the data on the NIST website, and requested additional data.

The pace of change in the database has slowed, but we have made a long-term commitment to maintain the database on the Materials Reliability Division's Website at: **http://www.boulder.nist.gov/div853/**. We continue to publicize the availability of the database at national technical meetings.

Different test procedures (*e.g.*, loading rates and dwell times) make some of the data inconsistent from laboratory to laboratory and so decrease the accuracy of the models. A Recommended Practice Guide (NIST SP 960-8) was written that recommends standardized procedures to facilitate the comparison of mechanical-property data within the electronics industry.

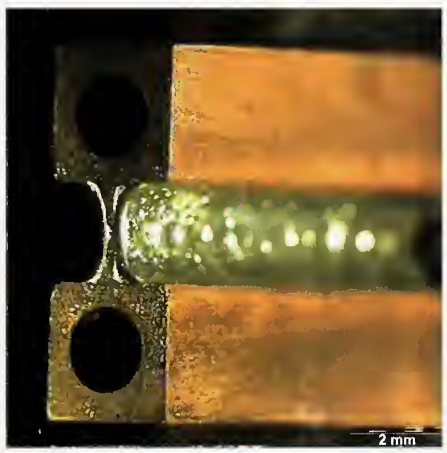

Figure 1: *Solder is cast between two copper blocks to make a "loaf" from which specimens are sliced off.*

A test method that used "miniature" specimens was developed to mimic the size of typical soldered joints. The purpose was to examine the effects of the size of the specimens (and hence the typical structures found in industry) and to fill in the gaps in the data for the lead-free solders. Solder is cast in a Ti mold between two copper blocks (Figure 1), and 200 μm specimens are cut from the blocks. The gauge length of the specimens is 300 μm. We can consistently make specimens with a known thermal cycle and maintain well-defined microstructure. Because the samples are sliced from a relatively large "loaf," a large number of samples can be made in a short time.

Contributors and Collaborators

Yair Rosenthal, Tom Siewert (Materials Reliability Division, NIST); Carol Handwerker (Metallurgy Division, NIST)

Nano- and Micro-Electronic Materials Characterization

As the scale of electronic devices is reduced, tools for characterizing materials properties and behavior at the nano- and micro-scale are required. We are developing and characterizing techniques to measure local properties, e.g., texture, strain, chemical homogeneity, and phase evolution, in materials used in nano- and micro-electronic systems.

John E. Blendell and Mark D. Vaudin

The characterization of nano- and micro-electronic materials requires different techniques than those used for bulk electronic materials. For example, optimizing the properties of multilayer systems requires knowledge of the structure and composition of interfaces at nearly atomic resolution. In ferroelectric thin films for ferroelectric random access memory (FRAM), local texture is known to have a significant effect on fatigue and imprint. The origin of strains at phase interfaces that cause microcracking can be determined from the structure of the surface near the crack. Examples of our research addressing these issues are highlighted below.

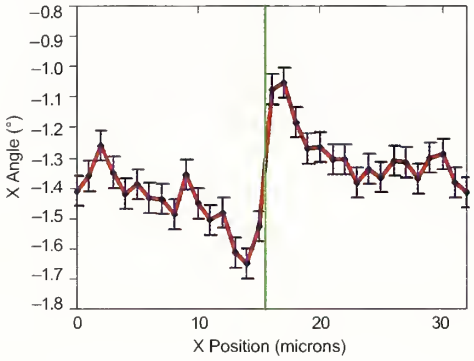

Figure 1: *Average tilt angle of lattice planes of $Al_xGa_{1-x}N$ thin films versus distance from a crack.*

A road block in the application of $Al_xGa_{1-x}N$ as light sources and detectors is the development of cracks during deposition of the films. Electron back-scatter diffraction (EBSD) was used to characterize the misorientation around individual cracks in 0.25 μm–1.2 μm thick AlGaN films on (111) silicon substrates. EBSD showed that the orientation of the AlGaN in the vicinity of each crack changed so that lattice planes in the film tilted away from the crack causing uplift of the specimen surface, which was also seen by atomic force microscopy (AFM). The basal plane orientation change across the cracks was typically 0.6° (Figure 1) with a measurement accuracy of the order of 0.05°. The width of the strain field varied from 2 μm to 15 μm in different specimens.

The presence of impurities or an intergranular liquid phase can significantly alter properties by affecting the motion of grain boundaries and transport or conductivity between grains. We have studied the influence of boundary misorientation and chemistry on the velocity of interfaces in $SrTiO_3$ single crystals of varying orientations. Crystals were bonded to dense textured polycrystalline $SrTiO_3$ ceramics; upon heating, the interface migrates into the ceramic. This experiment allows the isolation of key variables including crystallographic misorientation, impurity content, curvature, and boundary energy, leading to control over the nature of the grain boundaries, and the potential for improved properties.

Piezo-force microscopy (PFM) is used for characterizing individual domain orientations and the piezoelectric coefficient of ferroelectric thin films. Interpretation of results is complicated by highly localized, short-range interactions acting at the tip, as well as long-range interactions acting along the lever. The resulting distributed loads change the load applied at the tip by a factor of ≈ 3/8. Of greater importance is the impact of distributed loading on the angle along the lever. PFM measurements of piezoactuation can differ substantially from the true piezoactuation under conditions that have been modeled. Model calculations are supported by AFM measurements performed with interferometric lever detection and by PFM measurements on lead zirconate titanate thin films and triglycine sulfate crystals.

Silicon oxide-nitride-oxide multilayers are potential materials for charge storage structures in non-volatile memory devices; individual layers are 5 nm to 10 nm thick. Thorough microscopic examination of multilayers using electron energy loss spectroscopy, secondary ion mass spectrometry, and x-ray absorption spectroscopy revealed numerous details of the interface structure as a function of processing. There is a broadening of the nitrogen distribution across the nitride/oxide interfaces and reduction of the hydrogen content with increasing thermal budget in processing the top oxide. Also, radial-distribution functions are similar for differently processed silicon oxide layers.

Contributors and Collaborators

I. Levin, B. Huey, A. Scotch, D. Yoder (Ceramics Division, NIST); A. Davydov (Metallurgy Division, NIST); R. Leapman (National Institutes of Health, NIH); M. Kovler (Tower Semiconductor, Ltd.); W. Dawson, E. Sabolsky (NexTech Materials, Ltd.)

Superconformal Film Growth: Measurement and Modeling

State of the art manufacturing of microelectronic devices relies on superconformal deposition of copper in fine trenches and vias for on-chip wiring, or "interconnects." The NIST-developed Curvature Enhanced Coverage Mechanism is now used by industry to understand this superfilling process. More recent NIST research has demonstrated that the same mechanism explains the impact of catalysts on smoothing of surfaces during all types of electrodeposition. This is the first explanation of the surface stabilization process, a phenomenon that is as important for the filling of high aspect ratio features as the bottom-up superfill process itself.

Thomas P. Moffat and Daniel Josell

This project continues to explore novel, advanced means of meeting needs of the microelectronics industry for improved device metallizations. Much of the effort focuses on the Curvature Enhanced Accelerator Coverage mechanism originally shown by NIST researchers to explain "superconformal" (or bottom-up) feature filling with copper. The CEAC mechanism accounts for the impact of changing surface area on the coverage of adsorbed additives used in electrodeposition processes. Studies of this mechanism continue to yield exciting new discoveries. One particular result serves especially well to demonstrate the breadth of the superfill studies and the striking generality of the CEAC mechanism.

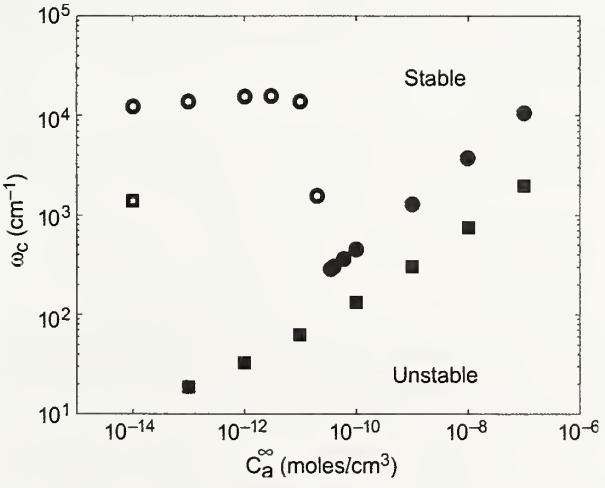

Figure 1: *The impact of catalyst concentration in the electrolyte on the minimum wavenumber for which a perturbation is stable (circles and squares are for different overpotentials). Substantial improvement in the range of conditions for which the surface is stabilized (up to two-orders of magnitude decrease of the critical wavelength) is evident.*

Researchers in the Metallurgy Division previously demonstrated the ability of the CEAC mechanism to explain key aspects of the bottom-up feature filling process that is known in the integrated circuit industry as "superfill." They have also extended it to superfill during electrodeposition of silver and chemical vapor deposition of copper. The CEAC mechanism has now been successfully extended to explain surface stabilization during electrodeposition of metals in electrolytes containing surfactant additives (Figure 1).

Such generality had been proposed in CEAC publications on feature superfill, but until this work, it had not been analyzed or proven. These results quantify the effect using a linear perturbation analysis; experimental evidence to support the model is also presented. Significantly, these results explain why remarkably dilute of additives known as "brighteners" or "accelerators" are so effective at preventing the roughening of surfaces even in the presence of destabilizing metal ion concentration gradients in the electrolyte.

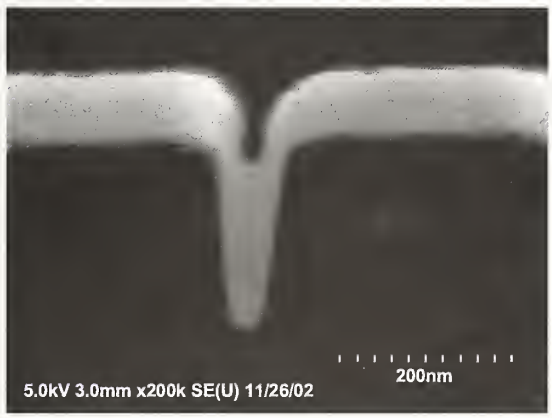

Figure 2: *Superconformal copper electrodeposition. Trench width is approximately 50 nm at mid-height. Note the smooth sidewalls.*

These results are of fundamental importance in the fabrication of high-aspect ratio advanced metallizations because smooth surfaces on the metal deposits are required for defect-free feature filling (Figure 2). Furthermore, these results provide understanding and direction in all electrodeposition processes providing brightening.

Contributors and Collaborators

D. Wheeler, S. Coriell, J. Mallett, W. Schwarzacher (Metallurgy Division, NIST); G. McFadden (Mathematical and Computational Sciences Division, NIST)

Lead-free Surface Finishes: Tin Whisker Growth

The U.S. microelectronics industry is moving towards Pb-free assemblies but lacks needed measurements and data comparable to that existing for Sn-Pb alloys. Protective layers, such as "pretinned" coatings on Cu leadframes and connectors, are required to maintain solderability of components during storage prior to assembly. A critical problem addressed by this project is that Pb-free coatings of nearly pure tin tend to grow "whiskers" which can cause catastrophic shorts across component leads.

Maureen E. Williams, Christian Johnson, and Kil-Won Moon

Development of Pb-free surface finishes is essential for the current move toward Pb-free microelectronics assembly, and tests which ascertain the tendency to form "tin whiskers" are in demand. NIST is providing leadership in two National Electronics Manufacturing Initiative (NEMI) whisker projects: identifying fundamental growth mechanisms and developing an accelerated test. Our goal at NIST is to provide an understanding of the fundamentals of the whisker formation, which will ensure that the test developed by the NEMI group will have widespread and general applicability.

Filamentary Sn whiskers (typically 1 µm diameter and several mm long) can grow from a Sn-based surface finish and cause electrical shorts and failure. Historically, Pb was added to Sn plate to prevent whisker growth as well as to lower cost. The current research program has focused on measuring effects of alloying additions on whisker formation in Pb-free Sn-rich deposits. The Sn-Cu system was chosen since Sn-Ag-Cu is the Pb-free solder of choice for industrial application. The goal is to substitute a different solute for Pb in the Sn-rich deposit in order to retard whisker growth.

Residual stress is generally believed to drive whisker growth in electroplated Sn. However, the origin of this stress has not been determined definitively. Our analysis of pure Sn and Sn-Cu deposits, combining a cantilever beam method for stress analysis with electron microscopy, indicates that Cu_6Sn_5 intermetallic particles in the Sn grains and along the grain boundaries of Sn-Cu deposits inhibit stress relaxation (Figure 1). Coarse intermetallic particles decorate grain boundaries with finer particles within the grains. The compressive stress in the pure Sn deposit decreased from an initial level of 14 MPa to zero after four days. In contrast, the initial compressive stress in the Sn-Cu deposit was 32 MPa and after twenty-three

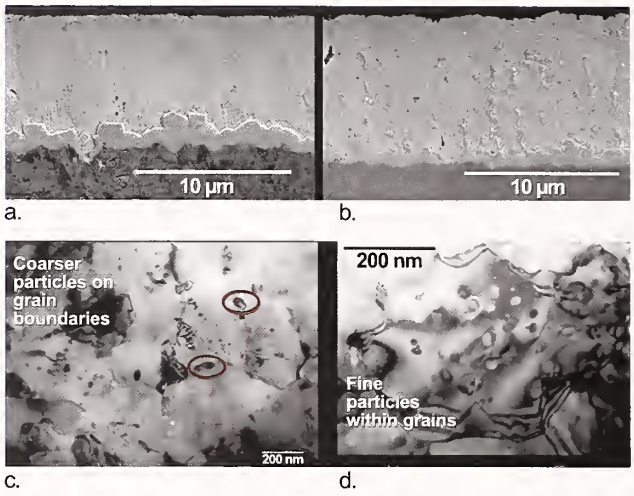

Figure 1: *(a) Polished section of pure Sn on Cu substrate; (b) Polished section of SnCu alloy on Cu substrate; (c,d) TEM photos of intermetallic particles on grain boundaries and in Sn grains.*

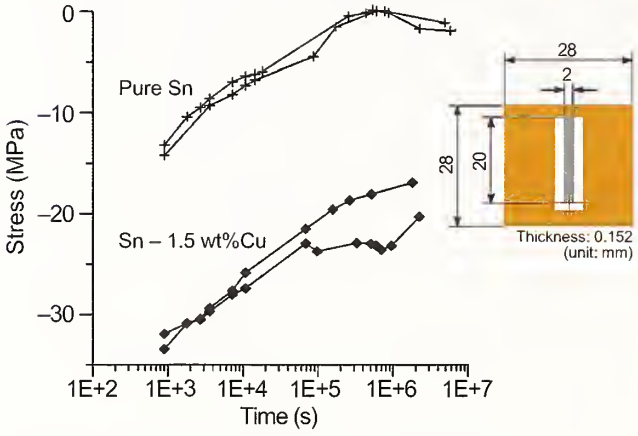

Figure 2: *Calculated stress levels from cantilever beam measurements of pure Sn and Sn-Cu electrodeposits.*

days was still 21 MPa (Figure 2). Whiskers were present on the Sn-Cu sample after only four days, but after 600 days, the pure Sn sample was still whisker-free. Since copper is a frequent impurity in electrodeposited Sn, unintendedly high, undocumented copper concentrations in commercial Sn deposits may have confounded controlled variables in previous studies. These results have been disseminated to the microelectronics community through NEMI meetings, including the March 2003 NEMI–NIST–TMS Workshop described in the Technical Highlights section.

Contributors and Collaborators

W.J. Boettinger, L. Bendersky, G.R. Stafford (Metallurgy Division, NIST); G. Galyon, N. Vo (NEMI project leaders)

Lead-Free Solders and Solderability

Solders and solderability are increasingly tenuous links in the assembly of microelectronics as a consequence of ever-shrinking chip and package dimensions and the international movement toward environmentally friendly lead-free solders. In collaboration with the NEMI Pb-Free Assembly Project, we are providing the microelectronics industry with measurement tools, data, and analyses that address national needs in the implementation of lead-free solders.

Ursula Kattner and Carol Handwerker

Since 1999, NIST has served a major role in the National Electronics Manufacturing Initiative (NEMI) Pb-Free Assembly Project to identify and move Pb-free solders into the microelectronics industry. (NEMI is an industry-led consortium of 65 manufacturers, suppliers, and related organizations brought together to facilitate leadership of the North American electronics manufacturing supply chain.) This move toward Pb-free solders is a direct result of the European Union ban, starting in 2006, on Pb-containing solders in electronic products.

The NEMI Lead-free Task Force and NIST have worked together to respond to the identified needs by:

- Identifying and providing the most important lead-free solder data for the microelectronics community, including the definitive database on thermodynamic properties of Pb-free alloys, and dessiminating such data on the NIST website. (See "Informatics and Visualization in Materials Data Delivery" in this volume.) This database allows the calculation of phase transformations in solder alloys containing Ag, Cu, Bi, In, Pb, Sb, and Sn, with additional data for Ag, Cu, and Sn with Ni, which is used in characterizing interactions between Pb-free solders and Ni-based surface finishes.
- Developing and widely disseminating "Recommended Practice Guide on Test Procedures for Developing Solder Data." (See Figure 1.)
- Providing a list of literature references on alloys, processing, reliability, environmental issues, and components for the implementation of lead-free solders.
- Completing the microstructure-based failure analysis on all thermally cycled assemblies as part of the NEMI's project's full-scale reliability trials.
- Providing chapters on the materials science of Pb-free solder alloys for three books on Pb-free solders.

In 2003, we have also served as an information resource to the microelectronics industry on issues related to the effects of alloy composition, reflow temperature, and furnace profiles for best melting and solidification behavior of solders when circuit boards are assembled, and to the effects of Pb contamination on alloy melting and assembly reliability.

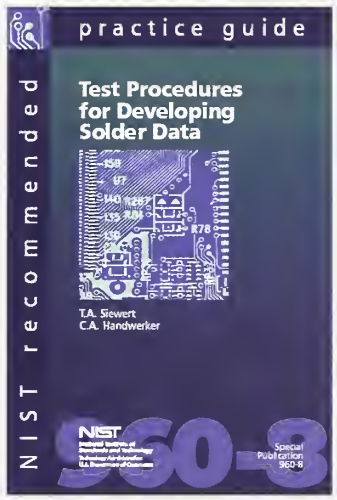

Figure 1: *"NIST Recommended Practice Guide on Test Procedures for Developing Solder Data."*

"The NIST group performed a significant service to industry by being the focal point for development of a reliable technology base to support the choice of a new lead-free alloy. They also led the way for further work on issues such as tin whiskers, which emerged from the initial lead-free work. NIST provided not only a strong technical basis but, by verifying reliability and comparing alternatives, enabled industry to choose an alloy based on extensive investigation. The prompt global establishment of a preferred alloy solution was critical for Motorola to be an early adopter of the technology."

Dr. Robert C. Pfahl, Jr.*, Director*
International and Environmental R&D
Motorola, *(retired)*

Contributors and Collaborators

W.J. Boettinger, K.-W. Moon, L.E. Smith, S.W. Claggett, M.E. Williams (Metallurgy Division, NIST); T. Siewert, C. McCowan (Material Reliability Division, NIST); J.P. Clech (EPSI, Inc.); J. Bath (Solectron); R. Gedney (NEMI); E. Bradley (Motorola); J.E. Sohn (NEMI, formerly Lucent); P. Snugovsky (Celestica); E. Benedetto (HP); R. Charbonneau (StorageTek)

Physical Properties of Thin Films and Nanostructures: Mechanical Properties of Low-κ Dielectric Films

Although crucial to the microelectronics industry, implementation of low-dielectric-constant (low-κ) films presents serious materials challenges. We apply different optical methods to these films to evaluate their critical properties: density/porosity, Young's modulus, and Poisson's ratio. The techniques provide complementary data and allow measurement of properties that are otherwise difficult to obtain.

Colm Flannery and Donna Hurley

Miniaturization in the microelectronics industry requires lowering the resistance-capacitance (RC) factor in order to achieve faster device switching. This requires replacing standard silica dielectrics with materials of a lower dielectric constant (κ). The most promising way to achieve this is to introduce nanometer-sized pores that reduce κ as porosity increases. An unwanted by-product is a drastic reduction of mechanical properties. The very low Young's modulus of porous low-κ films lessens the chance of their surviving the microelectronic chemical-mechanical polishing process and affects process reliability. Accurate values of film modulus must therefore be known. However, few tools are available to characterize such relevant thin-film properties and their dependence on porosity. Nanoindentation, a standard industry technique, is challenging on such soft films and generally tends to overestimate stiffness significantly. As an alternative, we are developing optical techniques to enable non-contact property measurement.

Brillouin light scattering (BLS) relies on a photon–phonon collision process where incident photons collide with ambient thermal phonons in the material. The frequency shift of the scattered photons, detected by a scanning Fabry–Perot interferometer, is characteristic of the acoustic phonon modes in the film. With BLS, we examined a series of methylsilsesquioxane (MSSQ) polymer films of varying porosity. We could detect both longitudinal and surface acoustic wave modes and, thus, could determine values for both Poisson's ratio ν and Young's modulus *E*. Figure 1, which plots the values of ν obtained in these films *vs.* porosity, reveals that ν decreases as porosity increases. This is important since the dependence of n on porosity is not well understood. Very few techniques have been able to provide experimental data to address this issue. BLS appears to be a very promising tool with which to explore this area.

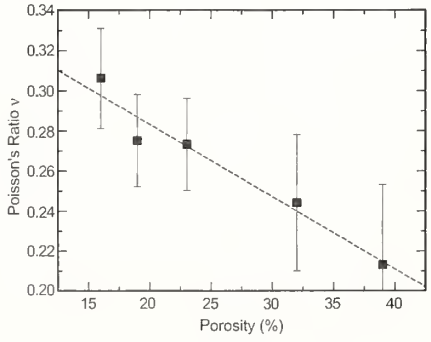

Figure 1: *Poisson's ratio vs. porosity for MSSQ films.*

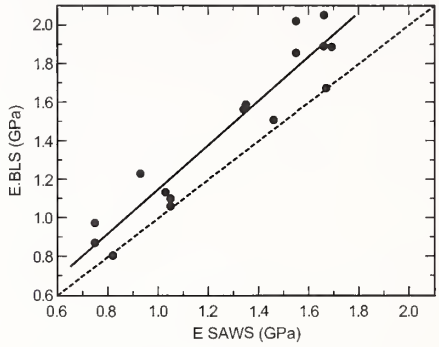

Figure 2: *Young's modulus determined by SAWS and BLS.*

In addition to BLS, frequency-dependent dispersion of laser-generated surface acoustic waves can yield accurate measurements of the density and Young's modulus of thin films. In FY03, we implemented a new SAWS apparatus optimized to inspect thin films on silicon and paid special attention to developing a robust data analysis procedure. Figure 2 compares values of *E* obtained by BLS and SAWS for a range of low-κ films. The results show a clear correlation but with a systematic difference between the techniques of 10–15 %. Reasons for this small discrepancy are being investigated. (SAWS density values have also been verified by x-ray reflectivity measurements).

We are also characterizing two-layer samples (low-κ film with a thin capping layer), interpreted using our newly-developed two-layer Green's function analysis code. Preliminary results show that SAWS is sensitive to the presence of capping layers as thin as 50 nm. Work in the coming year will concentrate on extending SAWS and BLS measurements to multilayer samples, analyzing measurement uncertainties, and developing a standard SAW thin-film data analysis procedure.

Contributors and Collaborators

S. Kim, V. Tewary (Materials Reliability Division, NIST); W. Wu (Polymers Division, NIST); J. Wetzel (Tokyo Electron America)

Physical Properties of Thin Films and Nanostructures: Molecular Electronic Interconnects

Electronic devices based on large molecular assemblages are being rapidly developed. Further progress is limited by the quality of the contacts joining these devices together. We are exploring various techniques to manipulate and join nanotubes to substrates. We are then developing techniques to probe the subsequent mechanical and electrical characteristics of these nanometer-scale connections.

Paul Rice

Molecular electronic devices such as carbon nanotube transistors have the potential to revolutionize the electronics industry by reducing circuit sizes dramatically and by increasing operational speed due to the inherent properties of the materials. Carbon nanotubes are currently one of the basic building blocks for molecular electronics. The electrical and thermal properties of these molecules theoretically solve numerous materials problems. However, even though, for example, their internal electrical conductivity is very high, the contact resistance between nanotubes is also quite high, limiting the current that can be passed from tube to tube. Using manipulation and fabrication techniques developed within the Division, we are exploring methods to characterize these interconnects.

Figure 1 shows an image of a popular technique called electron beam deposition (EBD) that is used for connecting nanotubes to substrates. In the scanning electron microscope (SEM), the beam is held on a spot where a connection is desired. The beam has enough energy to split hydrocarbon molecules, common contaminants in most SEMs. The resultant active carbon condenses on the nanotube and substrate to form a strong bond or weld.

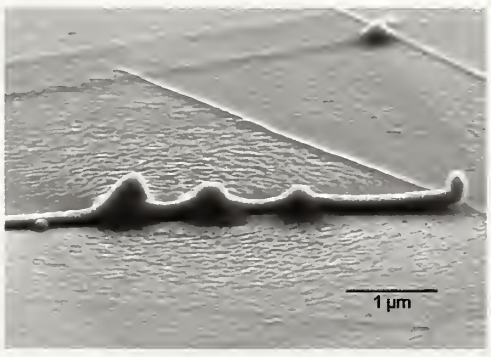

Figure 1: *SEM image of a 100 nm diameter multi-walled carbon nanotube attached by three welds to a Cr thin-film. The increase in size of the welds (from right to left) is due to increasing the time the electron beam was left focused on the nanotube.*

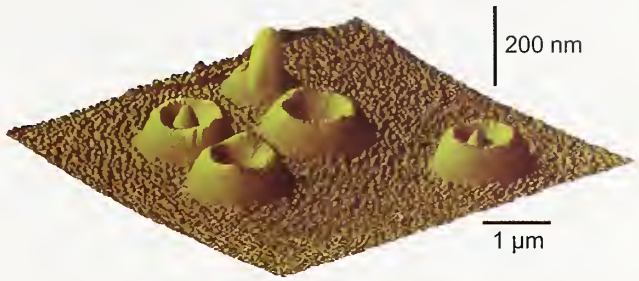

Figure 2: *AFM image of the effects of electron beam stigmation on EBD weld structures. The spike in the back is the result of a well-aligned electron beam.*

The quality of the EBD weld is highly dependent on the skills of the SEM operator. In FY03, we have been exploring the effects of beam collimation and stigmation on the weld. Figure 2 shows the variety of EBD weld structures that can be formed with different beam adjustments. Optimizing these variations in weld characteristics is an important step in ensuring the fabrication of high-performance interconnects.

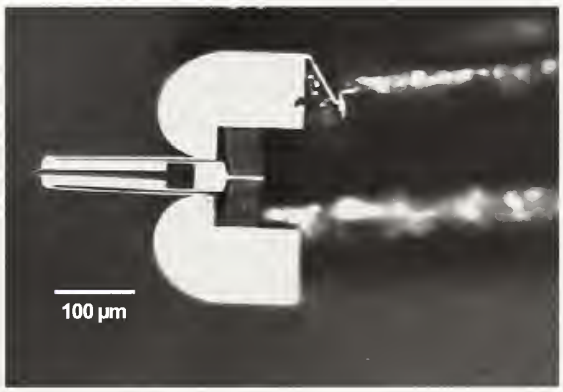

Figure 3: *Optical micrograph of tweezers for manipulating carbon nanotubes. The tips of the tweezers on the left are only a few microns long. They are actuated by thermal expansion of the silicon as an electrical current heats specific parts.*

In addition to controlling the interconnect fabrication process, manipulation of these small-scale structures is also critical for property characterization of these early-stage materials. With the help of researchers at the University of Colorado, we are developing tweezers capable of manipulating individual nanotubes for fabrication as well as characterization (see Figure 3).

Contributors and Collaborators

D.T. Read, R. Geiss, D.S. Finch (Materials Reliability Division, NIST); S.E. Russek, A.B. Kos (Magnetic Technology Division, NIST); A. Hartman (University of Colorado)

Micrometer-Scale Reliability: Strain in Photonic Semiconductors

The compound semiconductor photonics industry seeks to both measure and control strain that develops during the course of device fabrication. In the Materials Reliability Division, we are developing methods for measuring and mapping elastic strain distributions using electron diffraction. The methods are applied to phase transition-induced strains for the case of oxide formation in vertical cavity surface-emitting lasers, and to lattice parameter mismatch strains for self-assembled quantum dots.

Robert R. Keller and Roy H. Geiss

Vertical cavity surface-emitting lasers (VCSELs) present an attractive solution to many limitations faced by conventional edge-emitting lasers. Fabrication of aluminum oxide apertures for both electron and photon confinement in VCSELs is accomplished by wet thermal oxidation of AlGaAs between GaAs layers. Accompanying the transition is a volume contraction that exceeds 6 %. Thermal cycling during subsequent processing steps often results in delamination between the oxide and semiconductor interfaces, causing device failure. Our work with the Optoelectronics Division addresses the measurement and control of strain in VCSEL structures to minimize failure. We use both TEM and SEM-based electron diffraction to determine the strain states by means of measuring lattice spacings and angles. Compositional control during fabrication is used to tailor strain distributions. We describe here recent results on elastic strain mapping in the SEM.

Last year, we reported the exciting observation that electron backscatter diffraction (EBSD) pattern sharpness maps revealed a distorted region about the oxide growth front. Since that time, we have modeled the strain field using finite-element methods and have demonstrated mapping at much higher spatial resolution. Pattern sharpness shows a dependence upon all strain components since many reflections are used in the quantification. The shape and spatial extent of the distorted region in the resulting maps are consistent with the von Mises equivalent strain field expected about the oxide front, as determined by finite-element analysis. We are using kinematical electron diffraction theory to extract quantitative information regarding the magnitude of the strain gradient measurable in the patterns and maps.

Figure 1 shows an example of a high-resolution map where the beam was stepped in 10 nm increments. It reveals in detail the gradient in pattern sharpness normal to the interfaces (redder pixels indicate sharper patterns). We have determined that the orientation-dependent information volume for backscattered electrons has a diameter of approximately 25–30 nm in GaAs for the 15 kV electrons used in this scan. This map is therefore approaching the limit in terms of spatial resolution for this strain mapping method. We note that the resolution limit is somewhat smaller than the information volume diameter since we can overlap the sampling volume by means of the small step size and still detect differences from point to point. We are exploring improved resolution by decreasing the electron energies and by experimenting with camera positions.

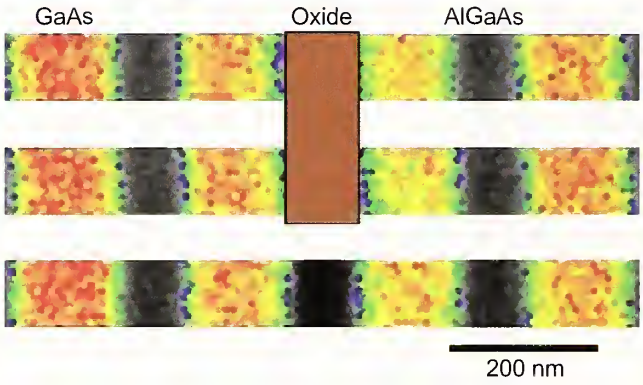

Figure 1: *High resolution EBSD pattern sharpness map, with 10 nm step size.*

This year, we began presenting some of our metrology results at professional society-sponsored conferences including the TMS Annual Meeting, the Summer Meeting of the Applied Mechanics and Materials Division of ASME, and the TMS Electronic Materials Conference. The prospect for using EBSD to both measure and map elastic strain distributions generated considerable interest, especially among those familiar with the technique. We feel that these developments have potential application to areas outside the photonics industry as well.

Contributors and Collaborators

T. Quinn, V. Tewary (Materials Reliability Division, NIST); A. Roshko, S. Lehman, K. Bertness (Optoelectronics Division, EEEL, NIST)

Wide Band Gap/Optoelectronic Materials

The Optoelectronics Industry Development Association roadmaps cite the need for standard reference materials (SRMs) and measurement methods to calibrate deposition processes and evaluate material properties. This project addresses those needs in the following areas: photoluminescence measurements of $Al_xGa_{1-x}As$ films for SRMs; photoreflectance measurements of band gap in InGaAsN; cathodoluminescence measurements to assess film quality in AlGaN; and Raman and photoluminescence measurements to evaluate stress and composition in $Al_xGa_{1-x}As$.

Albert Paul, Lawrence Robins, and Grady White

The NIST program to produce $Al_xGa_{1-x}As$ standard reference materials (SRMs) for the optoelectronics industry is nearing completion. Photoluminescence (PL) determined compositions of $Al_xGa_{1-x}As$/Ge films and AlGaAs lift-off films have been compared with results of inductively-coupled-plasma optical-emission spectroscopy (ICP–OES) measurements made in the Analytical Chemistry Division at NIST. Although Ge substrates eliminated biasing the ICP–OES results with Ga or As from GaAs substrates, there was concern that the Ge substrates would alter the $Al_xGa_{1-x}As$ band gaps. However, PL measurements confirmed that band gap energies for AlGaAs/Ge agreed with AlGaAs/GaAs. $Al_{.20}Ga_{.80}As$ SRMs are to be released in September 2003.

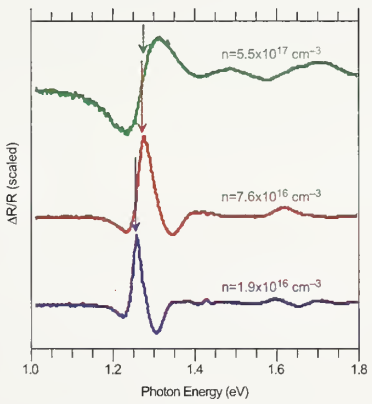

Figure 1: *PR of InGaAs films.*

Photoreflectance (PR) is a useful probe of the electronic structure of InGaAsN films, a new class of infrared optoelectronic materials. Figure 1 shows PR spectra of films with 8 % In, 0.4 % N, and varying silicon dopant and free carrier ("n") concentrations. The lines broaden and critical point energies shift upward with increasing "n". Arrows indicate the fitted band gap (lowest direct transition) energies. Higher-lying transitions (not labeled) are ascribed to splitting of both the valence and conduction bands in these alloys.

As part of a study of compositional, structural, and optical properties of AlGaN films, grown by either metalorganic chemical vapor deposition (MOCVD) or hydride vapor phase epitaxy (HVPE) on (0001) sapphire, the near-band-edge optical properties of the samples were probed by cathodoluminescence (CL) spectroscopy. Figure 2 compares low-temperature CL of films produced by different deposition processes. The near-band-edge CL lineshape is sensitive to compositional fluctuations and defect levels. The results suggest that recent HVPE grown films have improved homogeneity and crystalline quality.

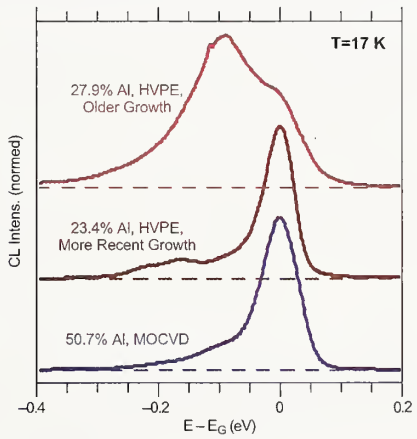

Figure 2: *CL of AlGaN films*

A paper, "Refractive Index Study of $Al_xGa_{1-x}N$ Films Grown on Sapphire Substrates," has been accepted by the *Journal of Applied Physics*.

Raman and PL spectra of $Al_xGa_{1-x}As$ have been calibrated in terms of stress and composition. Details are given in the Technical Highlights section of this report.

Contributors and Collaborators

Y.-S. Kang, M.D. Vaudin (Ceramics Division, NIST); T.A. Butler, G.C. Turk (Analytical Chemistry Division, NIST); A.V. Davydov, W.J. Boettinger, A.J. Shapiro (Metallurgy Division, NIST); K.A. Bertness, T.E. Harvey, N.A. Sanford (Optoelectronics Division, NIST); A.G. Birdwell (Semiconductor Electronics, NIST); D. Bryson, M. Fahmi, S.N. Mohammad (Howard University); S. Keller, U.K. Mishra, S.P. DenBaars (University of California, Santa Barbara); D.V. Tsvetkov, V.A. Soukoveev, A.V. Dmitriev (Technologies and Devices International, Inc.)

Phase Diagrams for III–V Thin Films and Metal Contacts

Commercialization of Group III nitride devices has been hindered by several technological and fundamental materials issues, including problems with making high quality GaN epilayers and bulk substrates and with fabrication of reliable electrical contacts. This project focuses on experimental and computational evaluation of Metal – Group III – N phase diagrams to be used as a roadmap for: a) optimization of growth and thermal processing of GaN and related nitrides and for; b) development of metallization information to enable the design of improved electrical contacts to GaN-based devices. For metallizations, a combinatorial approach is used for establishing the relationship between electrical properties, metallization compositions, and processing parameters.

Albert Davydov and William Boettinger

Gallium nitride-based semiconductors are used in blue-green and UV lasers, LEDs, photodetectors, and high-temperature/high-power electronic devices. The optimum growth conditions of GaN, choice of contact metals, and thermal processing limits for the device structures rely mostly on trial-and-error methods and are not fully understood. We believe that knowledge of the thermodynamics/kinetics in Metal – Group III – N systems can provide guidance for optimization of the device processing parameters.

In the Ga-N system, we use experimental and computational CALPHAD procedures to evaluate the thermodynamic and phase diagram data (Figure 1). A thermodynamically consistent model representation of the available data and our experimentally determined properties have resulted in reasonable estimates of missing critical data, such as melting/decomposition temperature of GaN as a function of nitrogen pressure. Results are now posted on the ONR National Compound Semiconductor Roadmap website (**http://ncsr.csci-va.com**) and can be used in optimizing growth and processing conditions for GaN-based devices.

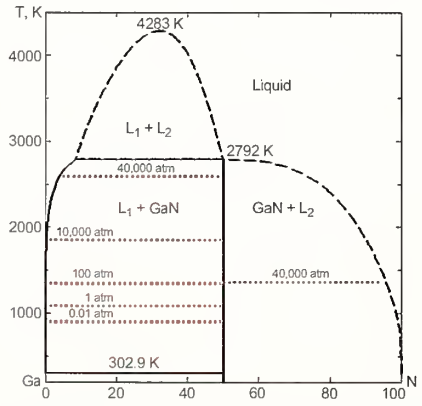

Figure 1: *Calculated Ga-N phase diagram with superimposed isobaric lines (dashed).*

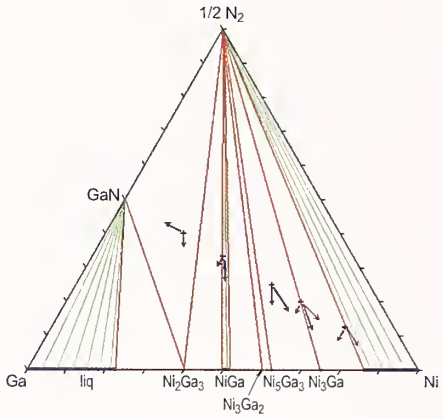

Figure 2: *Experimental data (points and arrows) and calculated (lines) for the Ni-Ga-N phase diagram.*

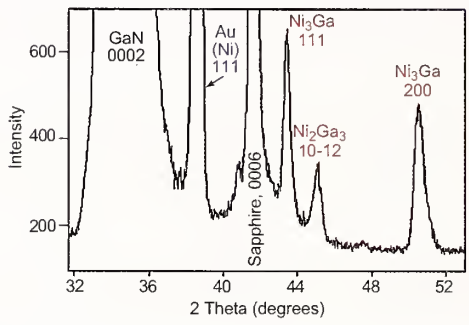

Figure 3: *XRD of Ni/GaN thin film structure (overcoated with Au) annealed at 800 °C: Ni_3Ga and Ni_2Ga_3 are formed.*

In 2003, the utility of phase diagrams in analyzing metallization choices was demonstrated using Ni as one of the most commonly used industrial contacts. The Ni-Ga-N phase diagram was calculated and verified experimentally (Figure 2). The diagram was used to interpret the interfacial reactions in the Ni/GaN thin film structures (see Figure 3). An experimental combinatorial study of Ni/Au metallization to GaN is now underway.

Contributors and Collaborators

L. Bendersky, U. Kattner, F. Biancaniello, D. Josell, A.J. Shapiro (Metallurgy Division, NIST); T.J. Anderson, O. Kryliouk (University of Florida); S. Noor Mohammad (Howard University); M. Master (TDI, Inc.)

Combinatorial Methods for Thin Films

In the search for new functional materials for use in modern microelectronics, various thin film oxides are under consideration. With the ability to locally measure properties of the films, combinatorial approaches using miniature thin film assays of varying compositions can be of significant impact to optimize the search. The combinatorial methodology is still in its early stages of development, and, therefore, understanding the fundamentals of synthesis of the combinatorial assays, as well as the relationships between crystal chemistry and physical properties of the assays, is of great importance.

Leonid A. Bendersky

The effectiveness of the combinatorial approach in the development of thin film electronic materials has been clearly demonstrated. In order to rapidly survey a large compositional landscape, assays with continuously changing compositions are synthesized, processed, and screened in a single experiment. Dielectric, magnetic, and other properties can be measured within compositional spreads using recently developed instruments with high spatial resolution, such as the microwave microscope and microSQUID. In early combinatorial materials research, the local microstructure and phase composition were largely unprobed. Through our ongoing collaboration with Professor Ichiro Takeuchi from the University of Maryland, we have demonstrated the value of using transmission electron microscopy (TEM) for understanding the deposition process and the correlations between physical properties and local microstructure.

In 2003, our primary focus was on using combinatorial research to demonstrate tunable bandgaps by doping a semiconductor ZnO (bandgap: 3.3 eV, hexagonal structure) with MgO (bandgap: 7.8 eV, cubic structure). Potential applications are for optical devices, including UV lasers, as well as transparent conducting layers for solar cells and phosphors. The $Zn_{1-x}Mg_xO$ thin film assays are prepared using pulsed laser deposition (PLD) with synchronized shutters. Multiple targets were alternatively ablated for atomic layer-by-layer deposition onto substrates with matching lattices, producing epitaxial films compositionally uniform in the growth direction and with one-dimensional compositional variation along the film plane. These epitaxial spreads were studied for bandgap by UV transmission and for microstructure by scanning x-ray microdiffractometer and transmission electron microscopy (TEM).

The results show a continuously changing bandgap for $x < 0.4$ and $x > 0.6$, suggesting possibilities of using the arrays themselves as photodetectors with a range of detection frequencies separately active at different locations within the film.

Scanning x-ray results showed three structurally different regions. TEM gave insight into the structural details. An especially important finding was for the $0 < x < 0.4$ region where, according to the x-ray diffraction, there is an extended solid solution of Mg in ZnO. TEM, however, identified a high density of planar defects and, according to high-resolution imaging, the defects appear to be layers of (111) MgO intergrown in the host lattice of ZnO (see Figure 1). Thus the effect of Mg ions on the electronic structure and bandgap of ZnO will be very different, at least conceptually, from the solid–solution model.

Other active areas of research include developing MOIF as a rapid imaging method to determine ferromagnetic phase boundaries, establishing the relationship between bulk properties and thin film properties in shape memory alloys, and measuring composition-dependent and structure-dependent properties of multiferroic materials.

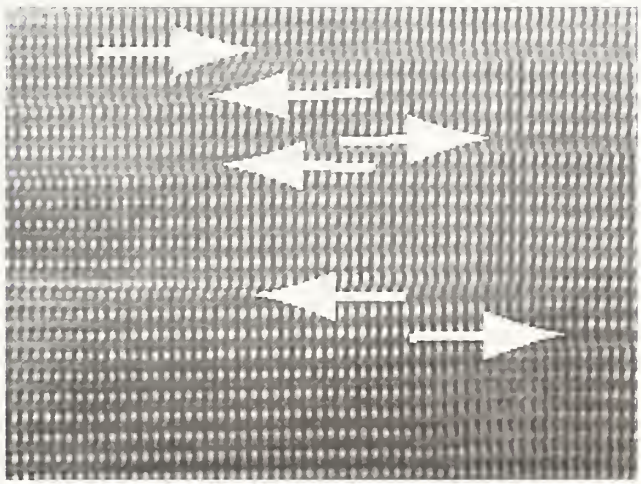

Figure 1: *Epitaxial ZnO-based phase (containing 10 at % Mg) with a high density of extended planar defects. HRTEM image showing the stacking fault-type nature of the defects and suggesting an accommodation of the excess MgO on the defect.*

Contributors and Collaborators

I. Takeuchi, K.-S. Chang (University of Maryland); M.J. Turchinskaya, R. Parke (Metallurgy Division, NIST)

Magnetic Properties and Standard Reference Materials

Users of magnetic materials, including the recording industry, the permanent magnet industry, and the manufacturers of electric motors and transformers of all types, need standard reference materials (SRM's) to calibrate instruments used to measure the critical magnetic properties of their starting materials. The Magnetic Materials Group develops such standards. We also investigate methods for improving the efficiency and accuracy of measuring and characterizing magnetic materials of industrial interest.

Robert D. Shull and Robert D. McMichael

In collaboration with scientists from universities, industry, and other Divisions at NIST, this project prepares magnetic materials that are important to the scientific and industrial communities and develops methods for the improved measurement of their properties. We develop models of hysteresis and magnetic time dependence that serve as a theoretical foundation for metrology of accommodation and aftereffect in magnetic recording and permanent magnetic materials. We also develop models for determination of the most efficient methods to fully characterize the hysteresis and magnetostriction in magnetic materials.

We develop and produce Standard Reference Materials for the calibration of existing and planned instruments used in the measurement of magnetic properties using the absolute magnetometer developed in our laboratory (*e.g.*, Figure 1). This year we have issued garnet magnetic moment SRM's useful for calibrating the most sensitive scales in SQUID and vibrating sample magnetometers. These SRM's provide, for the first time, a means for calibrating the measurements from high sensitivity alternating gradient magnetometers on an absolute basis. These small (1 mm diameter) single-crystal yttrium iron garnet spheres with a nominal mass of about 2.8 mg were measured using the Faraday technique after calibrating the magnetometer using the Thorpe–Sentfle method. Current work includes certifying platinum cylinders as paramagnetic susceptibility standards for the magnetics community. This standard reference material will be useful for calibrating magnetometers where an outside source of magnetic flux is undesirable. It will also be useful for determining the true zero field and zero moment values in magnetometers.

In order to inform the magnetics community of the availability of these recently prepared magnetic standard reference materials, a NIST booth on this topic was organized and manned at the last Magnetism and Magnetic Materials Conference (MMM, the big annual conference on magnetism in the U.S.). In addition, a brochure was assembled in collaboration with the Measurement Sciences Division of NIST, shown in Figure 2, and mailed to over 7,000 magneticians, with an electronic version sent by email to the participants of the above MMM conference.

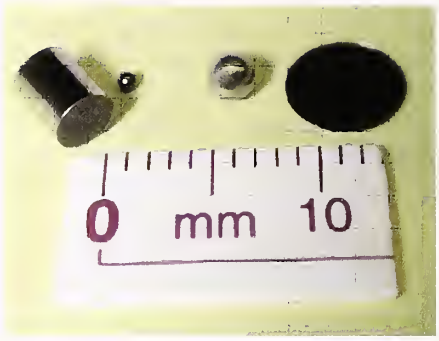

Figure 1: *Pt cylinder, YIG sphere, Ni sphere, and Ni disc SRMs.*

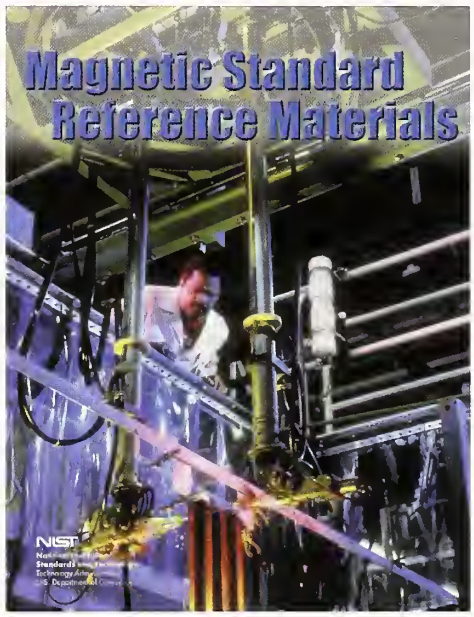

Figure 2: *Magnetic SRM brochure.*

Contributors and Collaborators

L.J. Swartzendruber (Magnetronix, Inc.); D. Twisselmann (Arete Associates, Inc.); D.Mathews, R. Drew (Metallurgy Division, NIST); S.D. Leigh (Statistical Engineering Division, NIST); D. Decker (Measurement Services Division, NIST); L. Bennett, E. Della Torre (George Washington University)

Magnetic Properties of Nanostructured Materials

In the past 10 to 15 years, there has been a remarkable improvement in the technology for materials preparation, resulting in today's capability of controlling morphology and features at the nanometer level. In magnetic materials, such control allows the fabrication of nm-thick (or separated) composite materials of dissimilar magnetism, leading to materials with novel magnetic character and unusual property combinations. We provide the understanding and metrology that allows U.S. industry to take advantage of these new materials.

Alexander J. Shapiro and Robert D. Shull

Present day high-density data storage is possible due to the giant magnetoresistance (GMR) spin valve, which is now used as the read head in magnetic disc drives. This structure is composed of two ferromagnetic (FM) layers separated by a thin non-magnetic layer. When an external magnetic field reverses the magnetization of one of the FM layers, the resistance of the composite changes. Consequently, one FM layer must maintain a constant magnetization during this process, usually accomplished by placing an antiferromagnetic (AF) layer adjacent to it so as to "exchange-bias" that FM layer. This results in a hysteresis loop that is shifted along the field axis as shown in Figure 1(a). Unfortunately, this exchange-biasing is not well understood.

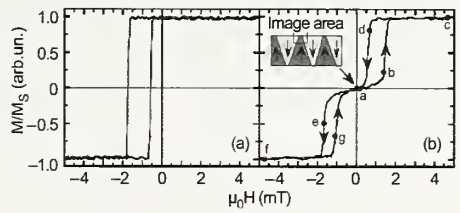

Figure 1: *Hysteresis loops for a NiFe/FeMn bilayer cooled under (a) constant and (b) alternating field conditions.*

Several years ago, we found we could elucidate some of the basics of the magnetization reversal process in such systems [V.I. Nikitenko, *et. al.*, PRB **57**, R8111 (1998)] by using the magneto-optic indicator film technique (MOIF) developed in our laboratory. This domain imaging technique enabled us to show for the first time that, contrary to popular thought, the two sides of the hysteresis loop are not symmetrical but are each governed by different mechanisms. This year, we have answered another key question regarding exchanged bias systems: do the domain walls in the AF move when the FM reverses its magnetization? MOIF observations were made of a NiFe (FM)/FeMn (AF) bilayer which had been ac-demagnetized above the Neel temperature of the AF but below the Curie point of the FM (Figure 1b). Application of the alternating field at elevated temperatures formed a demagnetized FM composed of striped domains with alternating magnetization vectors, shown in Figures 1(b) and 2(a), on top of coincident AF domains. When a field was applied to this bilayer to saturate the FM [Figures 2(c), (f)], there still remained a remnant image of the original domain pattern (Figure 2a), indicating the AF wall below the FM has not moved.

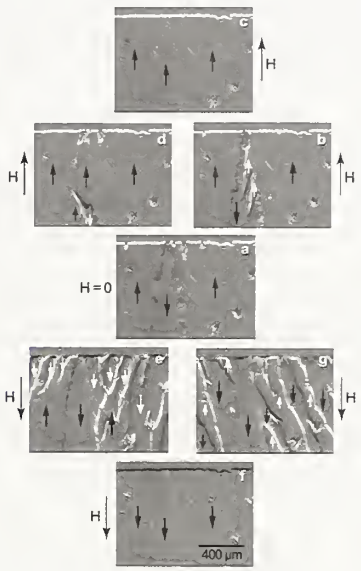

Figure 2: *MOIF images of domains in the FM at the conditions specified by the positions designated in Figure 1(b).*

Some AF spins in the region of the AF/FM interface, however, are changing during the FM reversal, as attested to by the fact that Figures 2(e) and (g) only show domain activity in the same areas for both field application and removal respectively, contrary to that for a normal ferromagnet. Similar observations have also been made on a different AF/FM bilayer, FeMn/$Fe_{76}Mn_6C_{18}$, wherein the initial coincident domain structure in the FM and AF was created by elevated temperature preparation under a low applied field.

As a result of these measurements, theoretical models may now be improved, and industry should now be able to better tailor spin valve processing to obtain improved reproducibility. In the past year, over 40 % of all papers on exchange-biasing have referenced our MOIF results.

Contributors and Collaborators

V. Nikitenko, V. Gornakov (Russian Academy of Sciences); C.L. Chien (Johns Hopkins University); H.-W. Zhao (Chinese Academy of Sciences)

Nanomagnetodynamics

This project provides the magnetic information storage industry with metrology for magnetization damping and magnetic inhomogeneity in thin film ferromagnets. Damping is expected to become a critical issue for magnetic information storage at GHz data rates, and inhomogeneity on the scale of 10 nm in recording media is important for increased storage density in the new generation of disk drives, which will use perpendicular magnetic recording.

Robert D. McMichael

The central issue in interpretation of ferromagnetic resonance line width data is the determination of how much of the ferromagnetic resonance line width is due to damping and how much is due to inhomogeneity. Ferromagnetic resonance is observed as a peak in the transverse susceptibility that occurs when the frequency of the driving field is close to the frequency of precession. The peak position can be used to determine sample average properties, but the width of the resonance peak, or "line width," is a combined effect of damping and inhomogeneity.

Existing simple models describe the contribution of damping to the line width. We have provided reliable models of inhomogeneity that are key to interpretation of line width data. These models describe the line width behavior as a function of frequency and applied field orientation for different types of inhomogeneity.

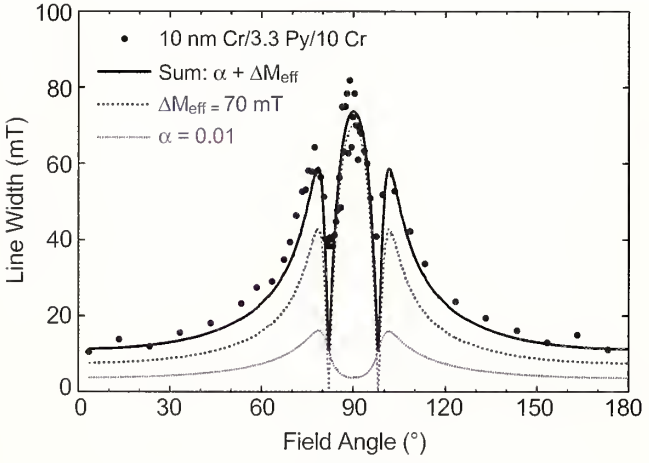

Figure 1: *Ferromagnetic resonance linewidth for a Cr/Permalloy/Cr trilayer as a function of applied field angle. This plot illustrates the ability to separate the linewidth into a damping component (pink line) and an inhomogeneous component (blue line) corresponding to 7 % variations in the effective magnetization.*

Neglecting the exchange and dipolar interactions that are characteristic of ferromagnets, local variations in magnetic properties would be expected to result in a distribution of local precession frequencies and a broadened resonance peak. However, interactions tend to synchronize the precession in neighboring regions, effectively "smoothing" the inhomogeneity, and reducing its effect on the line width.

Significant accomplishments in FY03 include:

- Development of a unified model of inhomogeneous line broadening in thin films. This model covers the full range of inhomogeneity and interaction strengths but is computationally too expensive to use for fitting. This model established that the transition from local to collective behavior is governed by the relative magnitudes of the inhomogeneity and the region-to-region coupling. See R.D. McMichael, D.J. Twisselmann, and Andrew Kunz, *Phys. Rev. Lett.*, **90,** Art. No. 277601 (2003).
- An approximation to the full calculation of inhomogeneous line broadening using the "two magnon" model in the strong coupling/weak inhomogeneity limit and local resonances in the weak coupling/strong inhomogeneity limit.
- Useful analytical approximations for the "two magnon" model for ultra thin films in the limit of zero damping.
- Measurement of the damping properties of Cr in proximity to Permalloy (Figure 1). These experiments imply that ferromagnetic resonance measurements in CoCr based hard drive recording media will not be hindered by excessive damping.
- Modeling of ferromagnetic resonance line widths in perpendicular recording media under development in industry.

Contributors and Collaborators

D.J. Twisselmann, W.F. Egelhoff, Jr., A.P. Chen (Metallurgy Division, NIST); Andrew Kunz (Lawrence University); H. Nakamura, M.E. McHenry (CMU); S. Rezende (Recife, Brazil); G.S.D. Beach, A.E. Berkowitz (UCSD)

Anomalously Large Low Temperature Intermixing in Metallic Thin Films

The objective of this program is to provide assistance to U.S. companies in the ultra-high density data storage industry, which includes such products as hard disk drives and magneto-resistive random access memory chips. Our work provides U.S. companies with significant competitive help by investigating the scientific issues underlying the manufacturing process. Often, this scientific understanding will point the way to improved manufacturing processes.

William F. Egelhoff, Jr.

As the scale of microelectronic devices shrinks, surfaces and interfaces play increasingly important roles as they become a larger fraction of the total device volume. Interfaces are especially important for the metallic thin films so common in layered device structures. Interfaces between thin films may appear to be abrupt at macroscopic length scales but diffuse at atomic length scales. Fortunately, when metallic thin films are deposited on one another at room temperature, there is generally little intermixing at the interface. Typically, if there is any intermixing, it is limited to one or two atomic layers. However, recent collaborative studies by NIST and the University of Durham have shown that such low-temperature intermixing can be far more extensive when Al and a transition metal (TM) are involved.

Thin film samples of the type "Al on TM" and "TM on Al" were prepared at the NIST Magnetic Engineering Research Facility and analyzed by grazing-incidence x-ray reflectometry (GIXR) at Durham. GIXR is an ideal technique for these studies since it is extremely sensitive to intermixing at interfaces. We find the intermixing profile perpendicular to the interface is usually well described by a Gaussian distribution, as expected, since diffusion processes often follow Fick's Law. The results are displayed in Table 1 as the full-width-at-half-maximum (FWHM) of the intermixed region. The FWHM results span the range from 0.1 nm for Al on W to 16.8 nm for Cu on Al. This Cu-on-Al result corresponds to approximately 100 atomic layers of intermixing. Such results are a great surprise to researchers in the field. For example, electronic properties for a thin film structure consisting of 2 nm Cu/1 nm Al/2 nm Cu were recently reported and analyzed as if the interfaces were atomically sharp. In fact, the sample must have been essentially a random alloy!

Among other combinations showing large intermixing were Mn on Al with 15.1 nm and V on Al with 9.4 nm. These surprising results suggest that the heat of alloying is driving much more extensive chemical reactions at the interface than had heretofore been known. These results have important implications for many microelectronic devices incorporating Al films. For example, problems in magnetic-tunnel-junction devices may be directly attributed to such phenomena. NIST is also developing solutions to such problems based on oxide barriers to suppress the intermixing.

Table 1: **The intermixing FWHM (in nanometers) for thin films of Al on transition metals and transition metals on Al**

TM Element	Al on TM	TM on Al
Ti	1.7	5.0
V	2.6	9.4
Cr	0.5	3.3
Mn	10.4	15.1
Fe	0.9	2.1
Co	0.8	6.8
Ni	1.4	7.9
Cu	2.8	16.8
Zr	1.0	5.1
Nb	0.8	3.6
Mo	1.3	3.4
Ru	0.8	5.2
Rh	0.4	4.7
Pd	4.8	5.6
Ag	2.5	4.5
Hf	2.0	4.4
Ta	0.1	0.9
W	0.1	3.5
Re	2.1	8.6
Os	0.1	7.1
Ir	0.2	5.4
Pt	1.9	4.5
Au	5.2	6.3

Contributors and Collaborators

R.D. McMichael (Metallurgy Division, NIST); M.D. Stiles (Electron and Optical Physics Division, NIST); C.J. Powell (Surface and Microanalysis Science Division, NIST); Readrite Corporation; Seagate Corporation; J.D.R. Buchanan (Durham, UK); J. Moodera (MIT)

Nanotribology and Surface Properties

Accurate adhesion/friction measurements at the nanoscale are needed in microelectromechanical systems (MEMS) and nanoelectromechanical systems (NEMS) devices. Lubrication by molecular assemblies at nanometer dimension is required to control the surface properties of device components and ensure durability. The magnetic storage industry also needs control of friction via lubrication in the push towards 1 Terabit/in^2 areal density and a fast data transfer rate. The head-disk interface space is shrinking to 3.5 nm, with a head speed of 40 m/s. Occasional contacts between the head and disk will test the strength and robustness of the carbon overcoat and lubricant layers which are continuously being reduced in thickness.

Stephen Hsu

Significant progress has been achieved in two areas: measurements for adhesion, friction, and lubrication at the nanoscale and establishing test methods relevant to magnetic hard disk performance (with input from the National Storage Industry Consortium.)

The nanofriction measurement activity aims to develop a constitutive equation for nanofriction to include surface force components and material characteristics. We set up a novel, multiscale friction apparatus, developed jointly with Hysitron, allowing friction measurements across nm to mm scales. Figure 1 shows friction data from a diamond tip sliding on silica for different tip sizes (tip radius). The coefficient of friction values show significant dependence on tip size. Future work in nanofriction comparing results among different scales will provide an understanding of how the scale affects frictional forces.

We continue to work with our external academic partners (UC Berkeley, UC Davis, and Ohio State) under the NIST Nanotechnology Extramural Initiative. This collaboration focuses on the development of friction measurement by three approaches: MEMS devices, AFM-based methods, and a novel ultra-high vacuum method. Results thus far have revealed that meniscus forces and electrostatic forces exert a significant effect on nanofriction. We are now quantifying these effects.

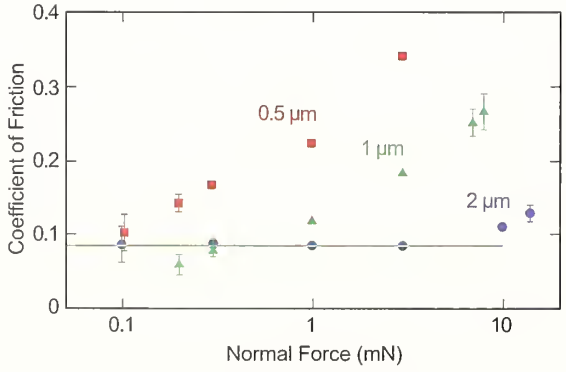

Figure 1: *Effect of tip sizes on friction.*

Significant progress has been made in establishing test methods for assessing the performance of the carbon overcoat and lubricant layers in magnetic head/disk interfaces. A high speed impact test was developed to simulate the occasional high-speed impacts that occur between the head and the disk media under the ramp-load and unload operating conditions. As the magnetic spacing continues to shrink, this type of contact could lead to data loss. In our test, a 1000 nm ridge is artificially created on a disk, and a ruby ball is used to collide with the ridge at 20 m/s. The impact force and the deformation are measured using an acoustic sensor. Recent improvements in the impact height control were achieved by installing capacitance probes to control the location and positioning of the ruby ball in the z direction. Crater imaging was also improved by using a new dual white light interferometer microscope. (See Figure 2.) Results show that the performance ranking of lubricants and overcoats agrees with field experience.

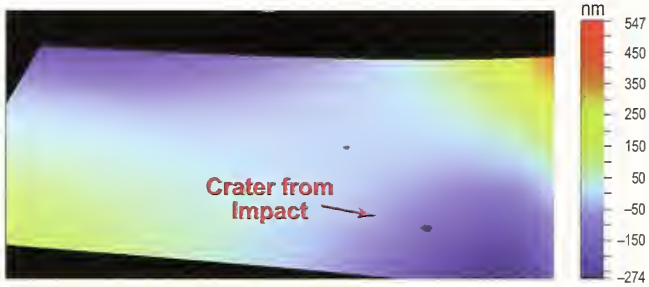

Figure 2: *Microscopic image of impact craters.*

A finite element model was developed last year to describe the stress distribution in the carbon overcoat/lubricant multilayer films. Recently, the model was improved by incorporating brittle fracture criteria for the carbon overcoat. This refinement allows the determination of the threshold stress level where data loss may occur.

Contributors and Collaborators

C. Ying, R. Gates, J. Chuang, D. Fischer (Ceramics Division, NIST); B. Bhushan (Ohio State); K. Komoupoulas (UC Berkeley); G. Liu (UC Davis); Y.T. Hsia (Seagate); J. Sengers (University of Maryland)

Metrology for Nanoscale Properties: Brillouin Light Scattering

A Brillouin-light-scattering facility is being developed for characterizing phonons and magnons at gigahertz frequencies in thin-film materials. The current focus of research is on providing information about the interactions between magnetic modes and thermal phonons, which play a central role in determining the switching times of magnetic-storage devices, spin-valve sensors, and other thin-film magnetic devices.

Ward Johnson and Sudook Kim

Technical Description

Methods that employ Brillouin light scattering (BLS) for the characterization of materials measure the intensity of spectral components of light that is inelastically scattered by acoustic waves (phonons) or spin waves (magnons). Fabry–Perot interferometric techniques are used to acquire accumulated spectra through repeated mechanical sweeping of the etalon spacing.

In this division, research employing BLS is focused primarily on interactions of magnons and phonons in ferromagnetic thin films. This subject is important with respect to maximizing the speed of magnetic-storage devices, spin-valve sensors, and other thin-film magnetic devices because the coupling of spin waves to thermal phonons determines the settling time of the magnetization during a switching event. BLS has the potential of becoming a particularly powerful tool for probing these interactions because it can detect both magnons and phonons at gigahertz frequencies. The aim of our research is to characterize changes in the populations of magnons and phonons induced by ferromagnetic resonant excitation.

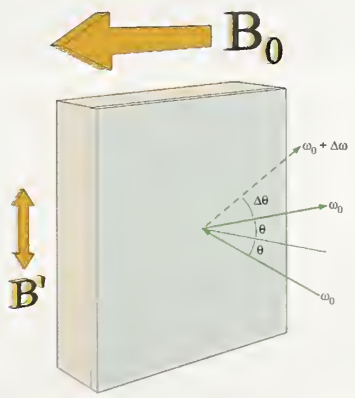

Figure 1: *Scattering of light off waves in a thin film in the presence of static and dynamic magnetic fields.*

Accomplishments

We have implemented techniques for electromagnetically pumping magnons during BLS measurements. As represented in Figure 1, an oscillating magnetic field B′ at gigahertz frequencies is superimposed on a constant magnetic field B_0 to drive spins into uniform precession (excite magnons with a wavevector of zero). Scattered light undergoes a frequency shift $\Delta\omega$ and a change in direction $\Delta\theta$ relative to the specular reflection, as a result of interactions with acoustic or magnetic waves in the film.

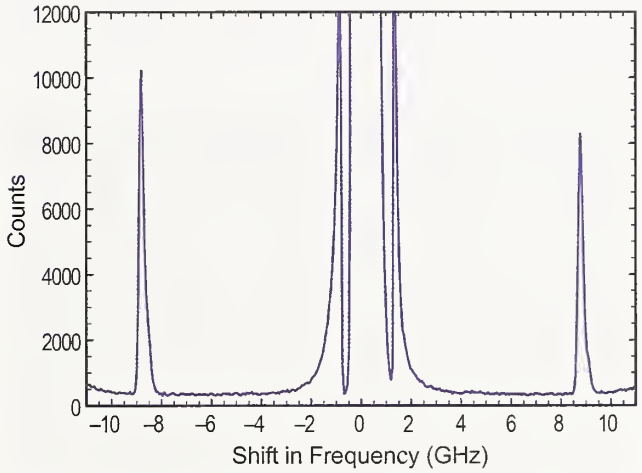

Figure 2: *Backscattered BLS spectrum showing 8.8 GHz pumped magnons in a film of $Ni_{81}Fe_{19}$ (0.9 % Tb).*

This implementation of magnon pumping in a backscattered configuration enables measurements on opaque films, which cannot be studied using forward-scattering techniques. Ongoing measurements are focused on permalloy ($Ni_{81}Fe_{19}$) thin films doped with Tb, which affects magnetic relaxation. An example of a pumped-magnon spectrum from a 50 nm film of $Ni_{81}Fe_{19}$ (0.9 % Tb) is shown in Figure 2. Counts in the range between –2 GHz and 2 GHz arise from a direct reference beam. Strong magnon peaks appear at the 8.8 GHz pumping frequency.

Contributors and Collaborators

P. Kabos (Radio-Frequency Technology Division, NIST); S. Russek (Magnetic Technology Division, NIST)

(This project was partially funded by the National Nanotechnology Initiative.)

Nanoscale Characterization by Electron Microscopy

Electron microscopy is used to characterize the structure and composition of materials at the nanometer scale to better understand and improve their properties. New measurement techniques in electron microscopy are being developed and applied to materials science research. The MSEL Electron Microscopy Facility serves the Metallurgy, Ceramics, and Polymers Divisions as well as other NIST staff and outside collaborative research efforts.

John E. Bonevich

Atomic-scale structure and compositional characterization of materials can lend crucial insights to the control of their properties. For instance, direct observation of local structures by transmission electron microscopy (TEM) provides an important information feedback to the optimization of crystal growth and processing techniques. Various characteristics may be observed such as crystal structure and orientation, grain size and morphology, defects, stacking faults, twins and grain boundaries, second phase particles — their structure, composition and internal defect structure, compositional variations as well as the atomic structure of surfaces, and interfaces.

The MSEL Electron Microscopy Facility consists of two transmission electron microscopes, three scanning electron microscopes, a specimen preparation laboratory, and an image analysis/computational laboratory. The JEM3010 TEM resolves the atomic structure and employs an energy selecting imaging filter (IF) and x-ray detector (EDS) for analytical characterization of thin foil specimens. The JSM6400 SEM employs electron backscattered diffraction/phase identification (EBSD) and EDS systems to characterize the texture and composition of materials.

Highlights from the EM Facility for FY2003 include:

- Facilities computer resources have been upgraded, providing streamlined user access and network file storage.
- Collaboration with the Semiconductor Electronics and Electricity Divisions (EEEL) to characterize quantum effects in confined Si devices.
- Characterization of the size and shape of III-V quantum dots, with the Optoelectronics Division (EEEL).
- Compositional mapping of electrodeposited nanowires with tunable magnetic properties, fabricated at Johns Hopkins University (Figure 1).

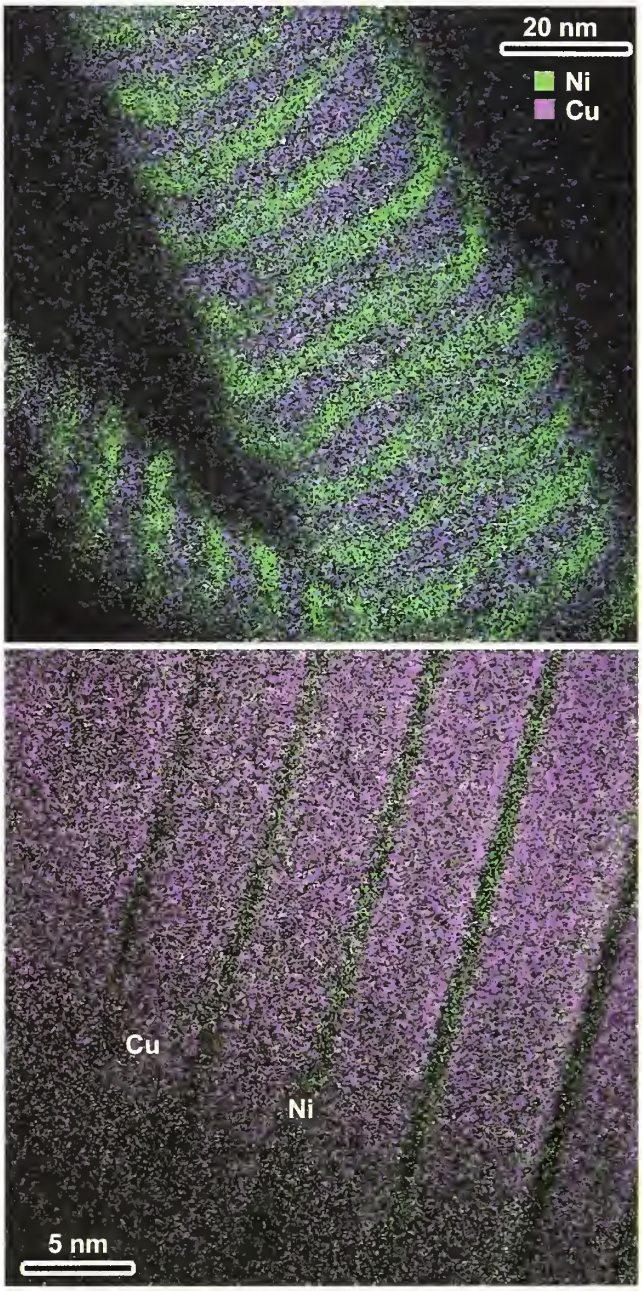

Figure 1: *Composition maps of Ni/Cu electrodeposited multilayer nanowires. Modulation of the composition wavelength provides a means to tune the magnetic properties as desired. The Ni layer thickness varies from 5 nm (top) to 1 nm (bottom).*

Contributors and Collaborators

D. Josell, T. Moffat, R.D. McMichael (Metallurgy Division, NIST); A. Roshko, S.Y. Lehman (Optoelectronics Division, NIST); E. Vogel, N. Zimmerman (Semiconductor Electronics Division, NIST); P. Searson (Johns Hopkins University)

USAXS Imaging: Microscope Development and Validation

Modeling the behavior of complex materials requires detailed knowledge of the underlying three-dimensional microstructure. Ultra-small-angle X-ray scattering (USAXS) imaging is a new class of synchrotron X-ray imaging techniques that uses USAXS as the contrast mechanism. The technique provides imaging and statistical data that cannot be obtained using any other experimental methods.

Lyle E. Levine, David J. Pitchure, and Gabrielle G. Long

USAXS imaging was developed by NIST researchers and was first demonstrated in May 2000. The primary advantages over existing X-ray imaging techniques are its inherently higher contrast and its USAXS-derived ability to provide quantitative data on object shapes and size distributions. USAXS imaging has broad applicability to a wide range of material systems including metals, ceramics, polymers, and biological materials. Over the past year, work has concentrated on two main areas. First, major improvements in the instrumentation have greatly improved the imaging capabilities, and second, a wide range of material systems have been explored to determine where USAXS imaging can have the greatest impact.

The USAXS imaging experiments are conducted on the UNICAT sector 33 insertion-device beamline at Argonne National Laboratory's Advanced Photon Source. A high-intensity, parallel, monochromatic X-ray beam passes through entrance slits that define the size, shape and position of the beam. Imperfections in the X-ray beam are removed using multiple Bragg reflections within a <111> channel-cut Si crystal referred to as the collimator. Within the sample, local density variations from the microstructure produce X-ray scattering at small angles. The X-rays leaving the sample are then angle-filtered using another pair of <111> Si crystals referred to as the analyzer. The only X-rays from the sample that can pass through the analyzer are those scattered by the microstructure at a specific angle. This angle can be selected by rotating the analyzer. Images are then formed by either exposing nuclear emulsion plates or using an X-ray camera system.

During the past year, several major improvements have been made in the instrumentation. These include new analyzer crystals whose surfaces were chemically polished to minimize image aberrations, a multiple-sample motorized rotation stage for doing stereo imaging and a motorized rotating goniometer stage for aligning the samples and then rotating them over 180° *in situ*. The most important improvement in instrumentation was the design, construction, and testing of a new high-resolution X-ray camera. In this device, the X-rays hit a single-crystal scintillator that converts them to visible light. The resulting image is then magnified using an optical microscope system using a cooled CCD chip, infinity-focus objective lenses, an auxiliary lens system to produce a real image on the CCD plane, and a mirror to shift the optical axis away from the X-ray beam. The spatial resolution of the camera is approximately 1 μm. Remote computer control is available for all operations of the USAXS imaging equipment, and sequences of images (such as during sample rotations) can be acquired automatically using macro programs.

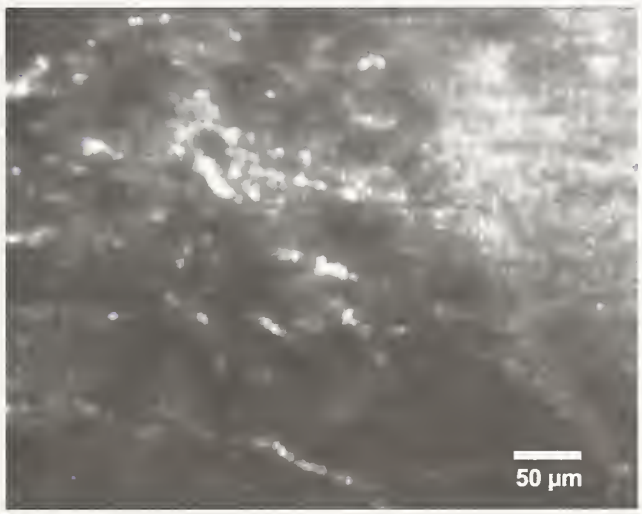

Figure 1: *USAXS image of density variations within the Allende meteorite.*

As examples of the technique's versatility, USAXS imaging has been successful at imaging creep cavities and cracks in copper, fatigue-generated voids in lead-free solder balls in microelectronic devices, silica beads embedded in polycarbonate and polypropylene, the Allende meteorite (see Figure 1), indentation crack surfaces in ceramics, artificial polymer tissue scaffolds, and fiber structures within bovine and human cartilage.

Contributors and Collaborators

J. Ilavsky (Ceramics Division, NIST); J. Dunkers (Polymers Division, NIST); P. Jemian (UNICAT); C. Muehleman (Rush Medical College); Denton Ebel (American Museum of Natural History)

Crystallographic and Phase Equilibria Databases

Crystallographic data models are used on a daily basis to visualize, explain and predict the behavior of chemicals and materials, as well as to establish the identity of unknown phases in crystalline materials. Phase diagrams are used throughout the ceramics industry to understand and control the complex phenomena which increasingly underlie advanced industrial material production and materials performance. Literally tens of thousands of structures and phase diagrams have been reported in the literature, all with varying degrees of reliability and completeness. This project develops, maintains, and disseminates comprehensive, critically-evaluated data in printed and modern computerized formats, along with scientific software to exploit the content of these databases.

Vicky Lynn Karen, Terrell A. Vanderah, and Peter K. Schenck

The Inorganic Crystal Structure Database (ICSD) is a comprehensive collection of crystal structures covering the literature from 1915. The ICSD database system now includes chemical and 3-dimensional structure information for more than 65 000 inorganic materials. The data and scientific software are licensed to instrument manufacturers, software vendors, and other third-party distributors as well as to individual researchers in industry and academia. Additional information about the ICSD can be found in the Technical Highlights section of this report.

To service the need for reliable phase diagram data, the NIST Phase Equilibria Data Center and the American Ceramic Society (ACerS) jointly publish a series of critically evaluated collections of phase diagrams. The series "Phase Equilibria Diagrams," originally published under the title "Phase Diagrams for Ceramists" (1964–1992), provides current, evaluated data on the phase equilibria of ceramics and related materials. These publications also provide bibliographic data, graphical representations, and analytical capabilities so that researchers have access to reliable, up-to-date data for use in designing, applying, analyzing, and selecting materials. The published portion of the database includes about 16 000 entries with 26 000 phase diagrams contained in nineteen books and a CD-ROM — over 53 000 units have been sold world-wide. Approximately 1000 new entries are collected from the primary literature each year.

Currently underway is a complete modernization to replace the outdated 1980's system with an integrated production facility using a relational structure that will facilitate electronic publishing in a variety of formats, including a web-based version. Much of this year's effort has involved assisting and working with on-site ACerS staff to design and build the new system, which must incorporate all of the scientific data relationships embodied in the original database.

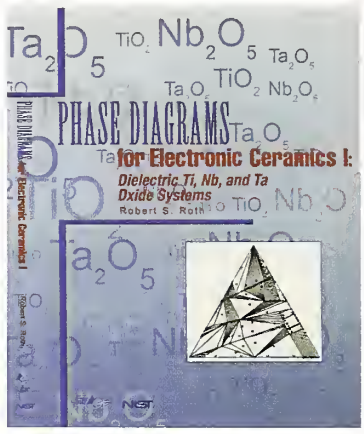

Figure 1: *The latest volume in the series "Phase Equilibria Diagrams" features systems of major interest to the fields of dielectric, ferroelectric, and piezoelectric ceramics.*

The latest database products completed this year include the topical volume, *Phase Diagrams for Electronic Ceramics I: Dielectric Ti, Nb, and Ta Oxide Systems*, edited by R.S. Roth (see Figure 1). This is the first volume of a new collection of phase diagrams focused on the increasingly important field of electronic ceramics. More than 1100 diagrams are presented along with commentaries written by knowledgeable associate editors. Also completed this year was an updated *Cumulative Index 2003* which provides comprehensive indexing of published equilibria data sorted by chemical system and author. In preparation is "Volume XIV — Oxides" (2004) which will contain a wide variety of metal, non-metal, and semi-metal oxide systems — more than 900 entries with 1300 diagrams are already available for inclusion.

Contributors and Collaborators

R.S. Roth, H. Ondik, M.A. Harne (Ceramics Division, NIST); H.F. McMurdie, C. Cedeno, J. You, X. Wang, N. Swanson, E. Farabaugh, M. Mecklenborg (The American Ceramic Society); Fachinformationszentrum Karlsruhe, Germany; D. Watson (Cambridge Crystallographic Data Centre, UK); A. Belsky, S. Young (Measurement Services Division, NIST)

Phase Equilibria and Properties of Dielectric Ceramics

Ceramic compounds with exploitable dielectric properties are widely used in technical applications such as actuators, transducers, capacitors, and resonators or filters for microwave communications. The commercial competitiveness of next-generation devices depends on new ceramics with improved properties and/or reduced processing costs. Phase equilibria determination integrated with systematic experimental/theoretical chemistry–structure–property studies contributes toward the fundamental understanding and rational design of these technologically important materials.

Benjamin Burton, Eric Cockayne, Lawrence Cook, Igor Levin, Michael Lufaso, and Terrell Vanderah

Next-generation ceramic packaging requires fabrication of multilayered structures that include embedded functional dielectric ceramics. Technical challenges include understanding and control of deleterious reactions at interfaces during firing. A detailed study of the system Ag-Bi_2O_3-Nb_2O_5-O_2 is in progress to develop a model of interfacial interactions applicable to other co-fired metal–ceramic systems. A partial phase diagram of the system has been determined, and includes a new compound, $Bi_5AgNb_4O_{18}$, which is also observed as a product in $Ag/BiNb_5O_{15}$ reaction couples. Surface diffusion was found to dominate mass transport of Ag at the reaction interface — this phenomenon could be important for co-firing metals with porous ceramics. Further modelling will incorporate kinetic aspects of interfacial reactions using equilibrium thermodynamics as a basis.

Important transducer/actuator materials include Pb-containing perovskite-type relaxor ferroelectrics. First-principles (FP) methods were successfully used to calculate the phonon frequencies for the prototype relaxor $PbMg_{1/3}Nb_{2/3}O_3$. In FP studies of $PbTiO_3$, the dipole moment generated by a nearest-neighbor Pb-O vacancy pair was calculated; the results demonstrate that local electric fields generated by defects strongly affect physical properties. Calculations were also performed for a Pb-free relaxor, $K_{1-x}Li_xTaO_3$. For small x, Li ions are displaced from centrosymmetric positions. The dominant mechanisms for Li hopping between off-centered positions and the resulting effects on the dielectric response were determined.

First-principles methods were also applied to the microwave dielectric system $(1–x)CaAl_{1/2}Nb_{1/2}O_3–xCaTiO_3$. The resulting model yields a dielectric constant that increases with increasing disorder, and increases nonlinearly with increasing x, in agreement with experiment.

Experimental studies of microwave ceramics include structural analyses (by x-ray and neutron powder diffraction) combined with dielectric property correlations of the technically important $Ba_3M^{2+}M^{5+}{}_2O_9$ (M^{2+} = Mg, Zn, Ni; M^{5+} = Nb, Ta) systems. In these systems, the M^{5+} cations tend to undergo a second-order Jahn–Teller distortion and hence shift from the centers of the $[MO_6]$ octahedra — this effect occurs simultaneously with 2:1 B-site cation ordering. Both phenomena influence dielectric response. Modeling of the crystal structures using bond valence methods is in progress to understand the interplay between the distortion and dielectric behavior.

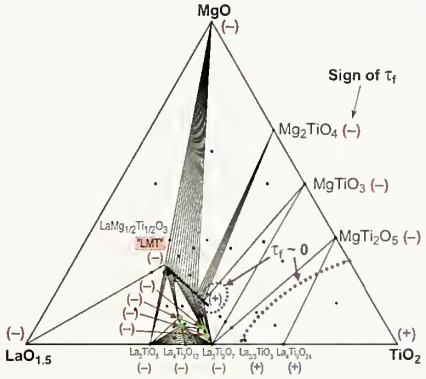

Figure 1: *Subsolidus phase relations in the La_2O_3–MgO–TiO_2 system (air, ≈1450 °C), sign of the temperature coefficient of resonant frequency (τ_f; in parentheses), and approximate locations of two regions of temperature-stable ($\tau_f = 0$) equilibrium mixtures (dotted lines).*

Subsolidus phase equilibria, crystal chemistry, and dielectric behavior were studied for the La_2O_3–MgO–TiO_2 system and for the ternary sections $LaMg_{1/2}Ti_{1/2}O_3$–$CaTiO_3$–La_2O_3 and $LaMg_{1/2}Ti_{1/2}O_3$–$CaTiO_3$–$La_{2/3}TiO_3$. Six phases form in the La_2O_3–MgO–TiO_2 system, and extensive perovskite-type solid solutions form in both ternary sections (see Figure 1). By mapping dielectric properties (relative permittivity and temperature coefficient of resonant frequency, τ_f; 5–10 GHz) onto the phase diagrams, the compositions of temperature-stable ($\tau_f = 0$) compounds and mixtures were predicted. From these studies, it was determined that the quaternary La_2O_3–CaO–MgO–TiO_2 system contains an extensive single-phase, perovskite-type volume through which passes a surface of temperature-stable compositions with relative permittivities in the range of 40 to 50.

Contributors and Collaborators

W. Wong-Ng, R.S. Roth (Ceramics Division, NIST); J.E. Maslar (Process Measurements Division, NIST); R. Geyer (Radio Frequency Technology Division, NIST); S. Bell (TRAK Ceramics, Inc.); K. Leung (Sandia); L. Bellaiche (University of Arkansas); U. Waghmare (JNCASR, India); S. Prosandeev (Rostov State University)

Phase Relationships in High Temperature Superconductors

Phase diagrams serve as "blue prints" for improved processing of high T_c superconductor materials. Of current interest are the $Ba_2RCu_3O_{6+x}$ (R = lanthanides and yttrium) superconductors. The construction of phase diagrams of these systems and the role of phase equilibria and kinetics in the formation of the $Ba_2YCu_3O_{6+x}$ phase using barium fluoride amorphous precursor films are important for rapid advancement of the RABiTS/IBAD coated conductor technology. By providing the phase equilibria data for optimal processing, high T_c technology will be advanced through reductions in cost and improvements in performance.

Winnie Wong-Ng, Lawrence P. Cook, and Igor Levin

In 2003, NIST materials research has continued to provide critical information pertinent to the development of practical superconductors. This project is an integral part of the Department of Energy intensive research program focused on high T_c wires and cables for high-impact commercial applications. Our effort included two principal groups of superconductors: (1) $Ba_2RCu_3O_7$ (Y-213 and R-213, R=lanthanide) coated conductors produced by rolling assisted biaxially textured substrate/ion beam assisted deposition (RABiTS/IBAD); and (2) MgB_2.

Part of our effort has been focused on the dependence of BaO-R_2O_3-CuO_x phase relations (under carbonate-free conditions to match the processing conditions of RABiTS/IBAD conductors) on both oxygen pressure, p_{O2}, and choice of lanthanides. This year, we have completed the study of three systems, with R=Gd, Eu and Ho. The trends of phase formation and tie-line relationships with respect to lanthanide size that were found previously for R=Nd, Sm, Eu, Gd, Ho, Y, and Er, were observed in the present work. Near the BaO-rich region, phase formation was very different from what was found previously for samples prepared in the presence of carbonate.

By mixing the smaller lanthanides R′ with the larger R in the $Ba_{2-x}(R_{1+x-y}R'_y)Cu_3O_{6+z}$ superconductor, both flux-pinning and melting properties can be tailored and optimized. A trend of the extent of solid solution formation with respect to the size of R was observed in $Ba_{2-x}(Nd_{1+x-y}R'_y)Cu_3O_{6+z}$ (R′=Gd, Y and Yb) and in $Ba_{2-x}(R_{1+x-y}Y_y)Cu_3O_z$ (R=Eu and Gd). There is considerable improvement of critical current density, $J_c(H)$, for samples with partial Y-substitution at high fields at 77 K as compared with that of Nd-213 and Y-213. This improvement is likely due to the increased flux pinning as a result of doping of Nd^{3+} in the Ba^{2+} site.

The "BaF_2 *ex-situ*" process is a promising method for producing long-length, high-quality Y-213 superconducting tapes. Previously, using a controlled-atmosphere differential thermal analysis system, we detected the presence of low temperature liquids in the multicomponent reciprocal Ba-Y-Cu//O,F system, which can be modeled in compositional space as a trigonal prism. This year, we initiated a study to understand the details of complex phase relations in selected Ba-Y-Cu//O,F subsystems: BaO-Y_2O_3-CuO_x-BaF_2, BaF_2-YF_3-CuF_2-CuO_x, BaF_2-Y_2O_3-CuO_x-YF_3, BaF_2-CuO, and BaF_2-Cu_2O. Our results explained the presence of low temperature melts, and confirmed the importance of p_{O2} in oxyfluoride melting reactions.

To control film properties, it is important to understand the details of Y-213 phase evolution from amorphous "BaF_2" films. High temperature x-ray diffraction has been successfully applied to a number of films deposited on $SrTiO_3$ model substrates (provided by Oak Ridge National Laboratory, ORNL). The phase formation sequences in the binary (BaF_2-Y_2O_3, BaF_2-CuO_x and Y_2O_3-CuO_x) and ternary (BaF_2-Y_2O_3-CuO_x) systems have been determined. Further studies of phase evolution of these films on both $SrTiO_3$ and RABiTS substrates will be conducted.

Understanding the interfacial reactions of Y-213 with buffer layers in RABiTS/IBAD films is critical to the development of coated conductor tapes. Since phase diagrams can provide information on how to avoid or control the formation of second phases, we have initiated a study of the BaO-Y_2O_3-CeO_2-CuO_x system (interaction of Y-213 with the CeO_2 buffer layer).

Efforts have continued on the measurement of enthalpy of formation and vapor pressure of MgB_2. Sources of the variability in these properties have also been determined.

Contributors and Collaborators

M. Vaudin (Ceramics Division, NIST); Q. Huang (NIST Center for Neutron Research); R. Shull (Metallurgy Division, NIST); R. Klein (Biotechnology Division, NIST); R. Feenstra (ORNL); T. Holesinger (Los Alamos National Laboratory); M. Rupich (American Superconductor Corp.); J. Kaduk (BP-Amoco); T. Haugan (U.S. Air Force); P. Canfield (Iowa State)

Metrology for Nanoscale Properties: Conductive AFM Using Carbon Nanotubes

The latest integrated electrical circuits, as well as microelectical mechanical devices, are dependent on sub-micron features with very high aspect ratios. We are developing a technique using carbon nanotubes mounted to atomic force microscope tips to probe the surface conductivity of these devices with nanometer resolution. The development of these tips also leads to probing high-frequency electronic circuitry and the electrical properties of biological specimens.

Paul Rice

We are mounting carbon nanotubes on the end of conductive atomic force microscope (AFM) tips to probe the surface electrical properties of various samples with nanometer resolution. Using these tips, we are attempting to map the sample surface conductivity and also to probe local electric fields on high-frequency circuits.

Carbon nanotubes have qualities that make them very desirable as AFM probes. They can be micrometers long and only nanometers in diameter allowing for probing devices with deep narrow features such as microelectrical and mechanical systems (MEMS). In addition, there are a variety of types of nanotubes that can have different electrical transport properties. A nanotube can be a ballistic conductor with very low resistance, a metallic conductor, or a semiconductor. The nanotubes are also very durable and can withstand multiple crashes while imaging. For example, we have found that a nanotube we mounted to an AFM tip will spring back after being bent back upon itself and still provide good quality images.

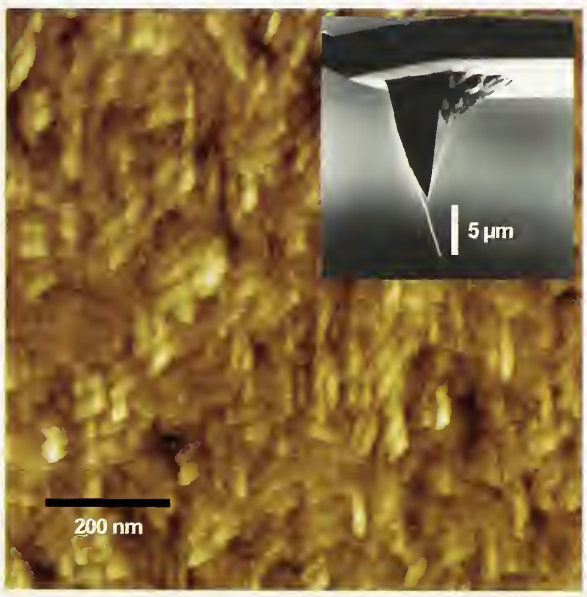

Figure 1: *The image above shows a topographic atomic force microscope image of sputter deposited thin-film niobium. The inset is a SEM micrograph of the AFM tip, fabricated at NIST, which took the AFM image. Attached to the end of the AFM tip is the carbon nanotube that actually probed the sample surface. This image demonstrates the resolution and durability of a carbon nanotube as used for AFM imaging.*

We are currently developing expertise in mounting nanotubes to AFM tips using the SEM. Figure 1 shows an AFM image taken with a nanotube attached to the AFM tip using our in-house technique. The image resolution is comparable to an image taken with a commercial AFM tip. Also, in this application, the nanotube provides extended capabilities for high-aspect-ratio probing, tip durability, and electrical conductance.

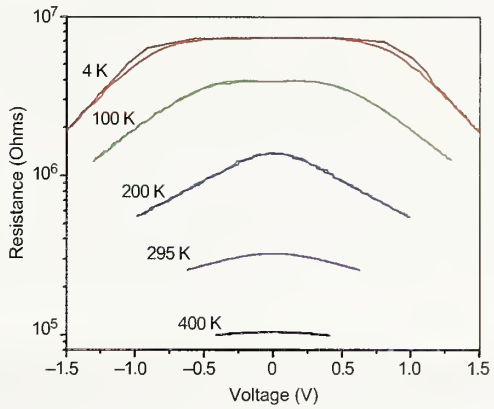

Figure 2: *Resistance versus voltage behavior of a multiwalled nanotube connected to a Au thin-film test structure using electron beam assisted deposition of carbon in the SEM.*

We are also testing the electrical properties of the nanotubes and their subsequent interconnects. Shown in Figure 2 is the resistance versus voltage behavior of a nanotube plus the effects of its interconnects. The resistance response to temperature indicates semiconductive behavior, while the voltage response indicates nonlinear effects possibly due to the interconnects.

Contributors and Collaborators

S.E. Russek (Magnetic Technology Division, NIST); P. Kabos (Radio Frequency Technology Division, NIST); D.S. Finch (Materials Reliability Division, NIST)

Physical Properties of Thin Films and Nanostructures: Multilayer Ceramic Components

A wide range of chemical compositions is now being produced commercially as nanopowders. The availability of ceramic materials in this size classification is particularly important for the electronic component industry. Nanopowders represent an enabling technology for achieving significant decreases in ceramic layer thickness, minimizing the size and prevalence of processing-induced defects, and boosting the overall performance of components ranging from capacitors to piezoelectric actuators. Quantification of these performance enhancements and their association with nanometer-scale microstructure control is a key objective within the Materials Reliability Division.

Stephanie A. Hooker

Surface-mount electronic components are widely used to accomplish both active and passive functions in state-of-the-art circuitry. Examples include capacitors, resistors, surge suppression devices, and temperature sensors. Recently, the multilayer fabrication process used to produce these electronic components has been employed to prepare miniature actuators. These piezoelectric ceramic devices (see Figure 1) provide precision, nanometer-scale motion in a small package and require very low power input, making them highly desirable for use in adaptive structural elements, biomedical pumps, and optical translation devices.

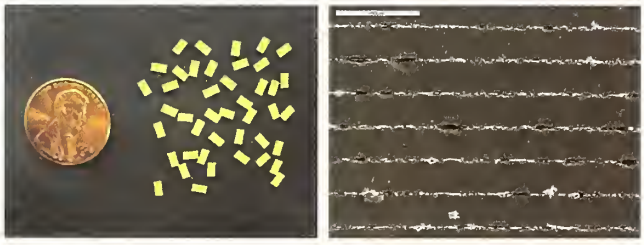

Figure 1: *Photograph & SEM image of typical mutlilayer components produced by Synkera Technologies.*

However, long-term cyclic fatigue, defined as a recoverable or non-recoverable change in polarization or displacement over time, is a recognized problem in piezoelectric actuators. One method to minimize actuator fatigue is to reduce both the size and prevalence of processing-induced defects within the ceramic layers, as these defects can grow rapidly during long-term exposure to electric fields. The emerging prevalence of submicrometer and, more recently, nano-sized ceramic powders offers the opportunity to achieve a high level of defect control in these components, significantly extending their operational lifetime and improving their overall electromechanical performance.

In FY03, a program was initiated to develop specialized test platforms and methodologies to systematically quantify the performance advantages of *nanometer-scale* microstructure control for multilayer actuator components under real-world operational conditions. This new capability combines measurements of dielectric properties, ferroelectric properties, and physical displacement with the simultaneous application of a range of external stimuli including both electrical and mechanical influences. Variables include the input waveform characteristics, loading and/or pre-stress condition, and method of attachment within the system.

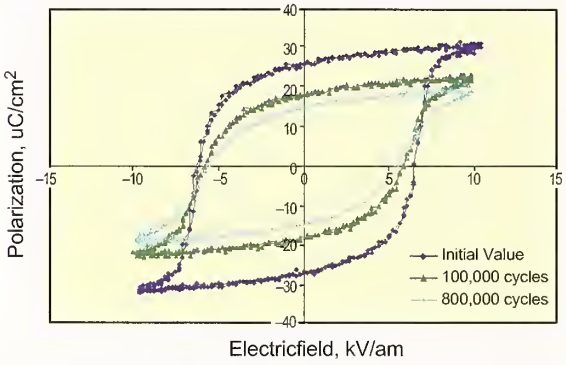

Figure 2: *Polarization degradation for one actuator device as a function of cyclic operation over time.*

To date, a series of microstructure-controlled multilayer actuators has been fabricated by our collaborator, Synkera Technologies, and fully characterized within the Materials Reliability Division of MSEL. Significant enhancements in polarization, electro-mechanical coupling, and resistance to short-term fatigue (see Figure 2) have been identified and correlated with microstructure evolution and grain growth. These results have clarified the importance of understanding the sintering characteristics of nanopowder materials and the relationship between initial precursor size, fired microstructure, and device performance. A more extensive follow-on investigation is currently underway, addressing alternative materials, additional process variables, and more comprehensive accelerated long-term fatigue testing.

Contributors and Collaborators

C. Kostelecky, D. Deininger, K. Womer (Synkera Technologies)

Physical Properties of Thin Films and Nanostructures: Mechanical Properties of Thin Films

We develop and apply noncontact, nondestructive tools to measure thin-film mechanical properties such as elastic modulus and residual stress. Optical methods are used to determine the frequency dependence of the velocity of surface acoustic waves. The information obtained can assist in developing new film materials. It is also valuable for predicting the reliability and performance of thin-film components.

Donna Hurley and Vinod Tewary

To successfully develop a new thin-film material, knowledge of its mechanical properties is often needed: to estimate surface residual stresses, to predict reliability or performance, or to assess film-substrate adhesion. Yet methods are generally limited to destructive tests or even "try it and see." Also, film properties usually cannot be extrapolated from those of bulk samples — if they exist.

We are developing nondestructive methods to quantify thin-film properties. We aim to relate physical properties like elastic moduli, residual stress, or adhesion to film microstructure, quality or performance. The approach exploits the behavior of surface acoustic waves (SAWs). The SAW velocity varies with frequency and depends on the film and substrate properties (Young's modulus E, Poisson ratio, density, and film thickness). We use laser ultrasonic methods to generate and detect SAWs over a broad frequency range. The SAW velocity-*versus*-frequency data are interpreted with a Green's function method to determine the film properties.

In FY03, we implemented a second SAW apparatus. Silicon and other materials are not opaque to infrared light and thus are ill-suited to the infrared detector in the original apparatus. The new apparatus uses a green laser in its interferometer, extending capabilities to a wider range of materials. In addition, a pulsed ultraviolet laser improves generation efficiency in polymer and other films. The apparatus is quite user-friendly, increasing accessibility to postdocs and visitors. This setup frees up our first apparatus for speculative experiments requiring more frequent reconfiguring of optical components.

Analysis capabilities were improved by extending the anisotropic Green's function inversion software to two layers. TiN films were analyzed with three different models: one elastically isotropic layer, one anisotropic layer, and two layers (isotropic TiN over hexagonal Ti). SEM images such as that in Figure 1 show a thin Ti interlayer, but, until now, we could not model two separate

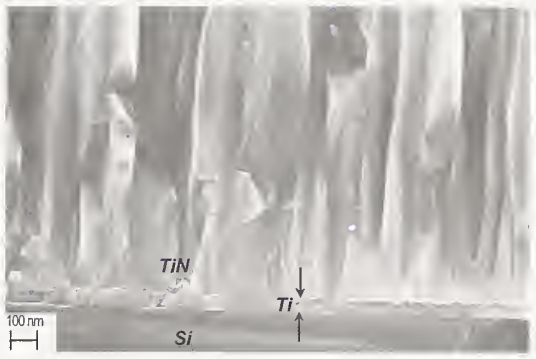

Figure 1: *SEM micrograph of TiN film showing preferential crystallite orientation and adhesive Ti interlayer (R. Geiss, NIST).*

layers. Of the three models, the velocities predicted by the two-layer model agreed best with experimental values. The nanoindentation and two-layer SAW values for E were virtually identical for the thickest film. Discrepancies in other films may be due to acoustoelastic effects or indentation substrate effects.

The two-layer model proved valuable in other cases. In a mini round-robin project for VAMAS TWA 22 begun this year, we examined oxide films (TiO_2 and SiO_2) on glass. SAW measurements on these transparent samples required the addition of a Cr topcoat. The Cr properties were fixed in the two-layer model using results from a sample with a single Cr layer. Preliminary nanoindentation results were in excellent agreement with the SAW results. Also, low-k dielectric films containing secondary capping layers were evaluated with this model (described in detail on the next page of this report).

Although nanoindentation is in widespread use, absolute validation by independent means is needed. The VAMAS project above is one example of our efforts to carefully compare SAW and nanoindentation results. We also performed similar comparisons on a Nb film. In that case, SAW data were obtained at both NIST and another laboratory on the same sample. By combining SAW and nanoindentation information so as to exploit the different sensitivity of each method to different parameters, we obtained a more consistent and complete set of values than possible with either method alone. We will pursue these and related issues (*e.g.*, ultimate uncertainty) during the visit of a guest scientist in late FY03.

Contributors and Collaborators

C. Flannery (Materials Reliability Division, NIST); D. Smith (Ceramics Division, NIST); N. Jennett (NPL, UK); U. Beck (BAM, Germany); D. Fei (Caterpillar)

Physical Properties of Thin Films and Nanostructures: Carbon Nanotube Composites

Carbon nanotube reinforcements can dramatically improve a wide range of material systems. Even at low volumes, nanotube additions can significantly impact electrical conductivity, heat dissipation, and mechanical durability. A key component of the high performance of nanotube composites is the ability to effectively disperse and/or align individual nanotubes within the matrix. This project addresses new measurement approaches that can bring to light information on tube distribution and alignment and provide important data for process optimization.

Stephanie A. Hooker

Carbon nanotubes (CNTs) have received considerable attention recently due to their remarkable combination of mechanical, electrical, and thermal properties. One avenue to effectively utilize these unique materials is to combine them with polymers, thereby creating *nanocomposites*. Incorporation of even small volumes of CNTs into various polymers has already led to demonstrated increases in electrical conductivity, Young's modulus, and hardness as compared to the non-reinforced matrix. As a result of these early findings, applications in multifunctional composites, EM shielding, static dissipation, thermal isolation, and flaw detection are being pursued.

However, one major challenge associated with the development of CNT composites is effective distribution of individual tubes within the matrix. To investigate the effects of this distribution on composite performance, various fabrication techniques are being evaluated, and the resulting mechanical, thermal, and electrical properties are being correlated with microstructure features such as tube alignment and tube-to-tube contact. In addition, impedance analysis is being investigated as a potential method to obtain critical information related to the tube-matrix interface.

Three approaches to composite fabrication have been selected for evaluation in this project: mechanical mixing, doctor-blade tape casting, and templated synthesis from the gas phase. Based on initial discussions related to the different processes, composite specimens with tube distributions ranging from completely random to fully aligned should be feasible.

In FY03, specimens were prepared by mechanically mixing 0 to 1 weight % single-walled nanotubes (SWNTs) with a polymer commonly used in microelectronic packaging. Impedance characteristics were determined from 100 Hz to 1 MHz and used to calculate parameters such as electrical conductivity (Figure 1). For this specific process, the data indicated that the individual nanotubes are randomly distributed, and percolation has not yet been achieved. Process variations for improved nanotube incorporation are currently in progress.

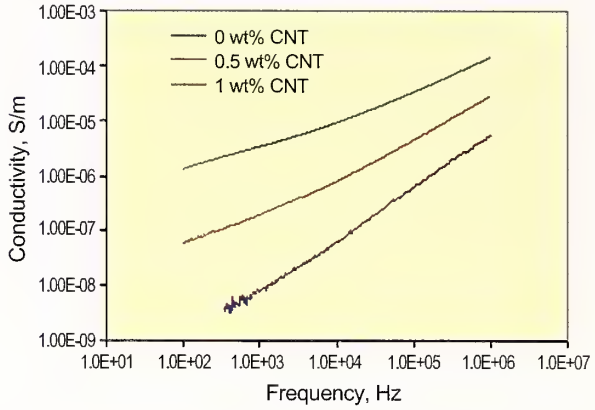

Figure 1: *Electrical conductivity of mechanically combined composites as a function of frequency. Specimens were provided by the University of Colorado at Boulder.*

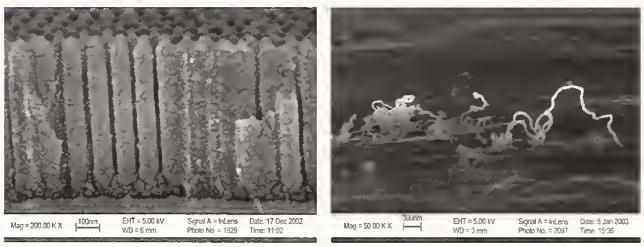

Figure 2: *Blank AAO template (left) and preliminary nanotubes grown inside and extending from an AAO template (right). Specimens were provided by Nanomaterials Research, LLC.*

In addition to randomly oriented composites, CNT arrays synthesized within the regularly aligned nano-sized pores of anodic aluminum oxide (AAO) (Figure 2) are also of interest for more advanced electrical characterization. Preliminary specimens have exhibited growth both within and beyond the porous template. Current research is focused on developing methods to contact and probe these CNT arrays.

Contributors and Collaborators

D. Finch, R. Geiss, P. Rice (Materials Reliability Division, NIST); D. Routkevitch, J. Alexander, O. Polyakov (Nanomaterials Research, LLC); V. Sundaram R.L. Mahajan (University of Colorado at Boulder)

Organizational Charts

Materials Science and Engineering Laboratory

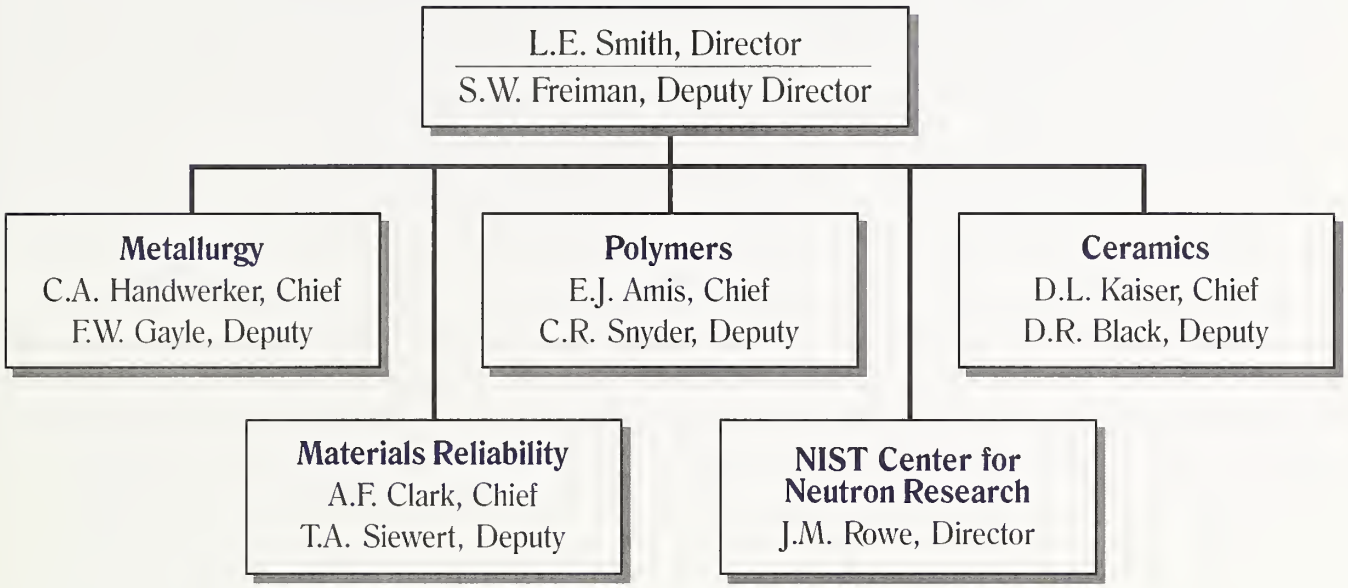

National Institute of Standards and Technology

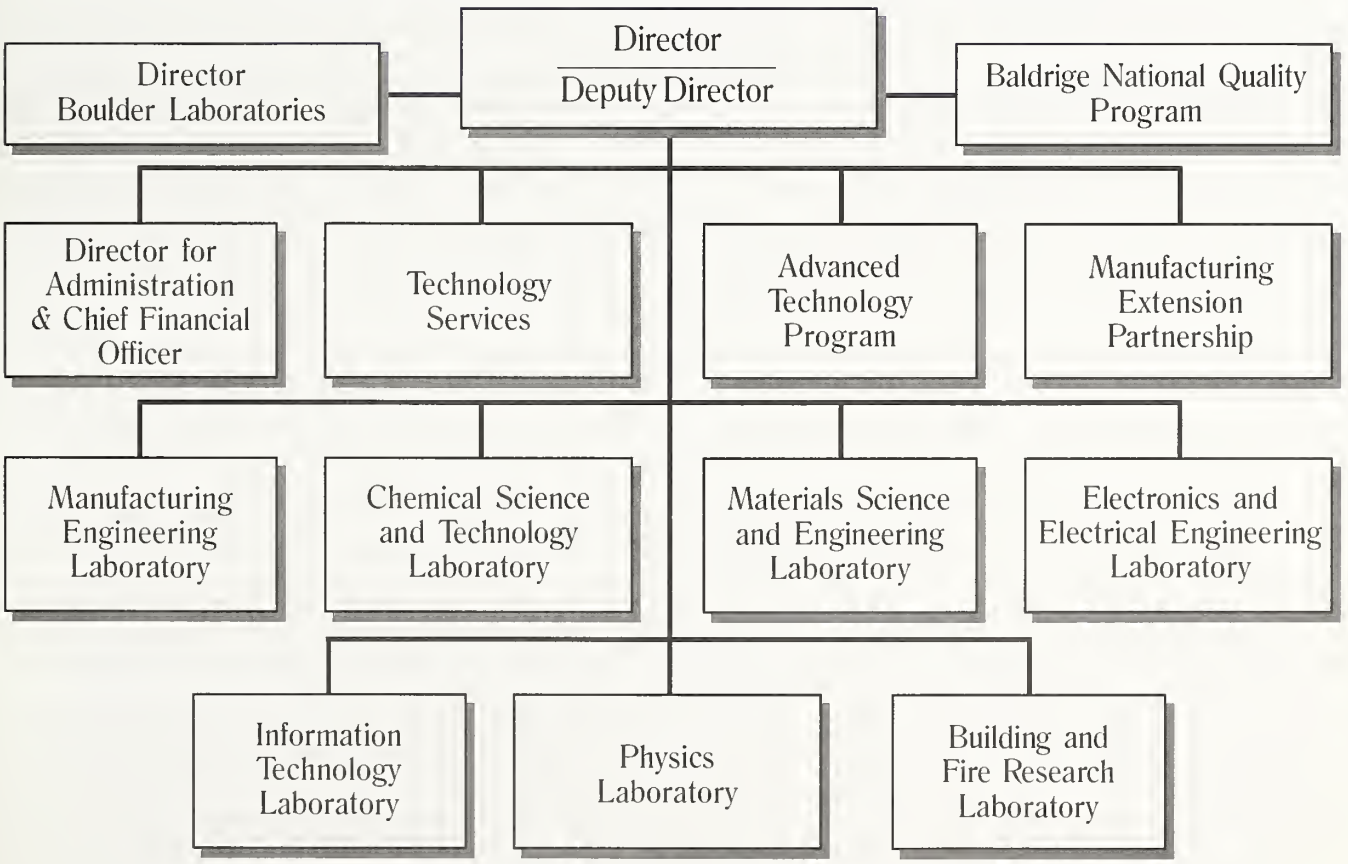

NIST